Towards engineering an artificial neural tube

Présentée le 15 octobre 2021

Faculté des sciences de la vie
Unité du Prof. Lutolf
Programme doctoral en biotechnologie et génie biologique

pour l'obtention du grade de Docteur ès Sciences

par

Jisoo PARK

Acceptée sur proposition du jury

Prof. D. Ghezzi, président du jury
Prof. M. Lütolf, directeur de thèse
Prof. E. Tanaka, rapporteuse
Prof. A. Kirkeby, rapporteuse
Prof. B. Treutlein, rapporteuse

■ École
polytechnique
fédérale
de Lausanne

2021

"Hope, at the end, connects us all
no matter how different we are."

Markéta Irglová

ACKNOWELDGEMENT

I am tremendously happy to have accomplished this thesis with a great story. This would not have been possible without all the people I met throughout the journey and all the lessons I learned from them. I would like to thank everyone for helping me during this journey and for being awesome companions.

First of all, I would like to thank my supervisor, Professor. Matthias Lütolf, who gave me this amazing opportunity to work on such an intriguing project and to be part of this lifelong team of great people. Especially, I really appreciate his patience and belief in me. As much as the project was challenging, I had quite a big struggle in the middle of my PhD with a lot of ups and downs, but he never gave up on neither me nor the project. Thanks to him, I could achieve my PhD project done as we planned initially. Danke vielmals! I also would like to wish him the best for his next adventure.

Also, I would like to thank all the committees for my candidacy exam, Professor Andrew Oates, Professor Selman Sakar, and Professor Carlotta Guiducci, for approving me to continue working on this project so that I could eventually defend my PhD successfully having the world-leading experts in this field as the juries. I would like to thank Professor Diego Ghezzi, Professor Elly Tanaka, Professor Agnete Kirkeby, and Professor Barbara Treutlein for being juries of my thesis defense and for sharing an invaluable discussion and insightful feedbacks. It was a great pleasure to share the outcome of my journey.

Additionally, I would like to thank my mentor, Andrew Oates, for being there to listen to me when I had hard times during my PhD and for giving me heartfelt advices with calm and happy vibe. Thank you!

I am also grateful for all the people from EPFL core facilities who made everyday lab life easier: BioImaging and Optics Platform for the help with the microscope and the image analysis, Gene Expression Core Facility for the help with quantitative analysis of transcriptomes, Histology Core Facility for providing the antibodies, Center of

MicroNanoTechnology for the general support for microfabrication, SV Store for taking care of delivery, SV Workshop for fixing instruments, Glassware Washing and Sterilization Facility for preparing clean wares ready, cleaning staffs for keeping the working environment clean.

Also, I would like to thank Sonja Bodmer from EDBB program who helped me with administration from the start to the end of my PhD journey always with her big smile and Sandra Roux from doctoral school who guided me the steps of thesis defense.

One of the biggest lucks I had was the awesome lab mates who made my everyday fun inside and outside of the lab and I would like to thank everyone of them:

Nikolce – for teaching me how to party,

Laura – for reminding me of different values in life,

Evangelos – for sharing the passion for teaching and medieval culture,

Gena – for the passionate discussion about morality,

Vincent – for helping my starting in the lab and for all the interesting discussions

Sara – for the powerful energy every day,

Marlen – for being an inspiration in the lab,

Yoji – for being a sugoi senpai,

Nathalie – for the sincerest heart and for making my PhD life interesting,

Delphine – for teaching me a real French and for the warm heart,

Sylke – for sharing fun moments which I miss,

Mark – for the funny group meeting presentations,

Andrea – for being an awesome friend,

Aleks – for sharing the passion for art and for introducing the life outside of the lab,

Stefanie – for teaching me about Korean TV series and for the sauerkraut,

Mehmet – for all the support and the warm hugs when needed,

François – for sharing genes having different parents and being my Swiss brother,

Sonja – for taking care of me warmly,

Moritz – for being awesome neighbor and always motivating,

Stefano – for being my science guru and youtube guru,

Mike – for being in the lab 24/7,

Olga – for giving me a lovely Russian nickname,

Nicolas – for sharing the passion for music,

Tania – for the kindness and always motivating,

Julia – for all the kind help and for always being supportive,

Saba – for being Sabamama sharing all the ups and downs during our PhD journey,

Lucie – for making the lab neat and for the happy laughter,

Sophia – for being my ENFP sister,

DJ – for the support with warm smile,

Antonius – for sharing all the good vibes with coffee, food, and surfing,

Fran – for being the king of muchachos with the calm aura,

Hwanseok – for being an amazing supporter and giver,

HaoAn – for tolerating my jokes and for the kind help,

Bilge – for being my holidays and sunshine in the lab,

Jakob – for the interesting conversation with random topics,

Ian – for inspiring me on a healthy diet,

Yann – for being Jesus in the lab,

Dustin – for being a cool Canadian rockstar,

3bla – for the orange blossoms,

Simone – for the "positiveness",

Julia Tischler – for being a kind and shiny star in the cell culture,

Maria – for being Spanish sunshine,

Si-Ying – for the language exchange and laughing at my jokes for HaoAn,

Francesca – for being Chiron.

I would also like to thank all the amazing people I met beyond the lab during my PhD for their support and the fun time:

Emma and Camilla from Advances in Stem Cell Biology Course 2017 in Paris,

All the members of BioScience Network Lausanne (BSNL),

Vytautas, Amandine, Alexandre, Robbie, Emil, Larisa, Valentine, and Enrico from Exposure Science Film Hackathon/SciFilmIt,

Peyman, Wilson, Antoine, and Jerome from Innosuisse Business Concept course,

All the members of Philophonia,

Ece from Schoonjans lab, Ece from Sakar lab, Eleonora from Ghezzi lab, Jai from D'Angelo lab, Dominique from Duboule lab, Irina from La Manno lab in EPFL, José from Martí lab in IBMB, Barcelona for being cool collaborator and awesome muchacho,

The Rezakhanis and the Vianellos,

and all my Korean friends in EPFL, especially Oh-hyeon, Joowon, Umji, Mintae, Sohyeong, Jihyun, Yeonju, Minji, Jiyeon, Sim, Mirim, and Songi, and Hae-In and Seungmin from Geneva.

I also would like to express my gratitude to my family in Switzerland and Korea:

Dear Joseph and Claudine, thank you for welcoming me warmly in the family and for all the beautiful and fun moments together. I will always remember the sunflowers you gave me that lightened up my thesis writing period.

Dear Nathalie, thank you for your unconditional love and support. The best thing happened during my PhD is you. You inspire me every day of my life. Thank you for sharing the life with me.

Dear my entire family in Korea, thank you all for always supporting me and believing in me. The most special thank goes to my parents who cherish me unconditionally with all their heart and encourage me every day. Thank you for always being there for me and being my shelter. I am very lucky and grateful to have you as my parents and the guide of my life. 감사합니다. I dedicate this thesis to you.

ABSTRACT

Given the developmental importance of the neural tube and the biological richness of its morphogenesis and patterning, it is somewhat surprising that its in-depth, real-time study is hampered by the availability of only a few models. Indeed, studies of neural tube development to date have been possible mainly through the use of animal models, which require labor-intensive, technically challenging, and low-throughput interventions. Additionally, the tracking of key cellular events in real-time, which is important for understanding various cellular processes, is complicated in animals. However, 3D organoids have emerged as faithful *in vitro* models that recapitulate key developmental processes to better study the emergence and function of organ development with greater experimental accessibility and reproducibility in real time. The development of neural tube organoids and their accessibility should help address the cellular organization and connectivity of the neural network, which previously seemed impossible.

There are many specific and tightly controlled events that must take place in a model to replicate *in vivo* neural tube development. In the developing mammalian embryo, the neural tube emerges by the formation of a tube through an invagination of the neuroectoderm, which is derived from the embryonic epiblast after gastrulation. The structure contains a single continuous lumen extending the entire length of the embryo, called the neural canal, which forms the early ventricular system that is critical for maintaining homeostasis and protecting central nervous system tissues. The neural tube develops to specify mature, region-specific cell types along both its anterior-posterior (AP) and dorsal-ventral (DV) axis in a remarkably sophisticated spatio-temporal patterning process controlled by morphogens and interactions with surrounding tissue types. Multipotent neural crest cells emerge, delaminate, and migrate out from the dorsal side of the neural tube and differentiate into a wide variety of cell types that contribute to the peripheral nervous system, the endocrine system, and the facial skeleton, amongst many others. Even though several *in vitro* neural tube models have been reported recently, to date, there is no suitable model that recapitulates the morphology, coordinated AP and DV patterning, and formation of the neural crest as *in vivo*.

Herein, I present a self-organizing neural tube organoid that is strikingly similar in morphology, cell-type composition, and patterning to the mouse embryonic neural tube. When exposed to a sequence of epiblast culture conditions and neural differentiation conditions in 3D Matrigel, single mouse embryonic stem cells develop into spontaneously elongating neuroepithelial tissues organized with key hallmarks of the neural tube. Single cell transcriptomics revealed the presence of regionalized cell types spanning the region from the midbrain to the spinal cord along the AP axis of the embryo. In long-term culture experiments for organoid maturation, I observed the emergence of neural crest cells and mature neurons. Furthermore, I developed a microfluidics-based system to promote a similar DV patterning to a neural tube. Also, maturation of neural tube organoid exhibited the emergence and migration of multipotent neural crest cells. Collectively, the accessibility and scalability of these organoids make them a unique model of the developing neural tube, allowing the study of key mechanisms involved in striking morphogenesis by self-organization, cell regionalization, neural crest development, and morphogen-triggered patterning *in vivo*.

RÉSUMÉ

Considérant l'importance du développement du tube neural ainsi que de la richesse biologique de sa morphogenèse et de sa structuration, il est quelque peu surprenant que son étude approfondie en temps réel soit entravée par le manque de disponibilité de modèles représentatifs en laboratoire. En effet, les études sur le développement du tube neural à ce jour ont été principalement possibles grâce à l'utilisation de modèles animaux, qui nécessitent un travail technique fastidieux, une expertise complexe à mettre en place et offrent une faible puissance statistique. De plus, le suivi des événements cellulaires clés du tube neural en temps réel, informations indispensables pour comprendre divers processus cellulaires, est compliqué voir impossible dans les modèles animaux. Récemment, une nouvelle technologie de culture cellulaire en trois-dimension (3D), appelée organoïdes, est apparue comme technologie clé pour la fabrication de modèles *in vitro* physiologiquement fidèles aux tissues et organes, récapitulant aussi les processus importants du développement. En utilisant ces organoïdes, il est désormais possible d'étudier le développement embryonnaire et les fonctions des organes avec une plus grande accessibilité expérimentale et reproductibilité en temps réel. Le développement d'organoïdes du tube neural offrant alors une accessibilité intrinsèque devraient aider à finalement comprendre en détail l'organisation cellulaire et la connectivité du réseau neuronal, un mécanisme auparavant difficile à élucider.

De nombreux événements spécifiques et étroitement contrôlés doivent avoir lieu dans un modèle pour mimer le développement du tube neural in-vivo. Dans l'embryon de mammifère en développement, le tube neural émerge de la formation d'un tube à travers une invagination du neuroectoderme, lui-même dérivé de l'épiblaste embryonnaire après gastrulation. Cette structure résultante contient une seule lumière continue s'étendant sur toute la longueur de l'embryon, appelée canal neural, qui forme ensuite le système ventriculaire précoce essentiel au maintien de l'homéostasie et à la protection des tissus du système nerveux central. Le tube neural finit son développement par la spécification des différents types de cellules matures propre au différentes régions le long de son axe antéro-postérieur (AP) et dorso-ventral (DV). Ce processus de structuration est remarquablement sophistiqué et contrôlé de manière spatio-temporelle par les morphogènes et les interactions avec les différents

tissus environnants. Les cellules multipotentes de la crête neurale émergent alors, se déstratifient et migrent hors de la face dorsale du tube neural pour se différencier en une grande variété de types cellulaires qui contribue au système nerveux périphérique, au système endocrinien et au squelette facial, entre autres. Même si plusieurs modèles de tube neural *in vitro* ont été décrit récemment, à ce jour, il n'existe aucun modèle approprié qui récapitule la morphologie, la structuration coordonnée AP et DV et la formation de la crête neurale du tube neural *in vivo*.

Dans ce travail, je présente un model d'organoïde du tube neural auto-organisé qui est surprenamment similaire au tube neural embryonnaire de souris en terme de morphologie, composition cellulaire et régionalisation. Une fois exposées à une séquence de conditions de culture d'épiblastes et de conditions de différenciation neurale dans du Matrigel en 3D, les cellules souches embryonnaires de souris se développent à partir de cellules unique en tissus neuroépithéliaux et s'allonge ainsi que s'organise spontanément en gardant les principales caractéristiques du tube neural. La transcriptomique unicellulaire révèle que la présence de types cellulaires régionalisés recouvrant les types de tissus allant du mésencéphale à la moelle épinière le long de l'axe AP de l'embryon. Dans des expériences de culture à long terme afin de générer des organoïdes plus matures, j'ai observé l'émergence de cellules de la crête neurale et de neurones matures. De plus, j'ai développé un système microfluidique afin de promouvoir une structuration DV similaire à un tube neural. Collectivement, le modèle d'organoïdes dévelopé dans ce travail est un modèle auto-organisé unique du tube neural en développement, permettant l'étude de mécanismes clés impliqués dans la morphogenèse, la régionalisation cellulaire, le développement de la crête neurale et la structuration déclenchée par des morphogènes externes *in vitro*.

Mots-clés : tube neural, organoïde, développement neural, transcriptomique unicellulaire, organe sur puce, microfluidique, structuration tissulaire, cellule de la crête neurale

Table of Contents

CHAPTER 1

Introduction

INTRODUCTION

Neural development

Neural development is the foundation of the entire nervous system in mammalian body and is responsible for the establishment of vital functions such as locomotion, respiration, and sensation[1,2]. Any developmental disfunction can directly lead to severe, often lethal, birth defects[3–7]. Thus, a deep understanding of how the nervous system establishes during development and how the tissue self-organizes to have proper structure with appropriate cell types in the right place and right time is key.

The major part of the neural tissues derives from epiblast, also known as primitive ectoderm, during gastrulation. The growth factors secreted from the notochord, located below the ectoderm, differentiate the ectodermal cells into neuroectodermal cells to then form the neural plate and the middle of the neural plate starts to groove downwards towards notochord and invaginate to form neural folds (**Figure 1**). The neural fold finally closes by fusion of each end of neural plate border in a tightly orchestrated process and this process is called neurulation[8–13]. The result of this process gives rise to an elongated tubular neuroepithelial tissue called the neural tube[14]. The rest of the ectoderm that lies on top of dorsal side of neural tube then becomes the surface ectoderm[15–17]. The neural tube contains a single continuous lumen, called neural canal, that extends through the entire length of the tissue[11,18,19]. This cavity further develops to be a ventricle where the cerebrospinal fluid is produced to play a critical role in maintaining homeostasis, cleaning and protecting central nervous system[20,21].
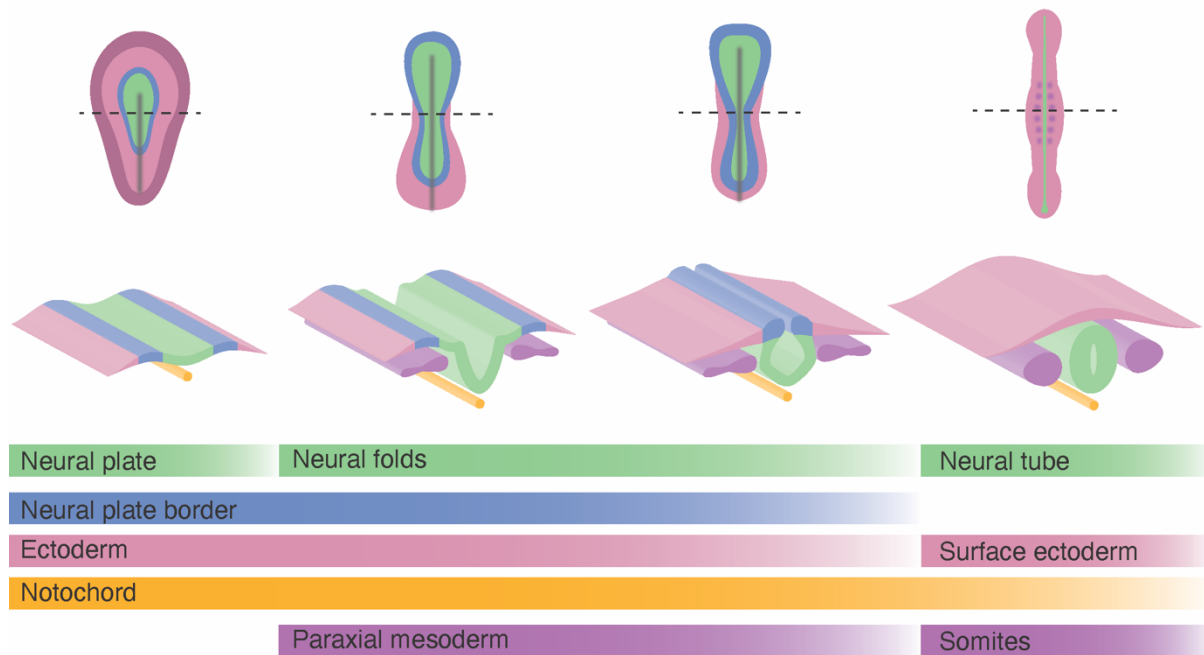
Figure 1. Scheme of the neurulation process for neural tube formation. After gastrulation, the growth factors from the notochord stimulate the ectoderm to be differentiated into neural plate. This neural plate then invaginates and forms the neural folds. Then the neural tube is constructed by the fusion of neural plate borders. After neural tube formation, the ectoderm above becomes the surface ectoderm and the paraxial mesoderm gives rise to the somites.

The neural tube develops to region-specific cell types along both its anterior-posterior (AP) and dorsal-ventral (DV) axis by a remarkably sophisticated spatio-temporal patterning process controlled by morphogens and interactions with its surrounding tissue types[22] (**Figure 2**).
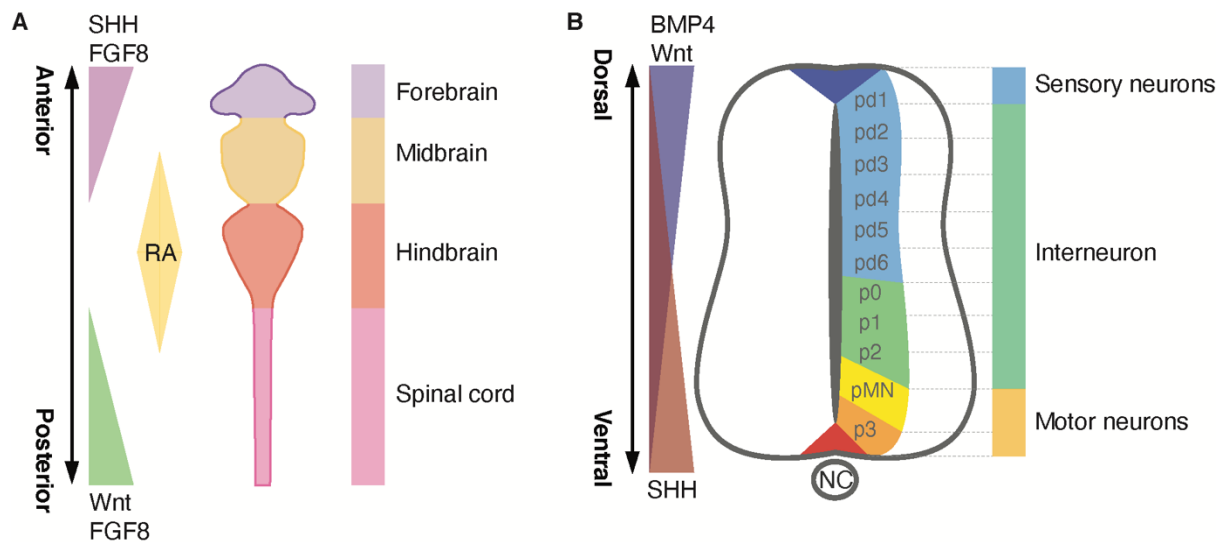
Figure 2. Spatial tissue patterning is driven by morphogen gradient in the neural tube. Morphogen gradients are an important biological event in developmental biology that provides the cells with positional information for precisely building tissue regions. The development of the neural tube is a good example of morphogen-driven tissue patterning. (A) Along AP axis, the neural tube is regionally specified into forebrain, midbrain, hindbrain, and spinal cord by the local signals: SHH and FGF8 at the anterior part, RA at hindbrain, and Wnt and FGF8 at the posterior part. (B) In DV axis, the anti-parallel morphogen gradient of BMP4 and Wnt from the roof plate at the dorsal pole and SHH from the floor plate at the ventral pole leads to the emergence of distinct precursors based on their position with different concentration combination of the morphogens from each pole. The precursors give rise to the sensory neurons (dorsal), interneurons (intermediate), or motor neurons (ventral).

Along the AP axis, the biochemical signals from the neighboring tissue pattern the neural tube. The main biochemical cues, also called morphogens, consist in a gradient of FGF8 and Wnt from the posterior to anterior direction, retinoic acid (RA) strongly expression locally form the hindbrain region, and SHH and FGF8 are strongly released at the very anterior part of the neural tube[23–25] (**Figure 2A**). These signals regionalize the neural tube; the anterior part becomes the brain and the posterior part becomes the spinal cord that forms central nervous system thus specifying the different cell types. The regionalization of central nervous system further results in region-specific specialized functions[1,2]. Forebrain, or prosencephalon, later forms the cerebrum, the thalamus, and the hypothalamus that are important for sensory processing, language, and memory. Midbrain, or mesencephalon, is involved in visual and auditory processing. Hindbrain, or rhombencephalon, forms the cerebellum, the pons, and the medulla oblongata that are critical for coordinating body movements and autonomic

functions crucial for survival. Beside the morphogens, there are also clusters of genes that regulate AP patterning, called Hox genes. Hox genes play an important role in providing positional information along AP axis for appropriate morphogenesis and local tissue patterning by diversified combinations of Hox proteins[26–30]. Especially, Hox gene expression is essential in hindbrain and spinal cord that generate the neural circuitry required for vital functions such as respiration, sensation, and locomotion. In general, Hox1-Hox5 genes are expressed in the hindbrain, while Hox4-Hox11 genes are detected in the spinal cord. Further, the spinal cord is composed of both sensory and motor nerves hence constituting the center for reflexes processing of external stimuli and locomotion control for accurate body movements. To coordinate reflexes and locomotion properly, a very sophisticated tissue organization along DV axis is required in the spinal cord.

The DV axis of the neural tube consists in a very precise spatial pattern of different cell types ruled by the morphogens released from the neighboring tissue. At the ventral side of the neural tube, the notochord releases a morphogen called sonic hedgehog (SHH) instructing the floor plate of the neural tube. Meanwhile, the surface ectoderm releases the morphogens called bone morphogenetic protein 4 (BMP4) and Wnt (**Figure 2B**) and promote roof plate formation at the dorsal end of the neural tube. These morphogens from each end of the dorsal and the ventral side of the neural tube form an opposing gradient that represses signals from each other. This cross-repressive interaction of morphogens defines the very distinct tissue specification found in the neural tube along the DV axis[31–37]. The cells at the dorsal side of the neural tube give rise to sensory neurons that convert external stimuli into action potentials and let the sensory information being transmitted to the central nervous system. At the opposite, the cells at the ventral side of the neural tube develop into motor neurons that innervate muscles for initiating movement. Lastly, the cells in the intermediate part become interneurons that connect sensory neurons and motor neurons and modulate the signals. Taken together, this morphogen-driven spatial patterning of the neural tube is essential for the fundamental function of the central nervous system.

Another key element of the neural tube development is the neural crest cells population. These cells emerge from the dorsal end of the neural tube, delaminate, and migrate to many different parts of the body and form a great variety of tissues (**Figure 3**). Neural crest cells are often called "the fourth germ layer" by virtue of their multipotency[38–41]. Although they emerge from the ectoderm, they can differentiate not only into ectodermal cells like neurons and glia, but also mesenchymal cells such as adipocyte and osteocyte, glial cells, cardiomyocytes. As much as they contribute to diverse tissues during development, its abnormal migration and differentiation can cause congenital neurocristopathies such as Treacher Collins syndrome which is a craniofacial disorder[42–44]. A deeper understanding of the plasticity, multipotency as well as migration of neural crest cells would lead to promising future treatment or prevention of neurocristopathies.
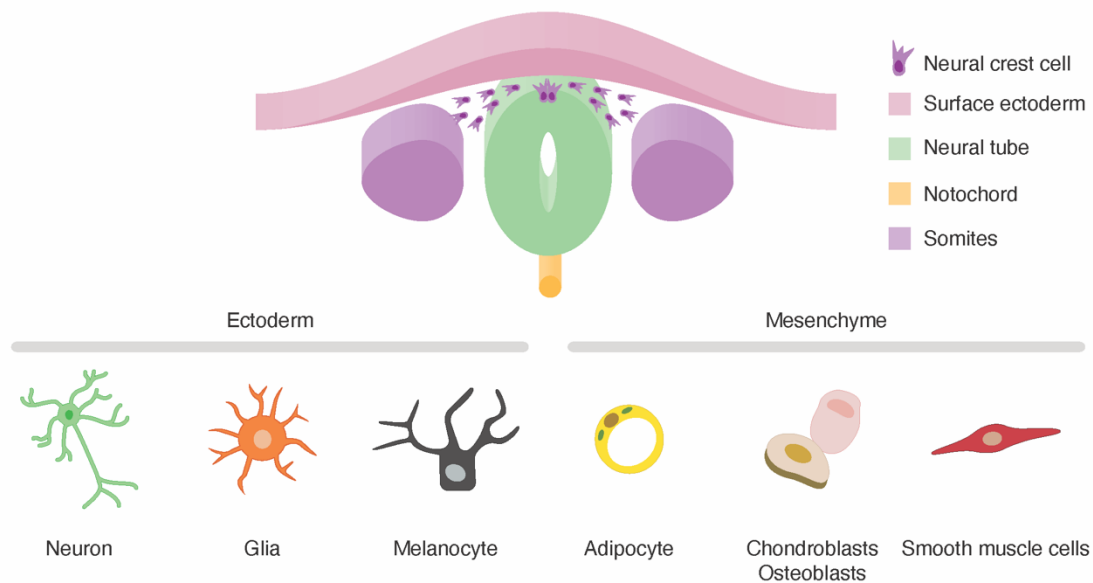

Figure 3. Neural crest cells are multipotent cells. Neural crest cells emerge from the dorsal pole of the neural tube, delaminate and migrate out between the neural tube and the surface ectoderm to many different parts of the body. They can be differentiated into a myriad of diversified cell types forming the peripheral nervous system, endocrine, and facial skeleton.

Collectively, neural development is among the most critical processes during embryogenesis directly link to fundamental functions of the body, from cognition, sensory, locomotion, to autonomic regulation and even skeletal formation through neural crest cells. Also, it is an excellent example for morphogenesis and tissue

patterning during development as abovementioned. For this reason, developing a mammalian model of developing neural tube with reliable accessibility and tractability would be a compelling tool for the field to understand neural development and to find potential treatments for related diseases.

In vitro organ model: Organ-on-a-chip and organoids

In vitro organ models refer to an in vitro tissue model that recapitulates the structure and function of the organ found *in vivo*. The goal of the *in vitro* organ model field is to develop a physiologically relevant model to understand the biology and disease in a more accessible and tractable way. To mimic the structure and function of the tissues *in vivo* closely, it is important to expose cells *in vitro* to a similar microenvironment than the one found in their native niches. To achieve this challenging endeavor, the engineers and biologists collaborated and suggested the two key interdisciplinary concepts; organ-on-a-chip and organoid. The common key hypothesis of both fields has been to transform the conventional two-dimensional *in vitro* culture systems into three-dimensional (3D) systems. This major switch already brought improvement in resembling the structure and function of organ *in vitro*.

Organ-on-a-chip

The concept behind organs-on-a-chip stemmed from the advent of BioMEMS (biomedical/biological microelectromechanical system) technology where microfabrication technologies were applied to solve yet pending biological challenges. This technology offered for the first time the possibility to create multicellular culture systems in 3D together with microfluidic perfusion systems to precisely control the presentation of biochemical cues and flow-derived stimuli. The combination of all the features found in microtechnologies enabled organ-on-a-chip system to provide cells with more relevant microenvironments thus promoting their growth into 3D tissues-like structures resembling the cytoarchitecture and their native physiological behaviors *in vivo*[45,46]. A key feature of organs-on-a-chip, is the capacity to provide biochemical cues in a graded fashion, a trait commonly found for precisely patterning and sizing tissues during embryonic development. This key aspect contributed to the generation of more complex *in vitro* model.
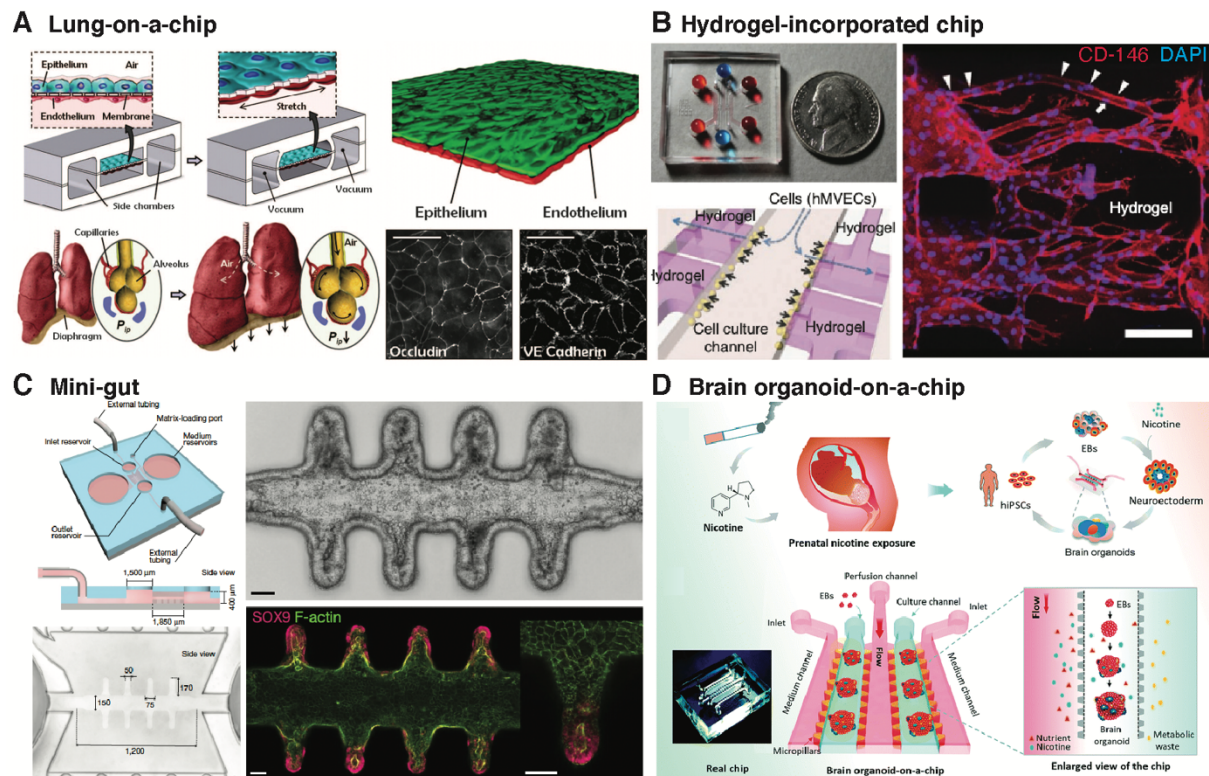
Figure 4. Organ-on-a-chip as an _in vitro_ model mimicking the key physiological features of organ _in vivo_ and its control on microenvironment. (A) The first described organ-on-a-chip, the lung-on-a-chip, mimics the alveolar-capillary interface by culturing the cells on the porous membrane and the mechanical activity of breathing lung of human by stretching the membrane with vacuum.[47] (B) Hydrogel-incorporated chips allow cell-cell or cell-matrix interactions analyses. The right-hand side figure shows the angiogenesis of human microvascular endothelial cells (CD-146+) in collagen by cell-matrix interaction.[48] (C) Mini-gut chip is also a hydrogel-incorporated chip but with microchannel generated by laser ablation. This approach allows the studies not only on cell-matrix interaction, but also effect of shape on tissue patterning. SOX9+ intestinal stem cells localised at the crypt-like structure shows that the shape affects the cell-fate patterning.[49] (D) Brain organoid-on-a-chip is an example system with the combination of hydrogel-incorporated chip and organoid, a 3D _in vitro_ organ model. This system suggests a new way to study organoid for disease studies and drug testing embracing both advantages of organ-on-a-chip and organoid.[50]

Figure 4 depicts the main classes of organ-on-a-chip. The first example ever described is the lung-on-a-chip[47] (**Figure 4A**). This model mimics the alveolar-capillary interface by culturing human alveolar epithelial cells and pulmonary microvascular endothelial cells separated with a porous membrane. In addition, by applying cyclic vacuum to the chamber, Huh et al. was able to recapitulate the breathing lung mechanical cycle. This example demonstrates that not only the biochemical environment of the organ, but also the mechanical activity of the organ can be

emulated *in vitro*. Then, hydrogel-incorporated chip was developed to add cell-cell interactions and cell-matrix interactions enabling more control and relevance to these advanced models. Typically, the hydrogel chamber acting as a barrier induces the formation of a biochemical gradient by diffusion through the matrix thus permitting the study of its effect on the cells. As an example, when human microvascular endothelial cells are cultured with collagen and VEGF gradient, a strong angiogenic response can be seen due to their reaction to the given environment[48] (**Figure 4B**). Recently, another increment of complexity was demonstrated in hydrogel-incorporated systems providing pre-shaped hydrogels, using laser ablation, in order to control stem cell localisation and their resulting morphogenesis. These, so called, mini-gut is an example where the hydrogel was laser-ablated to fabricate crypt-like microchannels to pattern the stem cell fate according to the shape of the hydrogel microchannels[49] (**Figure 4C**). SOX9^{+} intestinal stem cells localize preferentially at the crypt-like structures, suggesting that the initial shape of the matrix can affect the tissue patterning and self-organisation. The latest developments of hydrogel-incorporated chips enable the culture of organoids, a 3D *in vitro* organ model (to be discussed in this chapter), within the chips. Brain organoids were cultured in basement membrane extract (BME), e.g., Matrigel, on the chip and were treated with the nicotine to assess its effect on the tissue (**Figure 4D**). This system presents a novel way to study organoids for disease modelling and drug testing combining both the individual advantages of organ-on-a-chip and organoid. Taken together, organ-on-a-chip were developed to add various aspects of the native tissue physiology to improve *in vitro* models with the aim to understand organs and diseases *in vitro* more faithfully.

Organoid

Organoids are a miniaturized version of the native organs generated from stem cells grown in 3D and self-organizing to recapitulate the structure and function of organs *in vivo*[51,52]. They can be derived from embryonic stem cells, induced pluripotent stem cells, or adult stem cells by their capacities to self-renew and differentiate. To develop an organoid resembling a specific organ, it is essential to understand the tissue-

specific microenvironment *in vivo* such as their mechanical and biochemical cues. The standard approach is to culture the stem cells in BME resembling the complex extracellular environment of the tissue of interest with the relevant growth factors and morphogens. Here, the cellular and differentiation mechanisms knowledge that stemmed from traditional stem cell biology drove the *in vitro* modelling field to shift from two-dimension to 3D. This approach enables the stem cells to develop into tissue-specific organoids recapitulating the physiological relevant morphology and function of the organ by self-organization. This self-organization is the crucial asset retained in the stem cells even *in vitro* to catapult organoids as the best-in-class *in vitro* model for understanding the morphogenesis of the organ during development.

To date a great variety of organoids have been described[53–57] (**Figure 5**). Intestinal organoids were first described and showed the ability of single intestinal stem cells to reconstitute a 3D crypt-villus structure by self-organization in Matrigel without the mesenchymal cellular niche[55] (**Figure 5A**). This system also serves as an excellent example for symmetry-breaking morphogenesis in developing embryo. Secondly, cerebral organoid as one of the early developed organoids shows the key concept of organoid as an *in vitro* organ model facilitating the studies on complex human brain development and most importantly providing a unique accessibility to these, yet ununderstood, neuronal processes[57] (**Figure 5B**). After forming embryonic bodies and incorporating in BME with the neural induction medium, human pluripotent stem cell (hPSC) aggregates and self-organized in 3D into cortical tissue with clear epithelia consisting of cortical neurons. Specifically, the cerebral organoid-based microcephaly model suggests these as potential applications as disease models. Last, increasing studies demonstrate the capacity of pluripotent stem cells to recapitulate embryogenesis. Gastruloids resemble the gastrulation found in embryogenesis with a precise post-occipital spatial patterning in multiple axis and axial extension[56] (**Figure 5C**). Essentially, the elongation of gastruloids is resembling the axial extension of tail-bud composed of neuromesodermal progenitors (NMP) that induced by activation of Wnt signalling[29,58,59]. The level of organization found in these gastruloids highlights the stunning ability of pluripotent cells to develop by themselves when instructed by their surrounding environment.
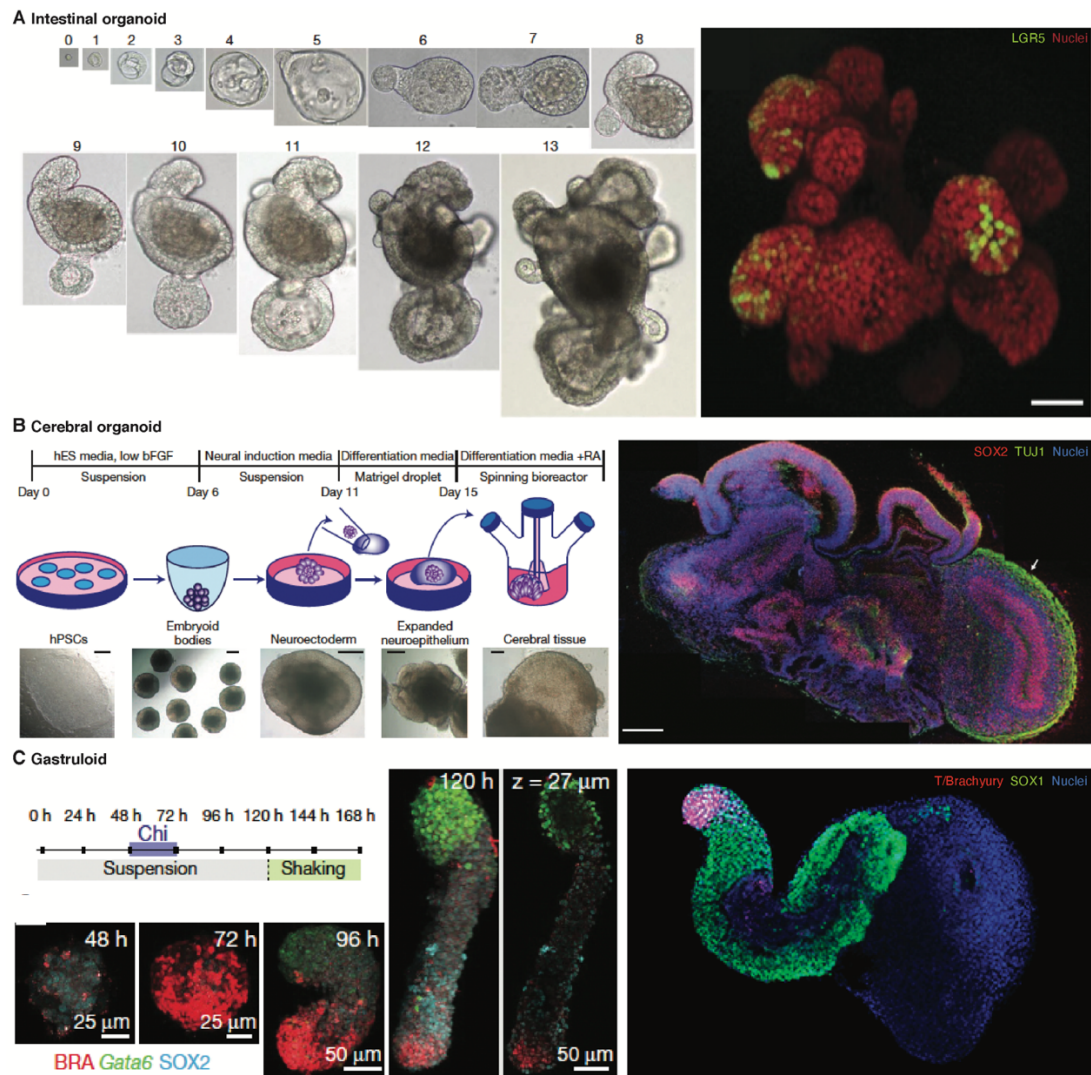
Figure 5. Organoids are 3D *in vitro* organ models harbouring the morphology and function of native organs by self-organization of the stem cells. (A) Intestinal organoid can be developed from a single LGR5+ intestinal stem cell self-organising and reconstituting the 3D structure resembling the crypt-villus of the small intestine.[55] (B) Cerebral organoid derived from human pluripotent stem cells recapitulating the cortical development.[57] (C) Gastruloid that mimics the gastrulation during embryogenesis with axial elongation and spatial patterning in multi-axis.[56]

The aforementioned *in vitro* model systems like organ-on-a-chip and organoid hold great advantages to answer yet unanswered questions in biology and medicine. More specifically, the level of accessibility to human biology of these *in vitro* models is a cornerstone for the advance of major fields such as personalized medicine, drug screening, and disease modeling (**Figure 6**). Developmental biology is equally impacted by this advance in understanding classically uncovered developmental process.
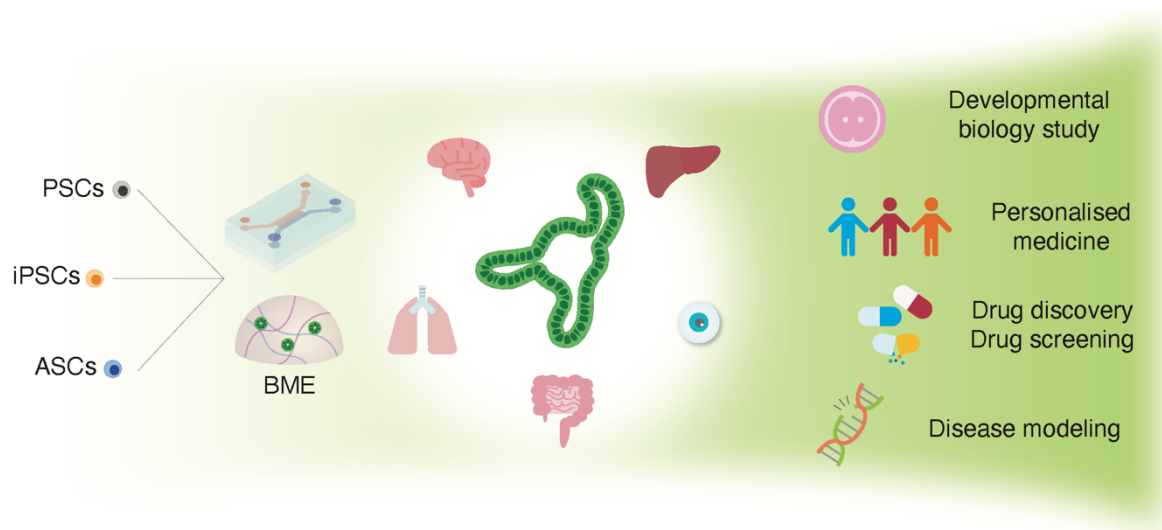
Figure 6. The overall key concept of *in vitro* organ model, organ-on-a-chip and organoid, and its potential applications. Pluripotent stem cells (PSCs), induced pluripotent stem cells (iPSCs), or adult stem cells (ASCs) can be developed into 3D organ-mimicking tissue when instructed by the adequate environment. For this reason, organs-on-a-chip and organoids are a promising approach to deliver more relevant biology *in vitro*. Many organ models have been described including brain, lung, and small intestine. These *in vivo* organ-like tissues are a useful tool for developmental biology study providing a great accessibility and tractability. Also, their physiological relevance to the organ *in vivo*, it can be used as a good platform for personalised medicine and drug screening. With the help of the advances in genetic engineering, these *in vitro* models have the capacity to reliably recapitulate diseases *in vitro* for a deeper understanding and a treatment for the disease.

In vitro neural tube model

To recapitulate the developing neural tube *in vitro*, it is crucial to understand its hallmarks beside the tissue patterning that previously described (**Figure 7**).
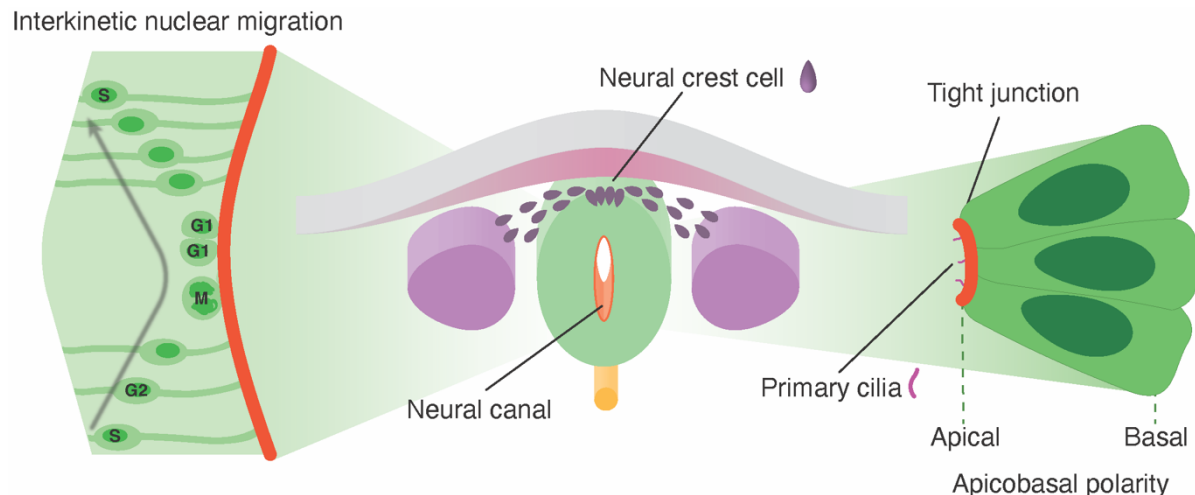

Figure 7. Hallmarks of the developing neural tube. As a result of neurulation, the neural tube adopts an elongated and apico-basally polarized tubular structure harbouring a cavity along the entire tissue length. This cavity is called the neural canal and is the earliest form of the ventricle that will later be filled with cerebrospinal, a key body fluid that maintains homeostasis and protects the neural tissues. The neural tube is composed of the neuroepithelium containing neuroprogenitors undergoing interkinetic nuclear migration during proliferation where the mitosis (M-phase) exclusively takes place at the apical surface. The neuroepithelium contains tight junction and primary cilia that are localised at the apical membrane. Also, neural crest cells originate from dorsal end of the neural tube and migrate to many different parts of body.

Upon neural tube closure, the neuroepithelial tissue organizes as a tubular structure with a single continuous lumen, called neural canal, harbouring apicobasal polarity that extends throughout the entire anterior-posterior length of the embryo[11,18–20]. This canal plays a critical role in maintaining homeostasis and protecting all tissues of the central nervous system[21]. The developing neuroepithelial cells undergo interkinetic nuclear migration to allow for an accurate polarization of the resulting tissue. Indeed, the cells migrate to the apical side of the neural tube to divide and migrate back on the basal side to build and stabilize the nascent epithelium. Interestingly, the cells in S-phase are found on the basal side of the tissue and the cells in M-phase found exclusively at the apical domain of the tissue[1]. In addition, the neuroepithelial cells

form tight junctions and primary cilia, structures that are localized at the apical membrane which is known to be essential for the tight regulation of the different following pathways; sonic hedgehog (SHH) and planar cell polarity (PCP)[3,60]. As shown with the cellular processes that composes its hallmarks, the neural tube is a fascinating tissue for its biological richness, its morphogenesis capacity and its patterning. However, it has been mainly possible through the use of animal models requiring labor-intensive, technically challenging, and low throughput interventions. Recently, to overcome these limitations, several *in vitro* neural tube models have been described each harboring a small subset of the above-described neural tube hallmarks.

The first neural tube models described aimed primarily at recapitulating the DV patterning of the neuroepithelial tissue *in vitro*. Meinhardt et al. proposed a neural cyst grown in Matrigel starting from single mouse embryonic stem cells (mESCs)[61] (**Figure 8A**). They reported that the patterned neural cyst was formed by self-organization and was able to break the symmetry *in vitro* to create a DV pattern with a roof plate (dorsal) and a floor plate (ventral) on each end of the cyst using a short RA exposition, named RA pulse, between D2 and D3. Their model is the first neural tube model demonstrating an apicobasally polarized neuroepithelial tissue including DV patterning via self-organization. Then, Ranga et al. have elucidated the key extracellular matrix (ECM) components involved in the formation of the neural cysts by using tunable fully-defined hydrogels[62] (**Figure 8B**). They demonstrated that laminin acts as the essential ECM component and that non-degradable fully-defined hydrogels with certain stiffness provide the optimal environment for the mESCs to form neural cyst with DV pattern. Zheng et al. extended this neural cyst approach with human pluripotent stem cells (hPSCs) and validated that RA pulse is the key factor inducing DV patterning by self-organization for human cells as well[63] (**Figure 8C**).
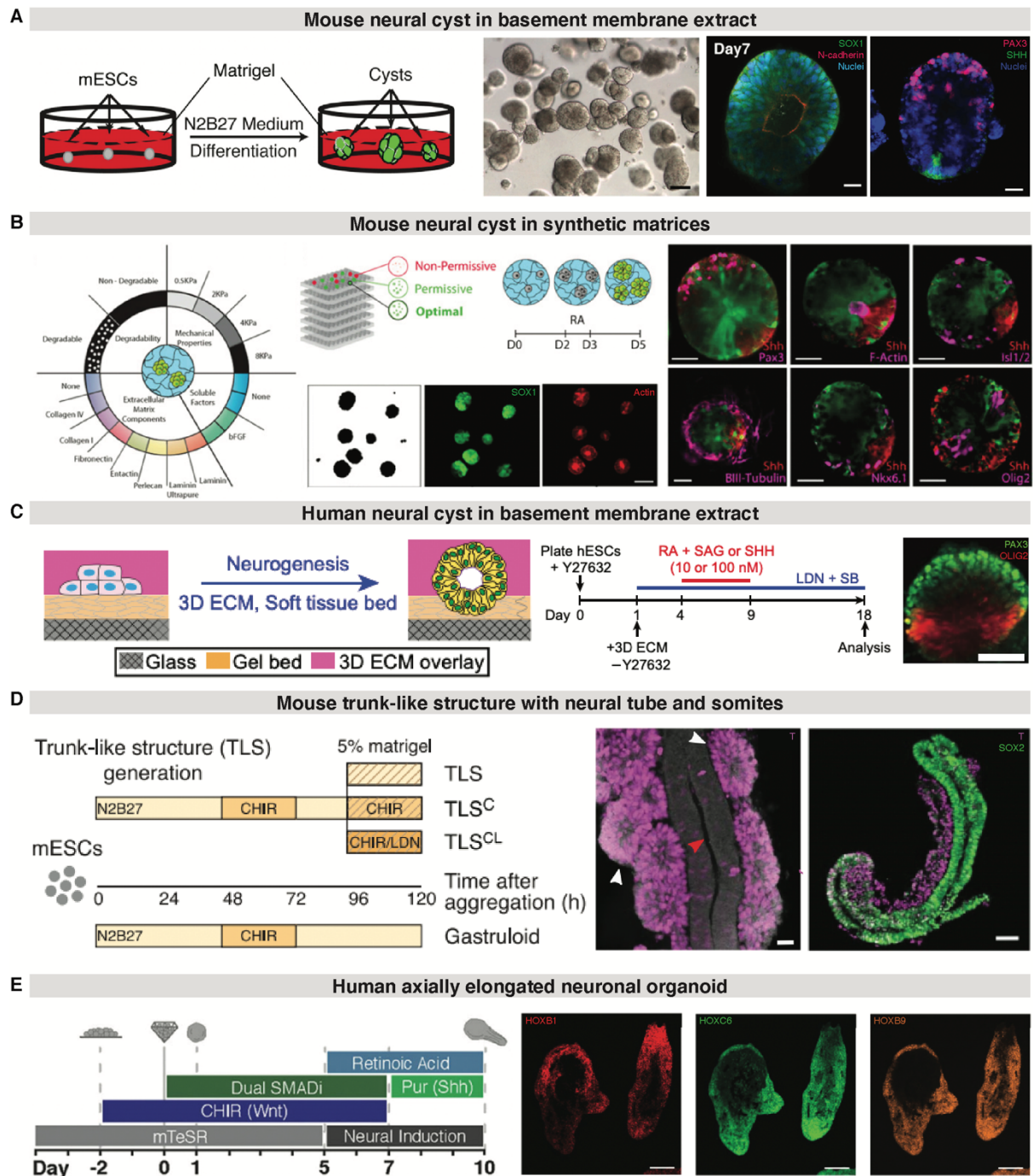
Figure 8. Organoid-based *in vitro* neural tube models mimicking the developing neural tube. (A) mESCs-based neural cyst cultured in BME showing apicobasal polarity and DV pattern upon RA pulse.[61] (B) mESCs-based neural cyst cultured with synthetic matrices with laminin and DV pattern upon RA pulse. Thanks to the tunability of synthetic matrices, biochemical and mechanical factors for neural cyst formation were screened for optimal conditions.[62] (C) hPSCs are also reported to form neural cyst with BME and neural induction media. RA induced DV patterning in human neural cyst as well.[63] (D) mESCs-based trunk-like structure harbouring neural tube and somites. The key factor of the system was to add BME to the gastruloid protocol.[64] (E) hPSCs-based neuronal organoid axially extended upon Wnt agonist. This organoid model showed AP patterning through the accurate expression of HOX genes.[65]

Following on the recent developments of gastruloid[56] (**Figure 5C**), several groups of scientists have developed axially elongated neural tube-like structure based on similar approach as the gastruloid. Veenvliet et al. developed a trunk-like structure (TLS) organoid harboring a neural tube together with somites by adding Matrgel to established gastruloid generation protocol[64] (**Figure 8D**). TLS reflects the morphogenesis of post-occipital embryos and lineage decision along development of the neural tube and the somite derived from NMP of tail-bud. Also, Libby et al. developed an axially elongated human neuroepithelial tissue by combining the classical neural induction protocol and the gastruloid protocol[65] (**Figure 8E**). This system shows AP patterning along the long axis of the organoid expressing distinct Hox gene expressing domains.

While most of the *in vitro* neural tube models are based on organoids, a few contributions focused on using organ-on-a-chip approach, to control morphogen delivery to the cells. Demers et al. developed a microfluidic device where the cells spatial patterning was directed in 2D by an orthogonal morphogen gradient of BMP4 and Purmorphamine (PM, SHH signalling pathway activator) mimicking that of the DV axis found in the native neural tube[66] (**Figure 9A**). The gradient is formed simply by the diffusion from the source to the sink. On the other hand, Rifes et al. suggested a microfluidic cell culture device where the gradient is generated by sequential diffusive mixing of two inlet fluids[67] (**Figure 9B**). Using this device, they could generate a gradient that mimics the WNT signaling gradient along the AP axis in early neural plate *in vivo* and thus could patterned the sheet of hPSCs accordingly. These studies show the potential of controlling tissue patterning by morphogen gradient *in vitro*.
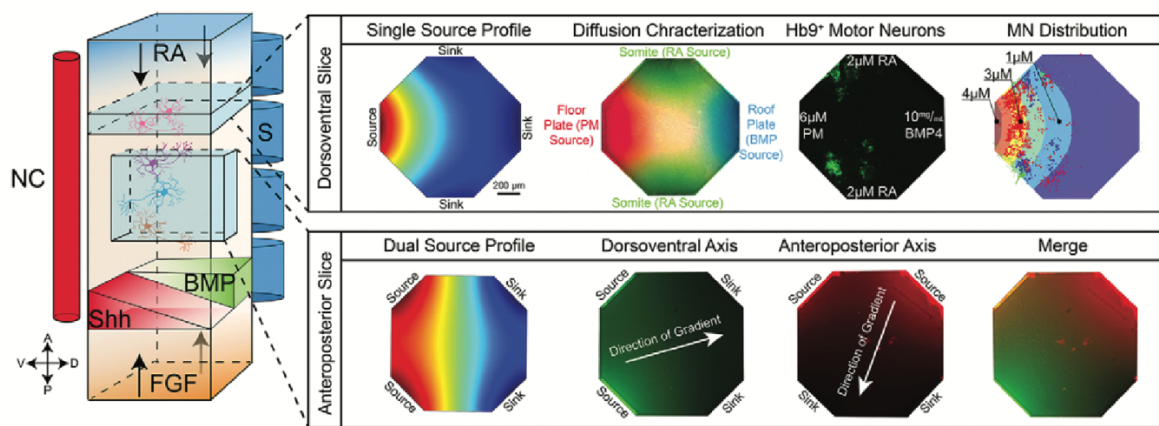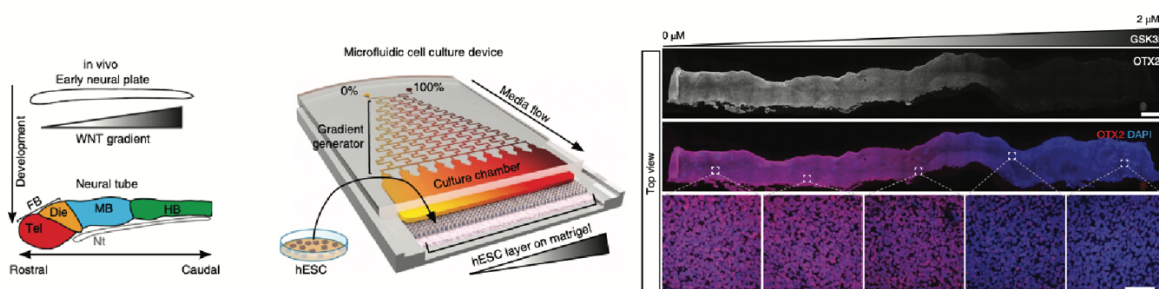
Figure 9. Organ-on-a-chip-based *in vitro* neural tube model mimicking morphogen gradient in neural tube. (A) A microfluidics-based system that resembles the gradient along DV patterning with BMP4 and purmorphamine (PM, SHH agonist). This gradient was treated to 2D cultured mESCs and the cells exposed to stronger PM differentiated into HB9+ motor neuron cells.[66] (B) A microfluidic cell culture device for Wnt gradient formation mimicking AP patterning of neural tube. hESCs were cultured on BME in 2D and the cells that were exposed to stronger Wnt differentiated into more posterior cell types.[67]

Overall, the above-described models demonstrate the capacity of stem cells in developing self-organizing according to the sets of environmental cues. This suggests that pin-pointing the appropriate mechanical and biochemical cues and providing them in a controlled spatio-temporal fashion would prove the key in developing a more accurate *in vitro* neural tube model.

Open challenges

As reviewed in this introduction, the neural development is a fascinating process not only for its impact on various prospective body functions, but also for its striking morphogenesis and tissue patterning capacity. Thanks to recent major advances in stem cell biology and bioengineering, several *in vitro* neural tube models have been described. These models could mainly recapitulate apicobasal polarity, primary cilia, tight junction, and interkinetic nuclear migration among all the hallmarks of the native neural tube *in vivo*. However, to date, there is no neural tube model with a single neural canal-like cavity surrounded by neuroepithelial cells and that are spatially regionalized in a physiological way. Also, as most of neural crest research is done with animal models that are easy to access and tractable such as chick embryo and zebrafish, but still differ significantly to human biology, there is a significant unmet need for a mammalian model to study neural crest cells biology. To date, it is almost impossible to observe real time neural crest cell delamination and migration in mammal leaving a large quantity of unknowns behind their true biology. More importantly, neural crest cells are major contributors in the development of various tissues, in consequence, many birth defects relate to abnormal neural crest cell behavior during development. Lastly, despite the current attempts of cell via morphogen gradients patterning using organ-on-a-chip technology, there is still no convincing demonstration of single organoid patterning in 3D as it requires a steep gradient at a very small scale is very challenging. Those challenges could be addressed by developing a model that more closely represents the tissue *in vivo*. Such a model of the neural tube would create a paradigm change in developmental biology and disease modeling in association with drug screening.

Motivation and objectives

Considering the previously described challenges in the current field, the general goal of this thesis is to develop a novel neural tube model recapitulating all the hallmarks of neural tube currently missing in state-of-the-art models. Especially, recapitulating the elongated tubular neuroepithelial tissue harboring a single neural canal-like cavity as future ventricle and the emergence of neural crest cells are unresolved. Moreover, the actual morphogen-driven tissue patterning in a single organoid has never been demonstrated which is the fundamental trait. Ultimately, a mammalian neural tube model demonstrating those missing key features would change the paradigm of the field to understand deeper about the neural development and find the treatments for related diseases. Thus, to overcome the current challenges in the field, the aims for this thesis have been determined as following:

Aim 1: To develop an artificial neural tube mimicking the morphology *in vivo*

: Using mouse embryonic stem cells, I will find a condition where the cells self-organize to be a neural tube organoid with an elongated tubular neuroepithelial tissue harboring a single neural canal-like cavity along the long axis of the tissue. Also, I will perform an in-depth characterization of the tissue to reveal whether it recapitulates the hallmarks of the developing neural tube *in vivo* as described previously.

Aim 2: To recapitulate neural tube patterning by spatiotemporally controlled delivery of morphogens

: By employing an organ-on-a-chip approach, I will develop a hydrogel-incorporated microfluidic device to spatially pattern the neural tube organoid developed from Aim 1 with morphogen gradients. I will demonstrate dorsal-ventral patterning of the native neural tube as an example to realize and validate the idea of morphogen gradient-driven tissue patterning *in vitro*.

Aim 3: To demonstrate the emergence, migration, and differentiation of neural crest cells.

: I will find a condition to stimulate the emergence of neural crest cells the neural tube organoids. Then, taking advantage of the good accessibility of the system, I will investigate the process of delamination as well as migration of these emerging neural crest cells. Finally, I will validate the multipotency of the resulting neural crest cells using the acknowledged marker for each cell type.

Reference

1. Dale Purves. *Neuroscience*. (Sinauer).

2. Kandel, E. *Principles of neural science*. (Appleton & Lange: McGraw Hill).

3. Valente, E. M., Rosti, R. O., Gibbs, E. & Gleeson, J. G. Primary cilia in neurodevelopmental disorders. *Nat. Rev. Neurol.* **10**, 27–36 (2014).

4. Botto, L. D., Moore, C. A., Khoury, M. J. & Erickson, J. D. Neural-Tube Defects. *N. Engl. J. Med.* 11 (1999).

5. Kaufman, B. A. Neural tube defects. *Pediatr. Clin. North Am.* **51**, 389–419 (2004).

6. Greene, N. D. E. & Copp, A. J. Neural Tube Defects. *Annu. Rev. Neurosci.* **37**, 221–242 (2014).

7. Copp, A. J. & Greene, N. D. Genetics and development of neural tube defects: Genetics and development of neural tube defects. *J. Pathol.* **220**, 217–230 (2010).

8. Colas, J.-F. & Schoenwolf, G. C. Towards a cellular and molecular understanding of neurulation. *Dev. Dyn.* **221**, 117–145 (2001).

9. Copp, A. J., Greene, N. D. E. & Murdoch, J. N. The genetic basis of mammalian neurulation. *Nat. Rev. Genet.* **4**, 784–793 (2003).

10. Schoenwolf, G. C. & Smith, J. L. Mechanisms of Neurulation. in *Developmental Biology Protocols* vol. 136 125–134 (Humana Press, 2000).

11. Shum, AlisaS. W. & Copp, AndrewJ. Regional differences in morphogenesis of the neuroepithelium suggest multiple mechanisms of spinal neurulation in the mouse. *Anat. Embryol. (Berl.)* **194**, (1996).

12. Smith, J. Neurulation: coming to closure. *Trends Neurosci.* **20**, 510–517 (1997).

13. Nikolopoulou, E., Galea, G. L., Rolo, A., Greene, N. D. E. & Copp, A. J. Neural tube closure: cellular, molecular and biomechanical mechanisms. *Development* **144**, 552–566 (2017).

14. Sadler, T. W. Embryology of neural tube development. *Am. J. Med. Genet. C Semin. Med. Genet.* **135C**, 2–8 (2005).

15. Ybot-Gonzalez, P. *et al.* Neural plate morphogenesis during mouse neurulation is regulated by antagonism of Bmp signalling. *Development* **134**, 3203–3211 (2007).

16. Nikolopoulou, E. *et al.* Spinal neural tube closure depends on regulation of surface ectoderm identity and biomechanics by Grhl2. *Nat. Commun.* **10**, 2487 (2019).

17. Ray, H. J. & Niswander, L. Mechanisms of tissue fusion during development. *Development* **139**, 1701–1711 (2012).

18. Kondrychyn, I., Teh, C., Sin, M. & Korzh, V. Stretching Morphogenesis of the Roof Plate and Formation of the Central Canal. *PLoS ONE* **8**, e56219 (2013).

19. Kaufman, M. H. Occlusion of the neural lumen in early mouse embryos analysed by light and electron microscopy. 18.

20. Tumani, H., Huss, A. & Bachhuber, F. The cerebrospinal fluid and barriers – anatomic and physiologic considerations. in *Handbook of Clinical Neurology* vol. 146 21–32 (Elsevier, 2018).

21. Xing, L., Anbarchian, T., Tsai, J. M., Plant, G. W. & Nusse, R. Wnt/β-catenin signaling regulates ependymal cell development and adult homeostasis. *Proc. Natl. Acad. Sci.* **115**, E5954–E5962 (2018).

22. Kiecker, C. & Lumsden, A. The Role of Organizers in Patterning the Nervous System. *Annu. Rev. Neurosci.* **35**, 347–367 (2012).

23. Martínez, S., Puelles, E., Puelles, L. & Echevarria, D. Molecular Regionalization of the Developing Neural Tube. in *The Mouse Nervous System* 2–18 (Elsevier, 2012). doi:10.1016/B978-0-12-369497-3.10001-9.

24. Schilling, T. F. Anterior-posterior patterning and segmentation of the vertebrate head. *Integr. Comp. Biol.* **48**, 658–667 (2008).

25. Yamaguchi, T. P. Heads or tails: Wnts and anterior–posterior patterning. *Curr. Biol.* **11**, R713–R724 (2001).

26. Philippidou, P. & Dasen, J. S. Hox Genes: Choreographers in Neural Development, Architects of Circuit Organization. *Neuron* **80**, 12–34 (2013).

27. Forlani, S., Lawson, K. A. & Deschamps, J. Acquisition of Hox codes during gastrulation and axial elongation in the mouse embryo. *Development* **130**, 3807–3819 (2003).

28. Aulehla, A. & Pourquie, O. More Than Patterning—Hox Genes and the Control of Posterior Axial Elongation. *Dev. Cell* **17**, 439–440 (2009).

29.   Deschamps, J. & van Nes, J. Developmental regulation of the Hox genes during axial morphogenesis in the mouse. *Development* **132**, 2931–2942 (2005).

30.   Deschamps, J. & Duboule, D. Embryonic timing, axial stem cells, chromatin dynamics, and the Hox clock. *Genes Dev.* **31**, 1406–1416 (2017).

31.   Wilson, L. & Maden, M. The mechanisms of dorsoventral patterning in the vertebrate neural tube. *Dev. Biol.* **282**, 1–13 (2005).

32.   Briscoe, J. & Small, S. Morphogen rules: design principles of gradient-mediated embryo patterning. *Development* **142**, 3996–4009 (2015).

33.   Jessell, T. M. Neuronal specification in the spinal cord: inductive signals and transcriptional codes. *Nat. Rev. Genet.* **1**, 20–29 (2000).

34.   Le Dréau, G. & Martí, E. Dorsal-ventral patterning of the neural tube: A tale of three signals. *Dev. Neurobiol.* **72**, 1471–1481 (2012).

35.   Dessaud, E., McMahon, A. P. & Briscoe, J. Pattern formation in the vertebrate neural tube: a sonic hedgehog morphogen-regulated transcriptional network. *Development* **135**, 2489–2503 (2008).

36.   Dessaud, E. *et al.* Interpretation of the sonic hedgehog morphogen gradient by a temporal adaptation mechanism. *Nature* **450**, 717–720 (2007).

37.   Sagner, A. & Briscoe, J. Establishing neuronal diversity in the spinal cord: a time and a place. *Development* **146**, dev182154 (2019).

38.   Simões-Costa, M. & Bronner, M. E. Establishing neural crest identity: a gene regulatory recipe. *Development* **142**, 242–257 (2015).

39.   Achilleos, A. & Trainor, P. A. Neural crest stem cells: discovery, properties and potential for therapy. *Cell Res.* **22**, 288–304 (2012).

40.   Soto, J., Ding, X., Wang, A. & Li, S. Neural crest-like stem cells for tissue regeneration. *STEM CELLS Transl. Med.* **10**, 681–693 (2021).

41.   Rekler, D. & Kalcheim, C. From Neural Crest to Definitive Roof Plate: The Dynamic Behavior of the Dorsal Neural Tube. *Int. J. Mol. Sci.* **22**, 3911 (2021).

42.   Sato, T. S. *et al.* Neurocristopathies: Enigmatic Appearances of Neural Crest Cell–derived Abnormalities. *RadioGraphics* **39**, 2085–2102 (2019).

43.   Pilon, N. Treatment and Prevention of Neurocristopathies. *Trends Mol. Med.* **27**, 451–468 (2021).

44. Vega-Lopez, G. A., Cerrizuela, S., Tribulo, C. & Aybar, M. J. Neurocristopathies: New insights 150 years after the neural crest discovery. *Dev. Biol.* **444**, S110–S143 (2018).

45. Zheng, F. *et al.* Organ-on-a-Chip Systems: Microengineering to Biomimic Living Systems. *Small* **12**, 2253–2282 (2016).

46. Azizipour, N., Avazpour, R., Rosenzweig, D. H., Sawan, M. & Ajji, A. Evolution of Biochip Technology: A Review from Lab-on-a-Chip to Organ-on-a-Chip. *Micromachines* **11**, 599 (2020).

47. Huh, D. *et al.* Reconstituting Organ-Level Lung Functions on a Chip. *Science* **328**, 1662–1668 (2010).

48. Shin, Y. *et al.* Microfluidic assay for simultaneous culture of multiple cell types on surfaces or within hydrogels. *Nat. Protoc.* **7**, 1247–1259 (2012).

49. Nikolaev, M. *et al.* Homeostatic mini-intestines through scaffold-guided organoid morphogenesis. *Nature* **585**, 574–578 (2020).

50. Wang, Y., Wang, L., Zhu, Y. & Qin, J. Human brain organoid-on-a-chip to model prenatal nicotine exposure. *Lab. Chip* **18**, 851–860 (2018).

51. Lancaster, M. A. & Knoblich, J. A. Organogenesis in a dish: Modeling development and disease using organoid technologies. *Science* **345**, 1247125–1247125 (2014).

52. Rossi, G., Manfrin, A. & Lutolf, M. P. Progress and potential in organoid research. *Nat. Rev. Genet.* **19**, 671–687 (2018).

53. Lee, J. *et al.* Hair-bearing human skin generated entirely from pluripotent stem cells. *Nature* **582**, 399–404 (2020).

54. Eiraku, M. *et al.* Self-organizing optic-cup morphogenesis in three-dimensional culture. *Nature* **472**, 51–56 (2011).

55. Sato, T. *et al.* Single Lgr5 stem cells build crypt-villus structures *in vitro* without a mesenchymal niche. *Nature* **459**, 262–265 (2009).

56. Beccari, L. *et al.* Multi-axial self-organization properties of mouse embryonic stem cells into gastruloids. *Nature* **562**, 272–276 (2018).

57. Lancaster, M. A. *et al.* Cerebral organoids model human brain development and microcephaly. *Nature* **501**, 373–379 (2013).

58.   Edri, S., Hayward, P., Baillie-Johnson, P., Steventon, B. & Arias, A. M. An Epiblast Stem Cell derived multipotent progenitor population for axial extension. *Development* dev.168187 (2019) doi:10.1242/dev.168187.

59.   Sambasivan, R. & Steventon, B. Neuromesodermal Progenitors: A Basis for Robust Axial Patterning in Development and Evolution. *Front. Cell Dev. Biol.* **8**, 607516 (2021).

60.   Bay, S. N. & Caspary, T. What are those cilia doing in the neural tube? *Cilia* **1**, 19 (2012).

61.   Meinhardt, A. *et al.* 3D Reconstitution of the Patterned Neural Tube from Embryonic Stem Cells. *Stem Cell Rep.* **3**, 987–999 (2014).

62.   Ranga, A. *et al.* Neural tube morphogenesis in synthetic 3D microenvironments. *Proc. Natl. Acad. Sci.* **113**, E6831–E6839 (2016).

63.   Zheng, Y. *et al.* Dorsal-ventral patterned neural cyst from human pluripotent stem cells in a neurogenic niche. *Sci. Adv.* **5**, eaax5933 (2019).

64.   Veenvliet, J. V. *et al.* Mouse embryonic stem cells self-organize into trunk-like structures with neural tube and somites. *Science* **370**, eaba4937 (2020).

65.   Libby, A. R. G. *et al.* Axial elongation of caudalized human organoids mimics aspects of neural tube development. *Development* **148**, dev198275 (2021).

66.   Demers, C. J. *et al.* Development-on-chip: *in vitro* neural tube patterning with a microfluidic device. *Development* **143**, 1884–1892 (2016).

67.   Rifes, P. *et al.* Modeling neural tube development by differentiation of human embryonic stem cells in a microfluidic WNT gradient. *Nat. Biotechnol.* **38**, 1265–1273 (2020).

CHAPTER 2

Self-elongating neural tube organoid

Self-elongating neural tube organoid

JiSoo Park[1], Matthias P. Lutolf[1,2,*]

[1] Laboratory of Stem Cell Bioengineering, Institute of Bioengineering, School of Life Sciences and School of Engineering, École Polytechnique Fédérale de Lausanne (EPFL), Lausanne, 1015, Vaud, Switzerland

[2] Institute of Chemical Sciences and Engineering, School of Basic Science, École Polytechnique Fédérale de Lausanne (EPFL), Lausanne, 1015, Vaud, Switzerland

[*] Correspondence: matthias.lutolf@epfl.ch

Abstract

Neural development is a fascinating process for its striking morphogenesis and tissue patterning. However, the study of mammalian neural tube development is limited by the lack of physiologically relevant *in vitro* models. Here, I demonstrate here a novel approach to generate self-elongating neural tube organoids harboring the essential hallmarks of the developing neural tube *in vivo*. This model is radically new tool to study the development of neural tube tissues. A variety of processes from cell fate decisions to whole tissue morphogenesis and its axial elongation are revealed with a great accessibility and tractability.

Introduction

In the developing mammalian embryo the neural tube emerges by invagination of the neuroectoderm derived from the epiblast after gastrulation. At the midline of the neuroectoderm, cells specified to the so-called neural plate, bend and fold into a characteristic tubular structure, the future neural tube[1,2] (**Figure 1**). This tubular structure contains a single continuous lumen that extends through the entire length of the embryo, called neural canal and it plays critical functions in maintaining homeostasis and protecting CNS tissues[3,4] (**Figure 7**). This neuroepithelial tissue establishes apicobasal polarity having the following hallmarks related to neurogenesis. First, primary cilia are localized at the apical membrane which are essential for the Sonic hedgehog (Shh) pathway and Planar cell polarity (PCP) pathway-driven neural tube specification *in vivo*[5,6]. In addition, the interkinetic nuclear migration is a characteristic feature of the developing neuroepithelium which includes the movement of the cells to the apical domain for mitosis[7–9]. Here, I present a self-organizing neural tube organoid which shows striking similarity in the morphology and cell developmental processes to the mouse embryonic neural tube. When exposed to a sequence of epiblast culture conditions and neural differentiation conditions in 3D Matrigel drop, single mESCs develop into spontaneously elongating neuroepithelial tissues harboring key hallmarks of the neural tube *in vivo*.

Results and discussion

To recapitulate neural tube development *in vivo,* I postulated that the generation of a self-organizing neural tube organoid must derive from an epiblast state. To generate such structures, I first embedded a suspension of single mESCs in Matrigel and promoted their differentiation towards epiblast fates and neural lineages, sequentially (**Figure 10**). Here, the cell density embedded in Matrigel was a critical factor in the procedure for generating self-elongating neural tube organoids. Strikingly, I could observe that the optimal cell density is different from cell line to cell line (**Table 1**). To physiologically mimic the neuroepithelium development *in vivo*, the cells were cultured for the first three days in serum-free N2B27 medium containing bFGF and Activin-A to guide them toward an epiblast state[10–12] (**Figure 10A**). The cells were then cultured in N2B27 to induce neural differentiation. I observed that mESCs form cysts and spontaneously elongate into structures harboring a continuous lumen and displaying characteristic features of the embryonic neural tube (**Figure 10B**).
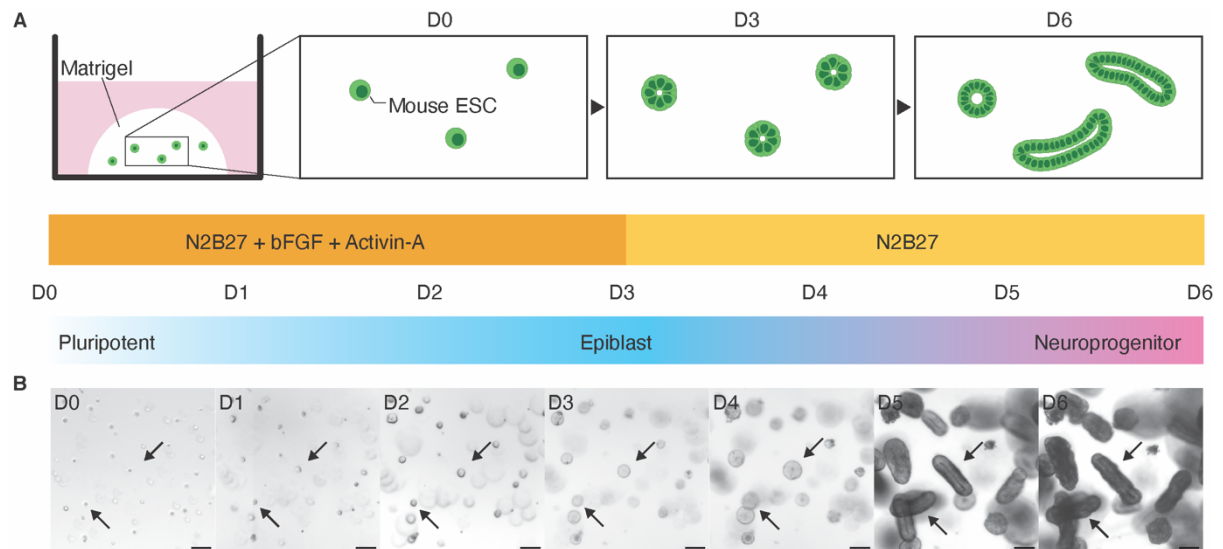
Figure 10. Schematic of self-elongating neural tube organoid culture in 3D along with the differentiation protocol. (A) Single mESCs were embedded in Matrigel and promoted to differentiate towards epiblast fates and neuroprogenitors, sequentially. On D3, the cells formed cystic structure and a significant fraction of these cysts evolved into self-elongating neural tube by D6. (B) Representative time course brightfield images of the organoids cultured from D0 to D6. The axial elongation takes place between D4 and D6. Black arrows indicate the progress of single mESCs developing into self-organizing neural tube organoids. All the scale bars are 100 μm.

Time-lapse imaging between D4 and D6 using a live cell actin probe to capture the lumen of apicobasally polarized organoids confirmed that the single neuroepithelial cysts indeed elongate and such elongation was concomitant with that of their lumen (**Figure 11A**). To understand the phenomena of elongation in a more quantitative way, I analyzed the elongation efficiency and elongation index. The efficiency of elongation was around 50% (**Figure 11B**) and the length and the elongation index increased drastically between D4 and D6 (**Figure 2C**).
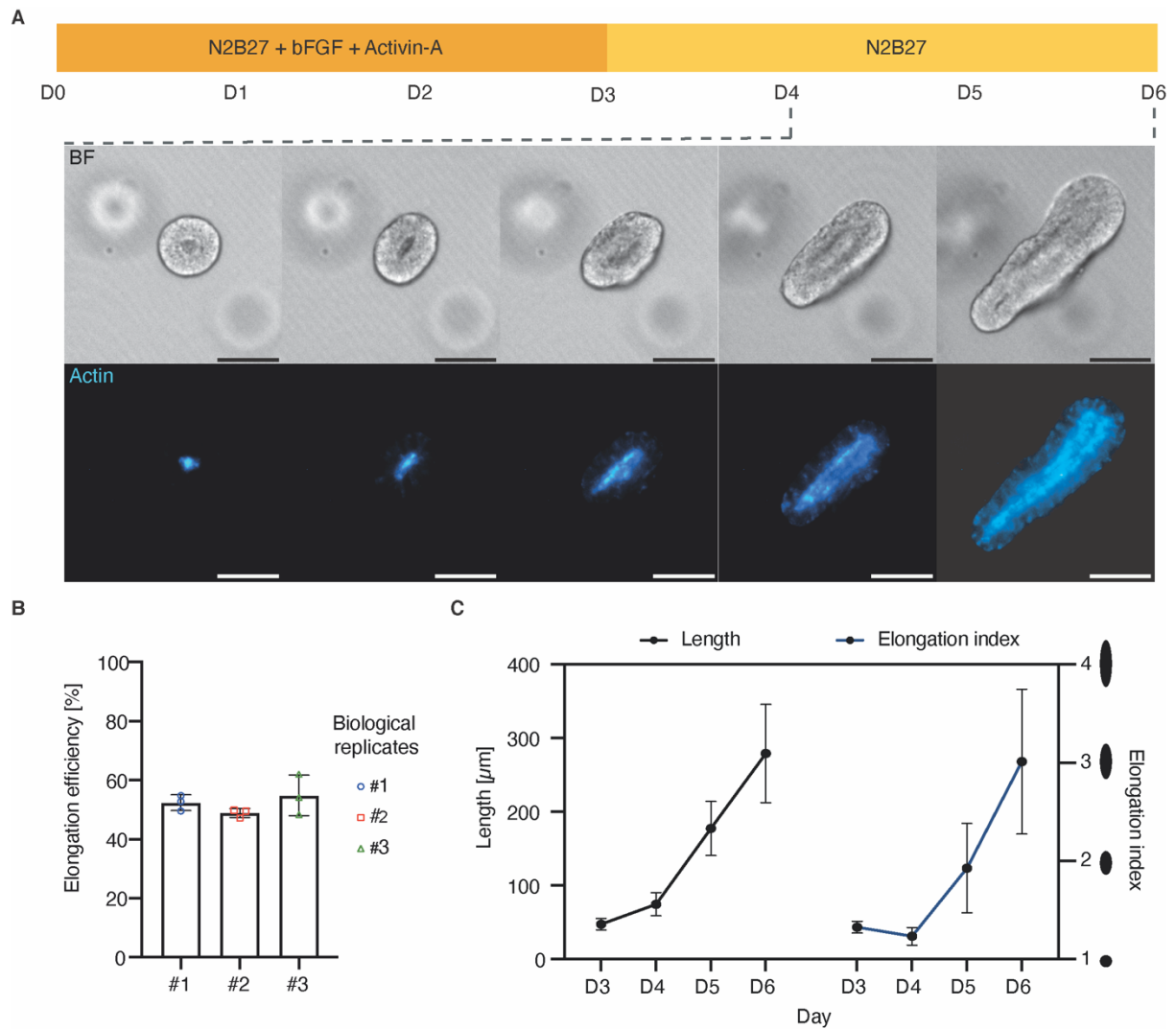
Figure 11. Axial elongation of self-elongating neural tube organoid. (A) Representative time-lapse images capturing the elongation of a neuroepithelial cysts into a tubular structure between D4 and D6. The images were obtained both in brightfield and fluorescence with a live cell actin probe to capture both the elongation of neuroepithelial cysts and their respective lumen. Surprisingly, the apicobasal polarization of the organoid was maintained during elongation. (B) Elongation efficiency of neuroepithelial cyst of three independent biological replicates. (C) Quantitative analysis of elongation in length as well as the Elongation index between D3 and D6. All the scale bars are 100 μm.

Also, with more magnified time-lapse imaging in combination with live actin probe, I could observe how the shape and size of the cells and the lumen change during the elongation process (**Figure 12**). The noticeable part is the forcefully tightened width of lumen over elongation which brought an extensive increase in aspect ratio of the

organoid. This might hint that there is a force that drives the striking morphogenesis to be further investigated.
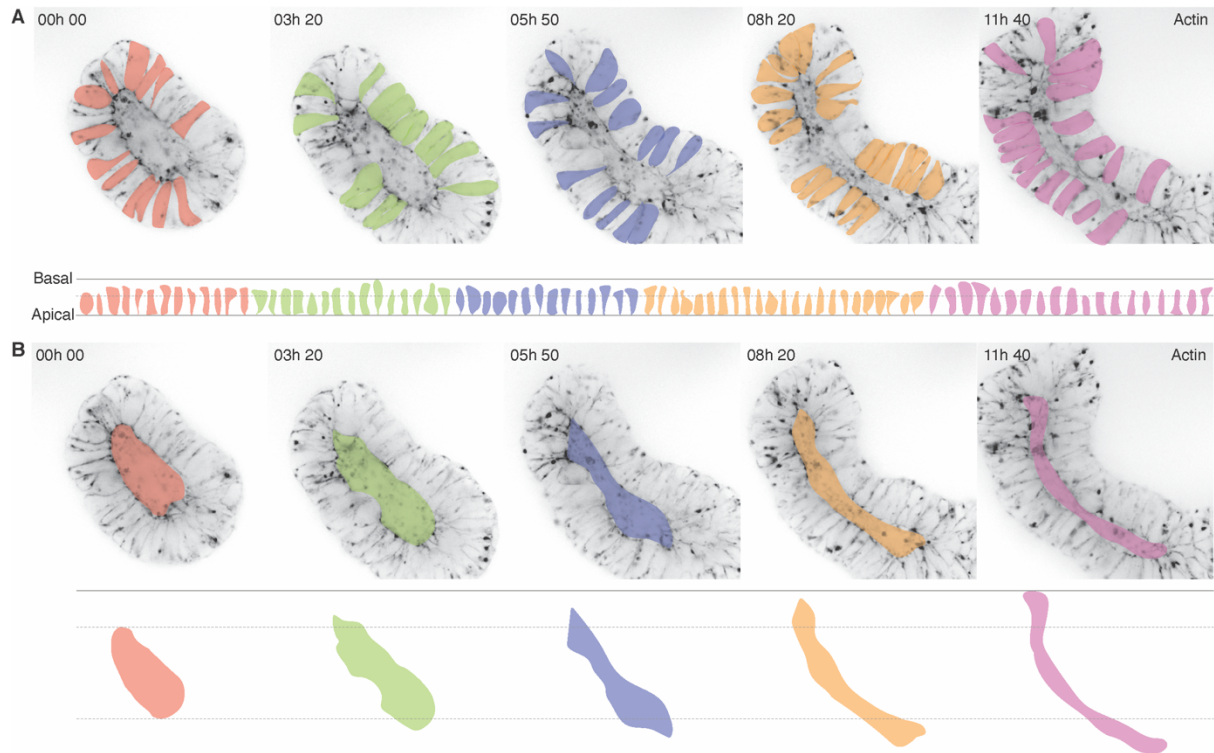

Figure 12. Time-lapse imaging between D5 and D6 reveals the progressive change of cell shape and lumen shape. (A) The overall changes in shape of each neuroepithelial cells over time can be monitored. (B) The shape and size of the lumen also can be measured in real time for further investigation to understand the mechanism of axial extension.

To characterize the similarities between organoids and the embryonic neural tube, I assessed the expression of key markers of the neural tube developing *in vivo*. This characterization revealed the progressive differentiation from a pluripotent state toward neuroprogenitor identities. Specifically, quantitative PCR (qPCR) analysis of organoids between D3 and D6 shows a gradual transition from epiblast to neuroprogenitor fate, with epiblast markers *Pou5f1* (also known as *Oct4*), *Otx2,* and *Fgf5* gradually decreasing over time, and neuroprogenitor markers *Sox1, Sox2,* and *Pax6* gradually increasing as the organoids develop (**Figure 13A**). Confocal

microscopy confirmed the transition in gene expression profiles at the protein level. The classic epiblast marker OCT4 is expressed at D3 but subsequentially lost at D6, while the neuroprogenitor markers SOX1 and PAX6 were absent at D3 but expressed later, notably at D6 (**Figure 13B**). I could also detect the presence of other key neuroprogenitor markers SOX2 and NESTIN in these D6 old organoids. (**Figure 14A**)
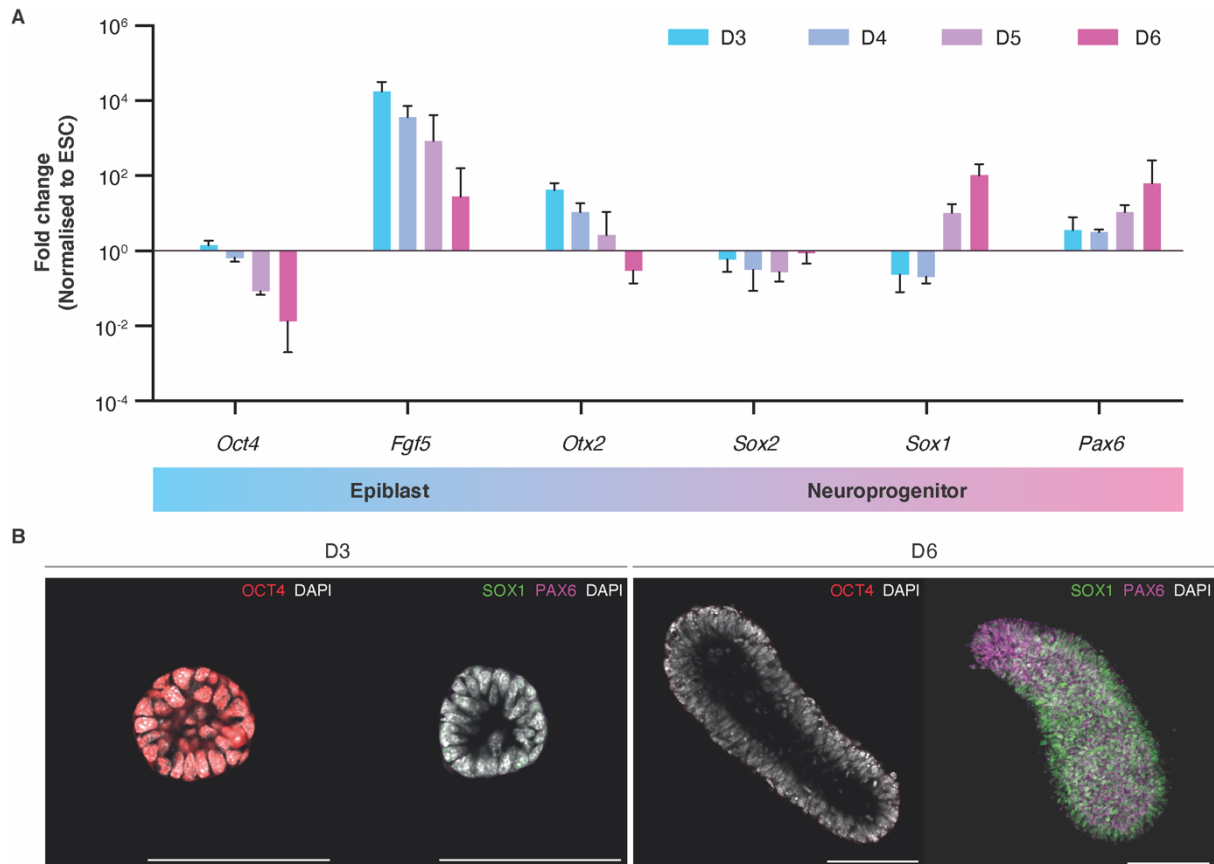

Figure 13. Time course of early developmental markers between D3 and D6. (A) Time course of early developmental marker expression as analyzed by qPCR between D3 and D6. The measured epiblast markers were *Oct4*, *Fgf5*, and *Otx2*, and the neuroprogenitor markers were *Sox2*, *Sox1*, and *Pax6*. (B) Immunofluorescent images showing the differentiation from epiblast (OCT4^{+}) to neuroprogenitors (SOX1^{+}, PAX6^{+}) in protein level.

In addition to neuroprogenitor markers, the organoids also exhibit key hallmarks of the tissue architecture of the embryonic neural tube. For instance, they also possess apicobasal polarity, as demonstrated by the apical localization of the tight junction

marker ZO-1 and the presence of apical domain markers Prominin-1 and PKCζ (**Figure 14B**). Lightsheet microscopy revealed a highly organized 3D structure of the neuroepithelium bounding the elongated lumen, which confirms that the lumen is indeed continuous throughout the organoid. This elongated tubular lumen resembles the neural canal of a developing neural tube, responsible in the formation of the early ventricular system that is essential for tissue homeostasis of the nervous system (**Figure 14C**). Also, confocal imaging confirmed the presence of primary cilia, marked by ARL13B, localized at the apical membrane of the organoids, which are essential for neural tube development *in vivo* (**Figure 14D**).
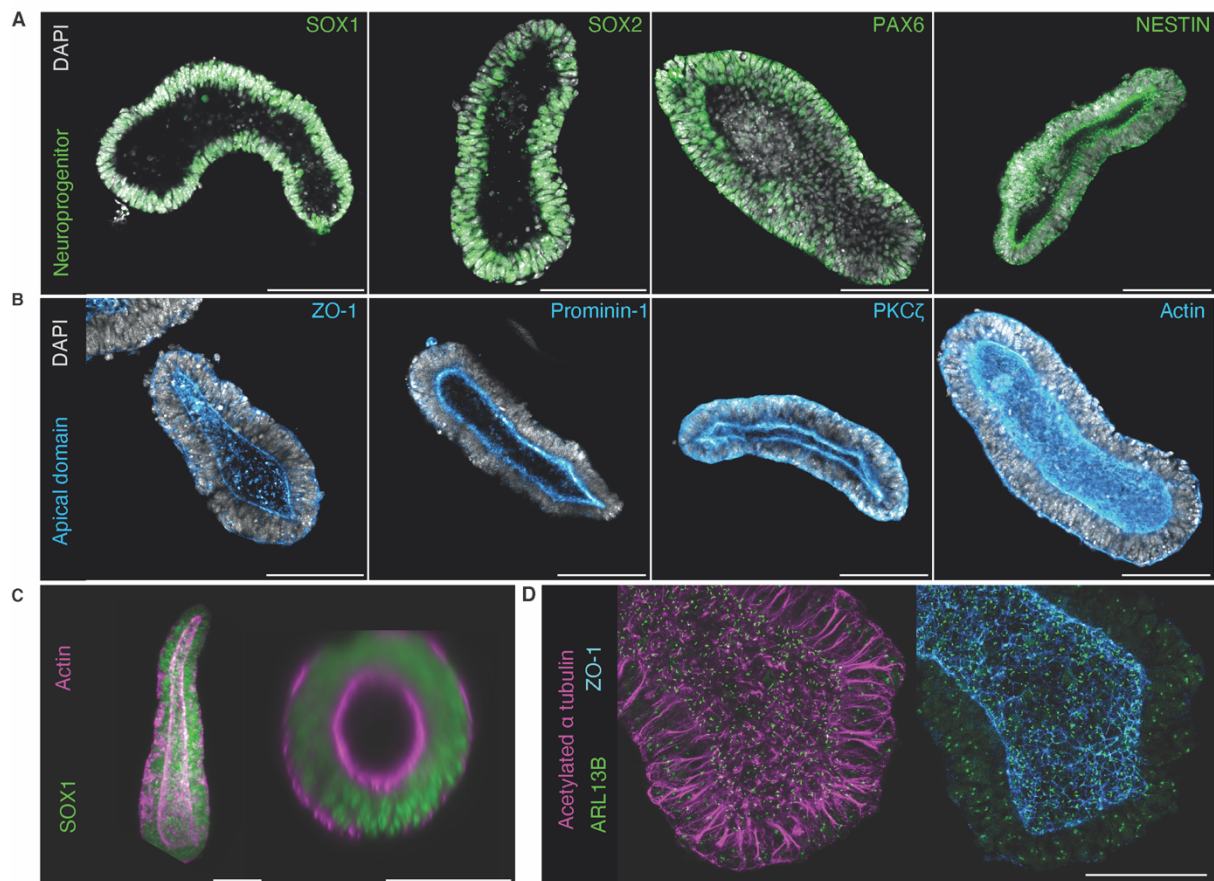
Figure 14. Characterization of hallmarks of the native neural tube in neural tube organoids. (A) Our elongated neural tube organoids are apicobasally polarized with a single elongated lumen, shown by the tight junction marker ZO-1, have an apical domain, shown by the restricted presence of Prominin-1 and PKCζ at the apical domain. (B) The neural tube organoids express neuroprogenitor markers such as SOX1, SOX2, PAX6, and NESTIN. (C) Light-sheet imaging confirms the presence of a single continuous cavity along the elongated axis. (D) Confocal microscopy revealed the presence of tight junctions (ZO-1) and primary cilia (ARL13B) in the apical membrane surface of the neural tubes similarly to *in vivo*.

Furthermore, the neural tube organoid demonstrates the characteristic interkinetic nuclear migration of neuroepithelial tissue in developing embryo. As the cells move to apical membrane for mitosis, the mitotic (M-phase) cells are exclusively found at the apical domain and the cells at other cell cycle phases are found more at the basal domain (**Figure 15A**). I performed time-lapse imaging using live actin probes and I could capture and thus confirmed the interkinetic nuclear migration movement of the cells in the neural tube organoids. For the mitosis, the cell moved to apical domain

and divided and its progeny cells went back to reconstitute the neuroepithelium (**Figure 15B**). This result shows that this model has a potential as a useful tool for studying and understanding the neurodevelopmental pathologies related to cell division of neuroprogenitors such as primary microcephaly. Primary microcephaly is caused by the failure in CNS growth by abnormal proliferative to neurogenic divisions of the neuroprogenitors. An accessible model like the presented neural tube organoid would facilitate elucidating the mechanism of the pathology in a tractable manner. To detect the proliferating cells in the organoid, a modified thymidine analogue 5-ethynyl-2'-deoxyuridine (EdU) labeling and an immunostaining against the proliferation markers, KI67 and Phospho-Histone H3 (pH3), were performed. The basal localization of EdU-labeled DNA synthesis phase (S-phase) cells and the apical localization of KI67+ or pH3+ mitotic cells (M-phase) are indicative of characteristic division patterns of interkinetic nuclear migration, a defining feature of cell behavior in the embryonic pseudostratified neuroepithelium (**Figure 15C**). Altogether, these results suggest that our neural tube organoids both physiologically and morphologically recapitulate key features of developing neural tube *in vivo*.
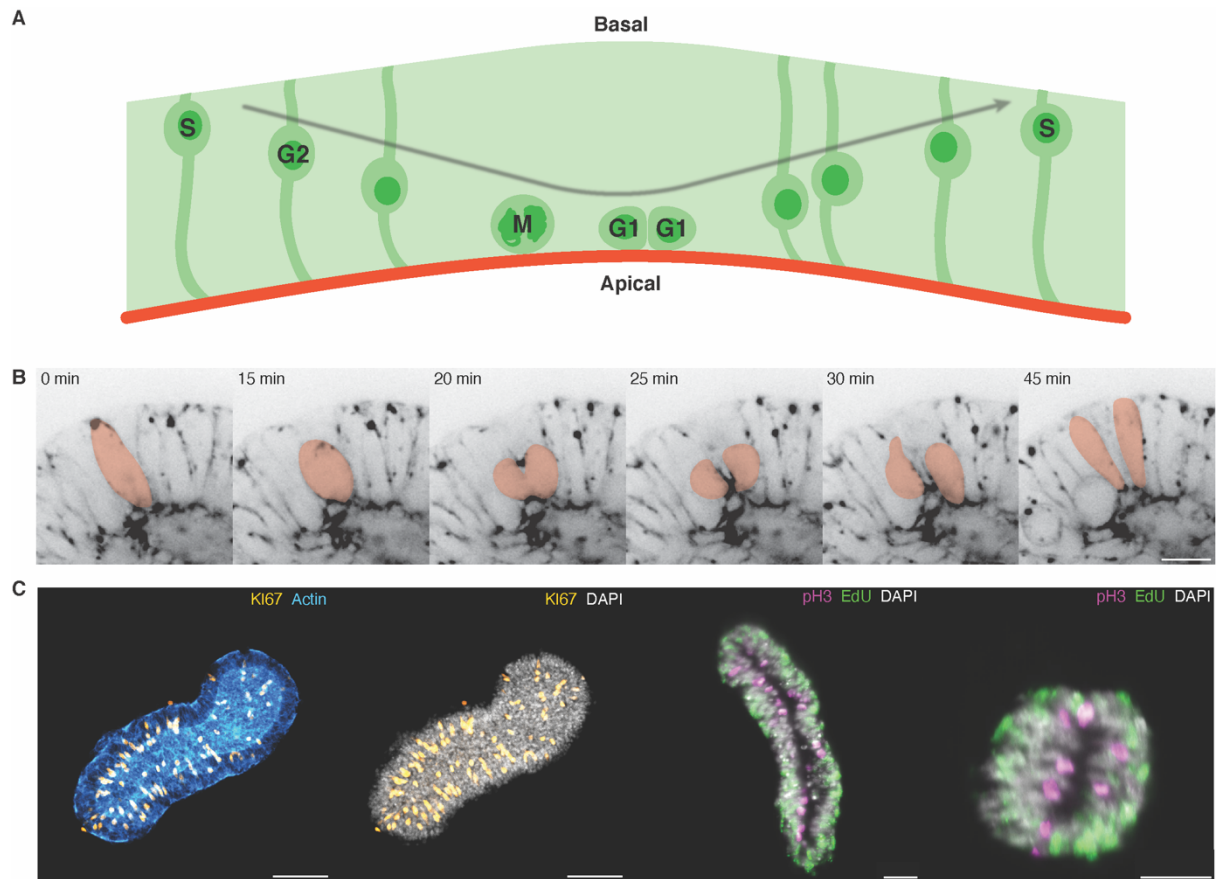
Figure 15. Neuroepithelial interkinetic nuclear migration was identified in neural tube organoid. (A) Illustration of interkinetic nuclear migration of the developing neuroepithelium in the embryo. (B) Time-lapse images revealed the cellular interkinetic nuclear migration in the neural tube organoids. The cells in the neural tube organoid moved to the apical membrane, divide, and go back to reconstitute the neuroepithelium. This cellular behavior is extremely close to the interkinetic nuclear migration of neuroepithelium found *in vivo*. Scale bar is 20 μm (C) Confocal and light-sheet imaging confirmed the presence of a single elongated lumen in the organoids with apically localised mitotic cells (KI67+ cells and pH3+ cells) and basally localised S-phase cells (EdU+ cells) indicating interkinetic nuclear migration. Scale bars are 100 μm.

Conclusion

I herein developed a novel *in vitro* organoid model that faithfully recapitulates the hallmarks of the developing embryonic neural tube, from its anatomy; with a neural canal, apicobasal polarity, primary cilia, interkinetic nuclear migration, to the cell composition. The key of this approach was to provide the mESCs the condition to differentiate from the pluripotent state to the appropriate neuroprogenitors population through an epiblast state. In addition, the cell density was a crucial element to be controlled when embedding the cells in Matrigel. I hypothesized that there is a strong contribution of paracrine signals for promoting the self-elongating phenomena of the organoid. This would need further mechanistic studies to be elucidated. This axial extension with a simultaneously elongating cavity of neuroepithelial tissue has never been reported to date, I thus show here a very unique model to understand the analogous morphogenesis during neural development. Also, thanks to its accessibility at the single cell level and in real time, this system is an inevitable tool to observe yet never observed phenomena and answer the questions unanswered mysteries of the neural tube establishment.

Materials and methods

Culture of mouse embryonic stem cells

Sox1eGFP;*BramCherry* double reporter[13] (SBr) and *Sox1eGFP* reporter[14] (SG) mouse embryonic stem cells (mESCs) were cultured in DMEM supplemented with 10% serum medium (10% ES-grade fetal bovine serum (FBS), 0.1 mM non-essential amino acids (NEAA), 1 mM sodium pyruvate, 3.44 mM GlutaMax, 0.1 mM beta-mercaptoethanol (β-ME), 100 U/mL Penicillin, 100 μg/mL Streptomycin) with 2i (3 μM CHIR99021, 1 μM PD025901) and 100 μg/mL LIF in a humidified incubator (5% CO_2, 37 °C). The cells were split every other day, by washing with PBS-/- and dissociating with Accutase for 2 min in room temperature. The cell suspension was collected in a tube and was centrifuged at 200 x g for 5 min. After centrifugation, the cell pellet was resuspended in 1 mL of 10% serum medium and the cells were counted with a haemocytometer. 85,000 cells were plated in 2 mL of 10% serum medium with 2i and LIF per each well of 6 well plate (Corning) and cultured in the humidified incubator. The cells were passaged every 2 days.

Neural tube organoid culture

mESCs were collected by washing with PBS-/- and dissociating with Accutase for 2 min at room temperature. The cell suspension was collected in a centrifuge tube and was centrifuged at 200 x g for 5 min. After centrifugation, the cell pellet was resuspended in 1 mL of 10% serum medium and the cells were counted with a haemocytometer. After cell counting, the cells were washed twice with PBS-/- and were resuspended in N2B27 (47.4% Neurobasal™ Medium, 47.4% DMEM/F-12 with 2.50mM GlutaMAX™, 1 mM GlutaMAX™ Supplement, 100 U/mL Penicillin, 100

µg/mL Streptomycin, 0.1 mM NEAA, 1 mM Sodium Pyruvate, 0.1 mM β-ME, 1% B27

Supplement, 0.5% N-2 Supplement) and embedded in Matrigel to a final concentration

of 1125 cells/10µL of Matrigel drop for SBr and 1000 cells/10µL of Matrigel drop for

SG (**Table 1**). 10 µL of the resulting Matrigel-embedded cell suspension were

deposited in each well of a 24 well plate (Corning). The cells in each well were cultured

in 500 µL of Epi medium (N2B27 supplemented with 12 ng/mL basic Fibroblast Growth

Factor (bFGF, Thermofisher, Cat#PMG0031) and 20 ng/mL activin-A (R&D Systems,

Cat#338-AC-010) for the first three days[10–12]. On D3, the Epi medium of each well was

substituted with 1 mL of N2B27. The medium of each well was substituted with 1 mL

of N2B27 on D5 and the cells were cultured until D6.

Cell Line	Cells/10µL Matrigel drop
Sox1eGFP;BramCherry double reporter (SBr)[13]	1,125
Sox1eGFP reporter (SG)[14]	1,000

Table 1. Embedding cell densities: self-elongating neural tube organoids require the optimal embedding cell numbers of each cell line.

Immunostaining

The organoids were collected from Matrigel drop by washing with PBS-/- and

dissolving the Matrigel using 4 mg/mL Collagenase-IV and 100 µg/mL Dispase I in

HBSS+/+ on a shaker in the incubator for 35 minutes. The organoids were fixed in 4%

paraformaldehyde (PFA) in PBS-/- for 30 min in room temperature. The organoids

were washed with PBS-/- for three times of 20 min, permeabilized in 0.2% Triton-X

100 in PBS-/- for 1 h and blocked in Blocking solution (3% Bovine serum albumin

(BSA) and 0.01% Triton-X 100 in PBS-/-) for 3 h to overnight. Primary antibody (**Table

2**) solution was prepared in Blocking solution, with 2 µg/mL of DAPI (**Table 3**). The

organoids were stained overnight on a low-speed orbital shaker in 4 °C. The organoids were thoroughly washed with PBS-/- every 30 min for 4 hours. Secondary antibody (**Table 4**) solution was prepared, treated, and washed the same way as primary antibody solution. For 5-ethynyl-20-deoxyuridine (EdU) incorporation to detect S-phase cells, the organoids from D6 were incubated with EdU for 1 hr and fixed with 4% PFA. Then, the EdU was detected using the Click-iT™ EdU Cell Proliferation Kit for Imaging with Alexa Fluor™ 647 dye (Invitrogen, Cat#C10340, **Table 3**) following the manual suggested by the manufacturer.

Target	Species	Dilution	Cat. No.	Supplier
OCT3/4	mouse	1:200	SC-5279	Santa Cruz Biotechnology
SOX1	goat	1:20	AF3369	R&D Systems
PAX6	rabbit	1:200	901301	BioLegend
CD133/Prominin-1	rat	1:200	14-1331-82	Invitrogen
SOX2	rabbit	1:1000	ab97959	abcam
Phospho-Histone H3 (Ser10)	rabbit	1:500	06-570	Merck
ARL13B	rabbit	1:200	17711-1-AP	Proteintech
Acetylated alpha tubulin (Lys40)	mouse	1:200	6-11B-1	Thermo Fischer
Nestin	mouse	1:100	ab11306	abcam
ZO-1	rat	1:8	R26.4C	DSHB
PKCζ	mouse	1:200	sc-17781	Santa Cruz Biotechnology
Ki67 (Sp6)	rabbit	1:200	MA5-14520	Invitrogen

Table 2. Primary antibodies used in immunostaining

	Dilution	Cat. No	Supplier	Purpose
Click-iT™ EdU Cell Proliferation Kit for Imaging, Alexa Fluor™ 647 dye	N/A	C10340	Invitrogen	S-phase cell detection
DAPI	1:500	D1306	Invitrogen	Nuclear dye
Alexa Fluor™ 647 Phalloidin	1:500	A22287	Invitrogen	Actin dye
sir-actin	1:1000	SC001	Spirochrome	Live cell actin dye

Table 3. Dyes used in staining: S-phase cell detection, nuclear staining, actin staining, and live cell actin imaging.

	Dilution	Cat. No	Supplier
Donkey anti-goat Alexa Fluor 647		705-606-147	Jackson ImmunoResearch
Donkey anti-goat Alexa Fluor 488		A-11055	
Donkey anti-mouse Alexa Fluor 568		A-10037	
Donkey anti-rabbit Alexa Fluor 647	1:500	A-31573	ThermoFisher Scientific
Goat anti-rat Alexa Fluor 647		A-21247	
Donkey anti-rabbit Alexa Fluor 568		A-10042	
Donkey anti-mouse Alexa Fluor 647		A-31571	

Table 4. Secondary antibody used in immunostaining

Confocal microscopy

Confocal images of organoids were obtained using LSM700 (Zeiss) on Inverted Zeiss AxioObserver Z1 (Bioimaging and Optics Core Facility, EPFL), equipped with 10×/0.30 air, 20×/0.80 air, and 63×/1.40 oil objectives, 405-nm, 488-nm, 555-nm and 639-nm lasers and controlled by ZEN 2010 imaging software (Zeiss). Images were analyzed using FIJI (NIH).

Light-sheet microscopy

The organoids were collected, fixed, and immunostained following the immunostaining method described above. *CUBIC-mount* (Sucrose (250 g of 50%, w/v), 125 g urea (25%, w/v), and 125 g N,N,N′,N′-tetrakis (2-hydroxypropyl)ethylenediamine (25%, w/v) dissolved in 150 ml of dH2O and brought up to 500 ml) was diluted with water to reach a refractive index of 1.453[15]. The organoids were embedded in 1% Agarose solution in a 1.5 mm diameter capillary (Cat# 701908) using a plunger and were cooled in 4 °C to allow for agarose gelation. The glass capillaries with agarose-embedded organoids were dipped in *CUBIC-mount* overnight in dark room at room temperature for tissue clearing. For imaging, the glass capillary with sample was mounted with sample holder and inserted into Top-fed Zeiss Lightsheet Z1. The Cell Chamber was filled with CUBIC-mount solution and the organoids in the capillary were located in the field of view using the plunger. Images were acquired with 20×/1.0 corr water W Plan Apochromat objective (for non-cleared samples) or 20×/1.45 corr clearing EC Plan Neofluar objective (for cleared samples). DAPI, Alexa Fluor 488, Alexa Fluor 568, and Alexa Fluor 633 were excited with 405, 488, 555, and 639-nm lasers, respectively. Images were analyzed using IMARIS (Oxford Instruments) and FIJI (NIH).

Time-lapse imaging

To observe how the organoid and its lumen elongate between D4 and D6, the organoids of each well were treated with 1 mL of N2B27 with Sir-actin (**Table 3**) and stabilized in the incubation chamber of the microscope at 37 °C with 5% CO_2 for 4 hours before imaging. Time-lapse imaging was acquired by either Nikon Eclipse Ti inverted microscope system (equipped with a 10×/0.30 air objective, 632-nm filters, DS-Qi2 and Andor iXon Ultra DU888U (Oxford Instruments) cameras and controlled

by NIS-Elements AR 5.11.02 (Nikon Corporation) software) or Visitron CSU-W1 (equipped with U PLAN S APO 60×/1.42 oil objective, sdc Cy5 filter, 50 µm Spinning Disk, ImagEMX2 camera, and controlled by VisiView software) and 647 nm laser for Sir-actin signal, and bright-field. The image was captured every hour between D4 and D6 (Nikon Eclipse Ti) or every 5 min between D5 and D6 (Visitron). Temperature was maintained at 37 °C with 5% CO_2.

Quantitative analysis of axial elongation of the neural tube organoids

Time-lapse images were analyzed using FIJI. Brightfield images of organoids were segmented by thresholding and Max Inscribed Circles function (FIJI function developed by O. Burri and R. Guiet, BIOP, EPFL) was used to fit circles in the segmented object. Axial length was determined by connecting the centers of the fit circles. Elongation index (10.5281/zenodo.4544370) was calculated by dividing Axial length by the diameter of the largest inscribed circle determined by Max Inscribed Circles function.

Gene expression analysis by quantitative PCR

The collected organoids were washed with PBS-/- and resuspended in lysis buffer. RNA was extracted immediately using the RNAeasy micro kit (Qiagen, Cat#74004) according to the manufacturer instructions with on-column DNase I (Qiagen) digestion. The extracted RNA concentration was measured using NanoDrop. cDNA was synthesised using iScript™ cDNA Synthesis Kit (BIORAD, Cat# 170-8891) according to the manufacturer's instructions using 1 µg of RNA of each sample replicate in Biorad thermocycler. Quantitative PCR analysis of mRNA levels for the genes on Primer list

was performed using *Power* SYBR™ Green PCR Master Mix (ThermoFisher Scientific, Cat# 4367659) on Applied Biosystems Quantstudio 6 Flex Real-Time PCR system. PCR primers were designed using NCBI Primer-Blast software (**Table 5**). Expression values of each gene were normalized to *Gapdh* expression value of each sample replicate using delta-delta CT method. The graph was plotted using Prism 8 (GraphPad) and error bars represent the standard deviation across three biological replicate samples.

Probe	Primer Forward	Primer Reverse
Oct4	TGG AGG AAG CCG ACA ACA ATG AGA	TGG TGC CTC AGT TTG AAT GCA TGG
Fgf5	TCT CCT TTT ATC TGC CCC CT	GAG CAG ATG CAC TCA TTC CA
Otx2	GCA GAG GTC CTA TCC CAT GA	CTG GGT GGA AAG AGA AGC TG
Sox2	CAT GAG AGC AAG TAC TGG CAA G	CCA ACG ATA TCA ACC TGC ATG G
Sox1	AGA CAG CGT GCC TTT GAT TT	TGG GAT AAG ACC TGG GTG AG
Pax6	CTA CCA GCC AAT CCC ACA GC	TTC GGC CCA ACA TGG AAC
Gapdh	GCA CAG TCA AGG CCG AGA AT	GTG GTT CAC ACC CAT CAC AA

Table 5. Primer sequences used for quantitative PCR

Acknowledgement

Reference

1. Colas, J.-F. & Schoenwolf, G. C. Towards a cellular and molecular understanding of neurulation. *Dev. Dyn.* **221**, 117–145 (2001).

2. Nikolopoulou, E., Galea, G. L., Rolo, A., Greene, N. D. E. & Copp, A. J. Neural tube closure: cellular, molecular and biomechanical mechanisms. *Development* **144**, 552–566 (2017).

3. Xing, L., Anbarchian, T., Tsai, J. M., Plant, G. W. & Nusse, R. Wnt/β-catenin signaling regulates ependymal cell development and adult homeostasis. *Proc Natl Acad Sci USA* **115**, E5954–E5962 (2018).

4. Kaufman, M. H. Occlusion of the neural lumen in early mouse embryos analysed by light and electron microscopy. 18.

5. Bay, S. N. & Caspary, T. What are those cilia doing in the neural tube? *Cilia* **1**, 19 (2012).

6. Valente, E. M., Rosti, R. O., Gibbs, E. & Gleeson, J. G. Primary cilia in neurodevelopmental disorders. *Nat Rev Neurol* **10**, 27–36 (2014).

7. Kosodo, Y. Interkinetic nuclear migration: beyond a hallmark of neurogenesis. *Cell. Mol. Life Sci.* **69**, 2727–2738 (2012).

8. Baye, L. M. & Link, B. A. Nuclear migration during retinal development. *Brain Research* **1192**, 29–36 (2008).

9. Spear, P. C. & Erickson, C. A. Interkinetic nuclear migration: A mysterious process in search of a function. *Develop. Growth Differ.* **54**, 306–316 (2012).

10. Vallier, L. *et al.* Early Cell Fate Decisions of Human Embryonic Stem Cells and Mouse Epiblast Stem Cells Are Controlled by the Same Signalling Pathways. *PLoS ONE* **4**, e6082 (2009).

11.   Brons, I. G. M. *et al.* Derivation of pluripotent epiblast stem cells from

mammalian embryos. *Nature* **448**, 191–195 (2007).

12.   Hayashi, K., Ohta, H., Kurimoto, K., Aramaki, S. & Saitou, M. Reconstitution

of the Mouse Germ Cell Specification Pathway in Culture by Pluripotent Stem

Cells. *Cell* **146**, 519–532 (2011).

13.   Deluz, C. *et al.* A role for mitotic bookmarking of SOX2 in pluripotency and

differentiation. *Genes Dev.* **30**, 2538–2550 (2016).

14.   Meinhardt, A. *et al.* 3D Reconstitution of the Patterned Neural Tube from

Embryonic Stem Cells. *Stem Cell Reports* **3**, 987–999 (2014).

15.   Lee, E. *et al.* ACT-PRESTO: Rapid and consistent tissue clearing and labeling

method for 3-dimensional (3D) imaging. *Sci Rep* **6**, 18631 (2016).

CHAPTER 3

Single-cell transcriptomic analysis of neural tube organoids

Single-cell transcriptomic analysis of neural tube organoids

JiSoo Park[1], Matthias P. Lutolf[1,2,*]

[1] Laboratory of Stem Cell Bioengineering, Institute of Bioengineering, School of Life Sciences and School of Engineering, École Polytechnique Fédérale de Lausanne (EPFL), Lausanne, 1015, Vaud, Switzerland

[2] Institute of Chemical Sciences and Engineering, School of Basic Science, École Polytechnique Fédérale de Lausanne (EPFL), Lausanne, 1015, Vaud, Switzerland

[*] Correspondence: matthias.lutolf@epfl.ch

Abstract

To understand the cell composition of the neural tube organoids, I performed single cell RNA sequencing of organoids from D3 and from D6 (i.e., beginning and end of the elongation). This single cell transcriptomic analysis revealed that neural tube organoid is composed of mainly neuroectodermal cells as well as of specific region cell types such as midbrain, hindbrain, and spinal cord. Furthermore, the analysis disclosed the differences, in terms of represented cell types, between self-elongating neural tube organoids and organoids that instead remain spherical.

Introduction

Recent advances in high-throughput sequencing technology have revolutionized biomedical research by allowing deeper understanding of the biological events under investigation through single-cell level resolution. Thanks to microfluidic technology, individual cells from a tissue of interest can be separated, uniquely barcoded, and then sequenced. Single-cell RNA sequencing (scRNAseq) thus provides new insights in understanding individual cells out of heterogenous populations of them, based on their distinctive gene expression profile. It allows to discover and detect rare cell types, to study heterogeneity in cell responses, and to track the trajectories of specific cell lineages in development[1–4].

After developing the novel neural tube organoid, I applied the scRNAseq technology to answer the following three main questions:

1) How does the organoid develop over time?

2) What kind of cell types compose the neural tube organoid?

3) What are the differences between the self-elongating neural tube organoid and the non-elongating neural tube organoid?

In order to do so, I established a convenient protocol to harvest organoids from their Matrigel embedding and I collected organoids at D3 and D6 of differentiation, to be processed for scRNAseq. Then, I analysed the raw sequencing data following standard workflows[5–8], identified the cell type composition of the neural tube organoid, and proceeded with further analysis.

Results and discussion

To better characterize the cellular diversity of the neural tube organoids and to better understand the temporal aspect of their differentiation from D3 to D6, I performed scRNAseq of cells isolated from organoids collected at D3 and at D6. (On D6, self-elongating neural tube organoids (SENT) and non-elongating neural tube organoids (NENT) were collected separately. I will specify SENT and NENT only to discriminate them for comparative investigation, but else, all the neural tube organoids refer to SENT by default.) To harvest organoids from their Matrigel embedding without damaging them, I adopted a novel practical protocol which includes treatment of the buffer solution with Collagenase IV and Dispase I with agitation throughout the protocol until the Matrigel dissolves completely. The collected organoids were then dissociated into single cells and were processed through the standard pipeline for scRNAseq[5–8] (**Figure 16**). In a microfluidic chip, cells were partitioned individually with their own unique barcode as to be later trackable for sequencing, thus allowing single-cell level exploration.
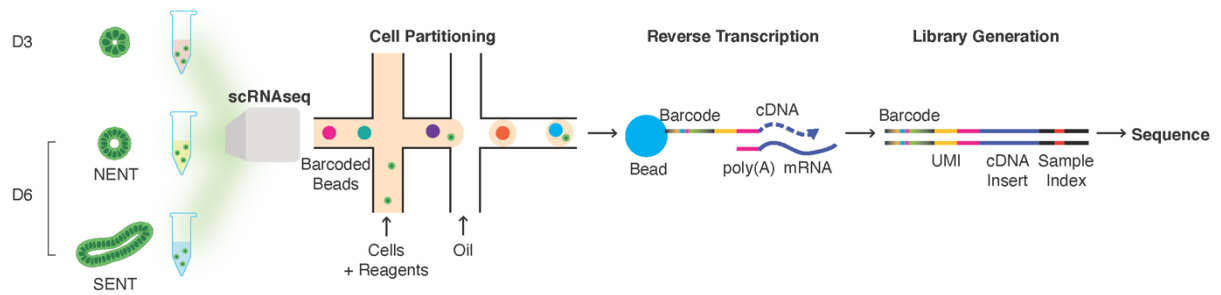
Figure 16. Scheme of the standard pipeline for scRNAseq. The organoids from D3 and D6 were collected and dissociated into single cells. 1) Cell partitioning: the collected single cell solution is loaded onto a microfluidic chip and individual cells are encapsulated in a droplet with a barcoded bead and the reagents for reverse transcription. Once the cells are lysed, the poly(A) tail of the mRNA binds to the bead. 2) Reverse transcription: cDNA tagged with the barcode for cell identification and a unique molecular identifier (UMI) for quantifying mRNA reads by reverse transcription. 3) Library generation: cDNA is amplified including a sample index to generate sequencing library. 4) Sequence: The pooled library is sequenced.

The acquired raw sequencing data were then processed following standard scRNAseq analysis workflow[5–8] (illustrated in **Figure 17**).
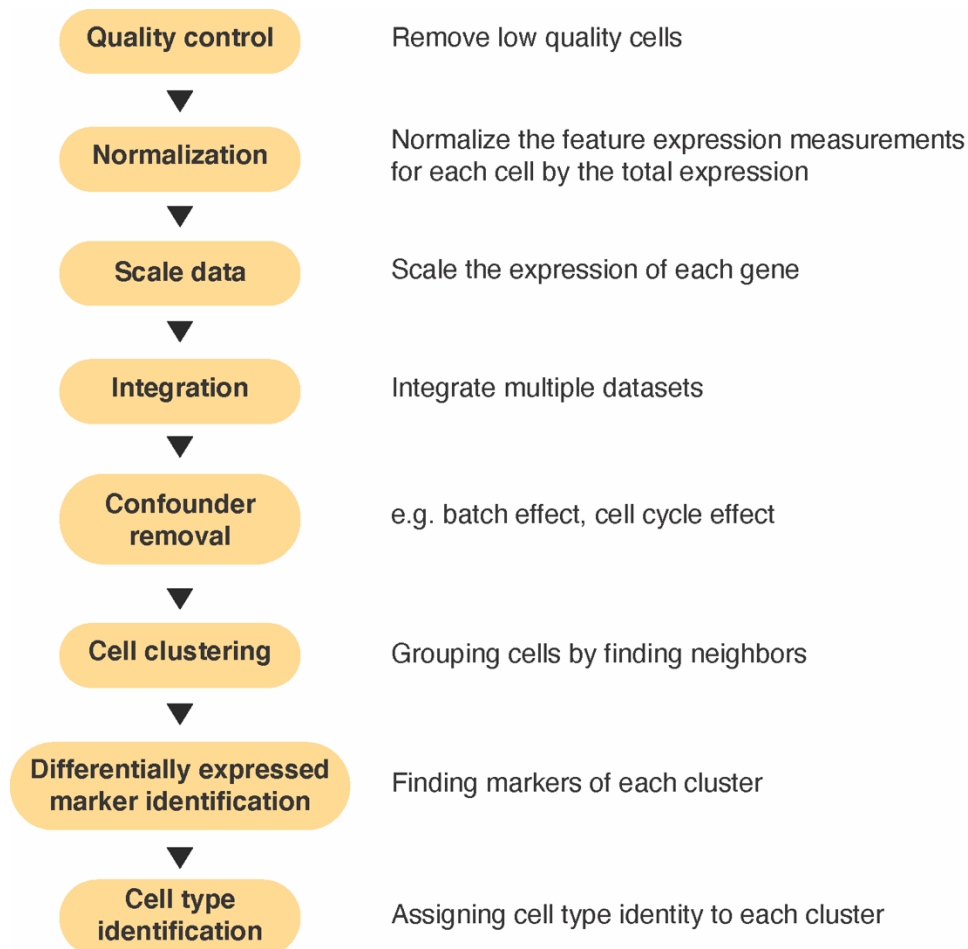
Figure 17. The standard workflow of scRNAseq analysis.

To understand how the cells in the organoids develop over time, cells from all three sample populations (D3, NENT, and SENT) were integrated and analysed. A clustering analysis using a shared nearest neighbor modularity algorithm followed by analysis of the markers characterizing each cluster (**Figure 18**) identified a total of 11 cell types across the analyzed differentiation window (**Figure 19**).

Figure 18. Canonical markers of various cell types throughout the neural development were found in neural tube organoid. Heat map of the top markers of each cell types from D3 and D6 neural tube organoids. Pluripotent cells and epiblast cells express high level of *Nanog*, *Pou5f1*, *Utf1*, and *Otx2* and caudal epiblast cells express also the caudal genes like *Cdx2* and *Wnt8a*. Surface ectoderm cells express high level of *Krt8* and *Krt18* and neuroectoderm cells express *Crabp1, Crabp2, Sox1,* and *Sox2*. Midbrain cells exclusively express *En1* and *En2*, Mid/hindbrain cells express *Egr2, Nnat,* and *Ppp1r1b* as the boundary between midbrain and hindbrain *in vivo*. Spinal cord cells express the hox genes from level 1 to 9 and *Pax6*. There is a small population of posterior mesoderm expressing *T* and *Mesp1* and proliferating cells expressing *Top2a* and *Mki67*.
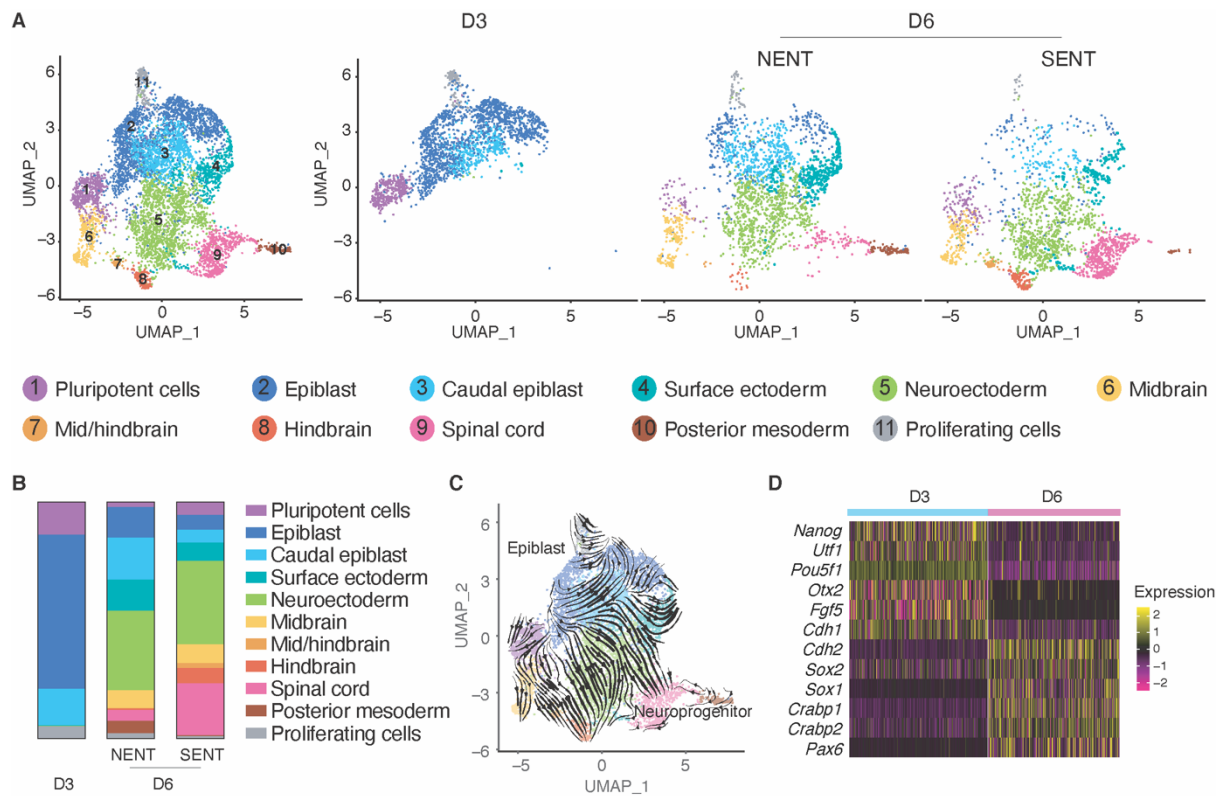
Figure 19. Single-cell transcriptomics of the neural tube organoids from D3 and D6. (A) UMAP projection[9] of organoids from D3 and D6 determining 11 cell types and the composition ratios of each cell types are shown in B. (B) D3 organoids are composed of mainly epiblast and caudal epiblast cells, while D6 organoids are composed of mainly neuroectoderm and its derivative cell types like midbrain, hindbrain, and spinal cord. (C) UMAP projection with trajectories inferred from RNA velocity with the arrow flows that represent calculated velocity trajectories. The RNA velocity stream flows from top to bottom, representing neural differentiation from an epiblast-like state. (D) Heatmap with scaled gene expression of early developmental markers in D3 and D6 organoids showing transition from epiblast to neuroprogenitors. A phenotypic transition characteristic of early neural development *in vivo*, Cadherin switching from E-cadherin (*Cdh1*) to N-cadherin (*Cdh2*) between D3 and D6 could be observed as well.

Accordingly, D3 organoids appear to be predominantly composed of cells with early epiblast-(*Pou5f1*+, *Utf1*+, *Otx2*+, *Fgf5*+) as well as caudal epiblast- (*Cdx2*+, *Nkx1.2*+, *Wnt8a*+) identities (**Figure 19A, B, D, Figure 20A**). Meanwhile, the major population of the cells from D6 organoids expresses markers of neuroectoderm (*Sox1*+, *Sox2*+, *Crabp1*+) and of its derivatives (**Figure 19A, B, Figure 20**). As discussed in Chapter 2, we thus confirm that the early epiblast-like cell population induced by Epi medium found at D3 decreases over time to be replaced by a cell population harboring more

mature neural lineage fates induced by neural differentiation medium (**Figure 19A, B**). The trajectories inferred from RNA velocity[10] support this transition from epiblast to neuroprogenitors (**Figure 19C**). We could also observe cadherin profile switching from E-cadherin (*Cdh1*+) to N-cadherin (*Cdh2*+) between D3 and D6, a phenotypic transition characteristic of early neural differentiation *in vivo*[11,12] (**Figure 19D**). More interestingly, our analysis demonstrates that organoids at D6 are composed of neuroectodermal cells with diverse axial identities ranging from the midbrain (*En1*+ and *En2*+), to the hindbrain (*Egr2*+, *Ppp1r1b*+), and to the spinal cord (*Hoxb7*+, *Hoxb9*+) (**Figure 18** and **Figure 20**). A population with surface ectoderm identity (*Krt8*+, *Krt18*+) could also be detected at D6, at a higher proportion in NENT than in SENT (**Figure 19B**). The existence of surface ectodermal cells (KRT8+) was confirmed by immunofluorescent imaging on NENT and SENT (**Figure 21**).
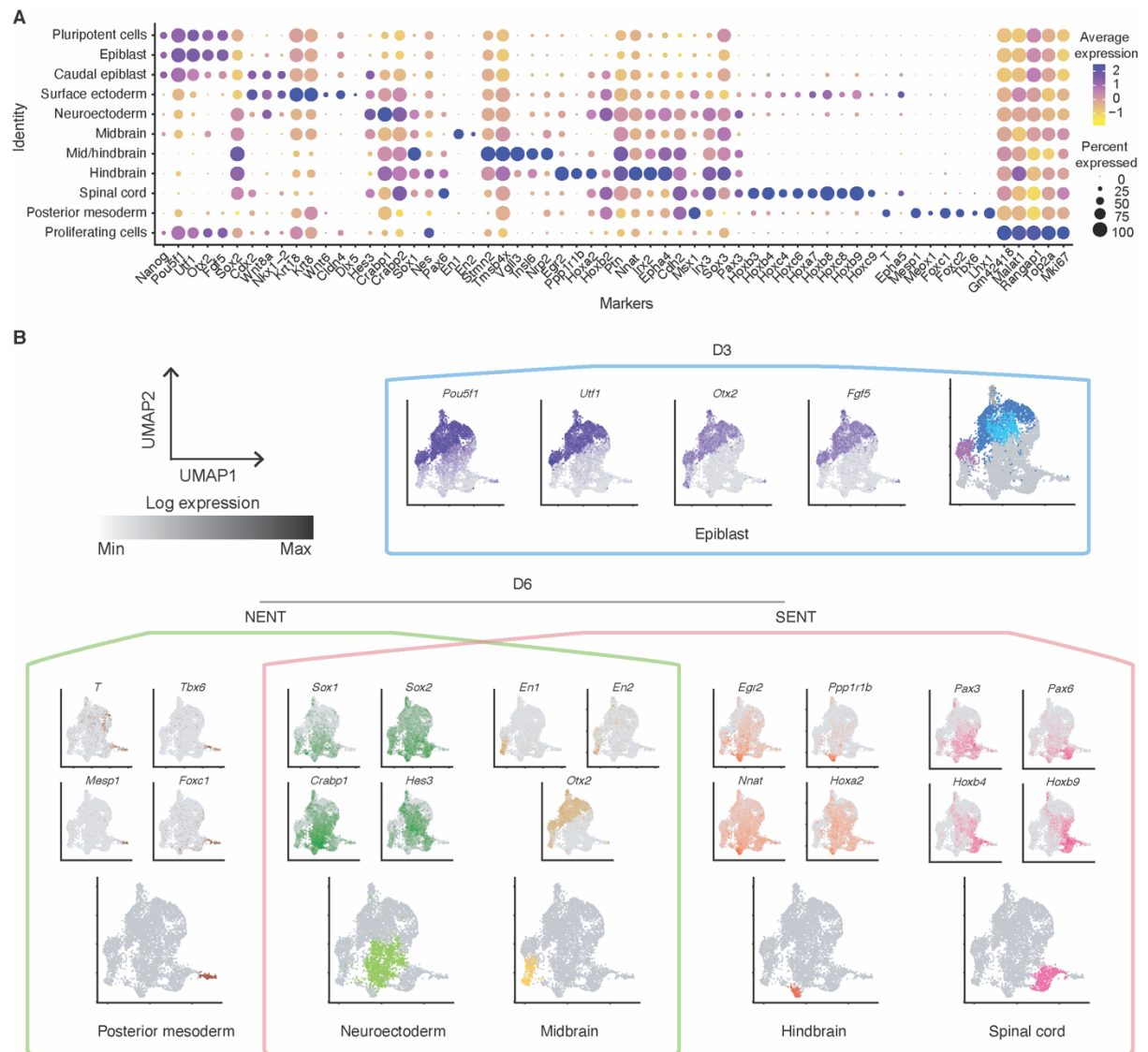
Figure 20. Key markers of each identified cell type and their expression level. (A) Dot plots showing key markers of each identified cell cluster and their expression level and the percentage of the cells expressing the markers. (B) The markers of each cluster defining the cell type: early epiblast cells of D3 organoids and neuroectoderm and more specified cell types along the AP axis of the neural tube, from midbrain to spinal cord, of D6 organoids.
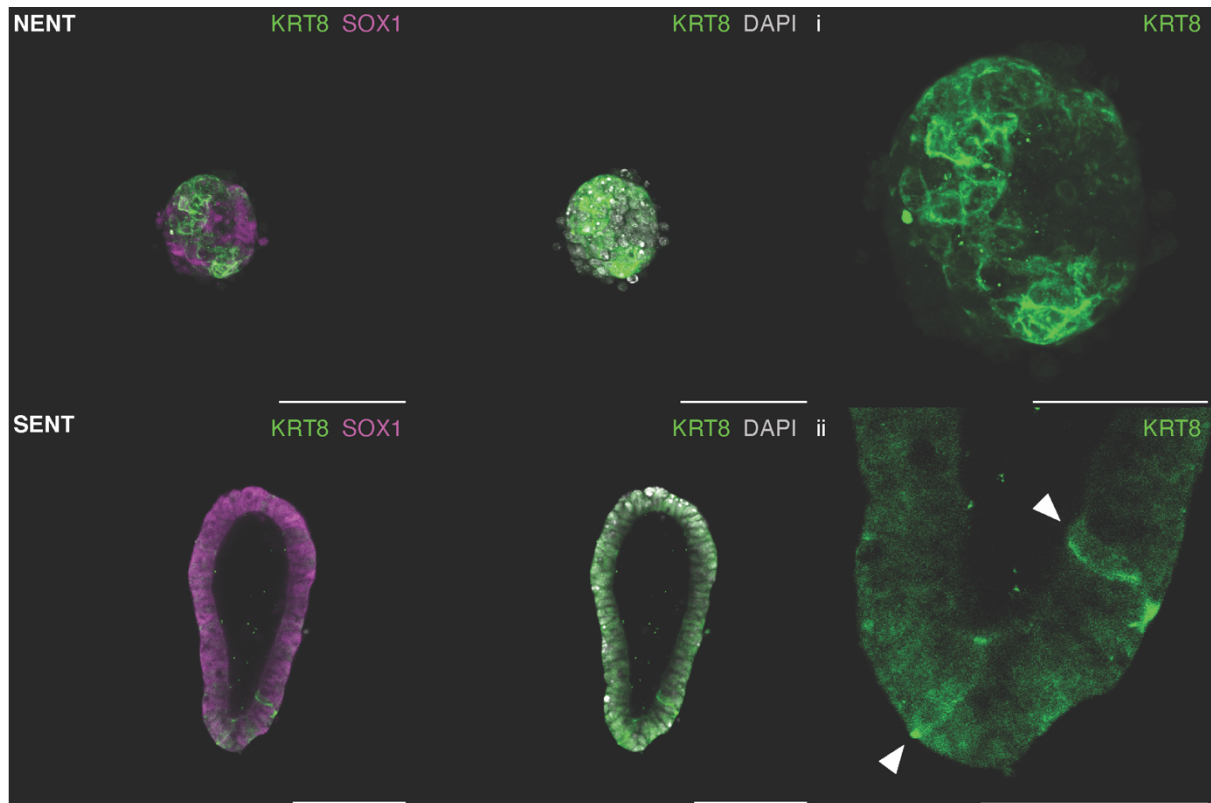
Figure 21. Surface ectodermal cells exist in D6 organoids. NENT organoids possess a greater number of surface ectodermal cells (KRT8+) than SENT organoids. All the scale bars are 100 μm and 50 μm for i-ii.

To assess the extent to which the cell types identified through this analysis resemble the cells *in vivo*, I compared the organoid dataset to available datasets of peri- and post-gastrulation mouse embryos. Indeed, Pijuan-Sala et al. have reported a single-cell transcriptional profiles of mouse embryos from E6.5 to E9.5, and developed an instructive atlas about mouse gastrulation and early embryogenesis[13]. I extracted the scRNAseq data of E8.0, E8.25, and E8.5 mouse embryos, combined them with D6 neural tube organoid data, and aligned them to see their overlay (**Figure 22**). The UMAP projection[9] of integrated datasets shows a good match of the identified cell types between the organoid and embryo. Clearly, the neural tube organoid cells fall on top of the atlas cell clusters that are related to neural tube development, such as Forebrain/midbrain/hindbrain and Spinal cord clusters. Collectively, the single-cell transcriptomic analysis confidently suggests that the neural tube organoids mirror the cell types related to neural tube development of *in vivo* mouse embryos.

Figure 22. The cell types identified in neural tube organoid resemble the neural tube development-related cell types of *in vivo* mouse embryo. The datasets of D6 neural tube organoid and the mouse embryo of E8.0, E8.25, and E8.5 were integrated and aligned. The cells of D6 organoids place on top of the cell types like Forebrain/Midbrain/Hindbrain, Spinal cord, and Rostral/Caudal neuroectoderm as identified from the scRNAseq analysis. This overlay confirms the cell identification analysis was properly performed and the neural tube organoid indeed mirrors the cell types *in vivo*.

Having shown that neural tube organoids undergo a transition from epiblast to neuroectodermal types, and that these recapitulate embryonic identities, I then focused on whether the single cell dataset could help explain the difference between organoids that elongate by D6 and organoids that instead remain spherical. To assess the difference between NENT and SENT, the two sample populations were thus analysed separately from D3 (**Figure 23**). As **Figure 23** shows, the majority of the cell types were conserved from the previous analysis (**Figure 19A**).
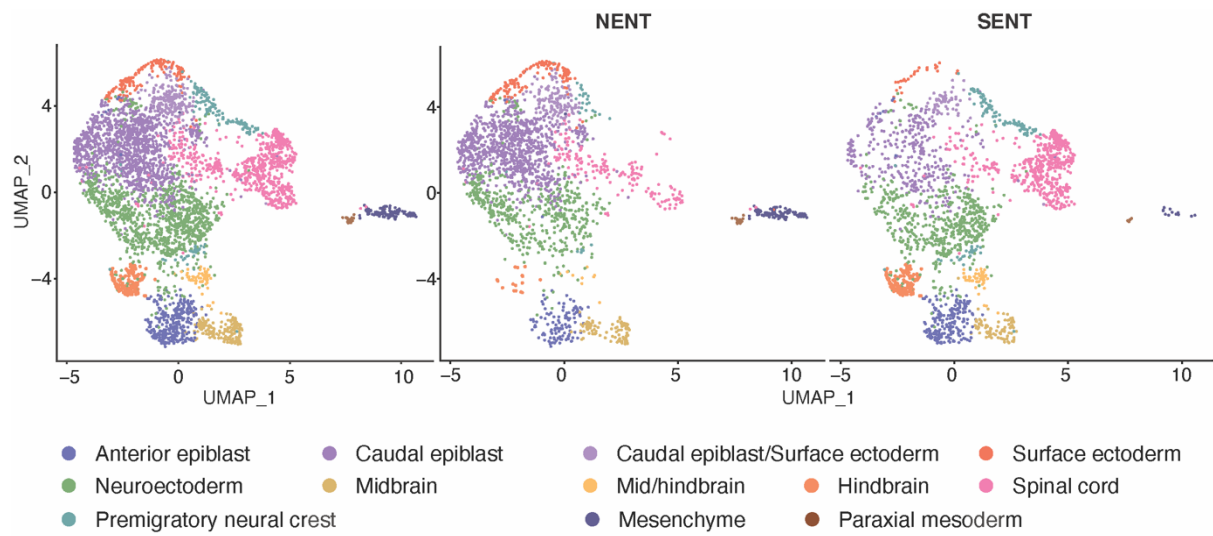

Figure 23. Single-cell transcriptomics of the neural tube organoids from D6. UMAP projection of the D6 neural tube organoids revealed 12 cell types. Most of the cell types are conserved from the previous analysis but it also revealed a new cell type cluster, premigratory neural crest cells, which resides between the surface ectoderm and spinal cord.

Broadly, NENT and SENT both share epiblast, neuroectoderm, and midbrain cell clusters. Yet, mid/hindbrain, hindbrain, and spinal cord cell clusters are preferentially found in SENT while surface ectoderm and mesenchyme cell clusters are preferentially found in NENT. Considering that NENT and SENT were cultured under exactly the same conditions, such difference in cell types is remarkable. Specifically, SENT develop more posterior cell types (such as hindbrain and spinal cord) compared to NENT, which express posterior Hox genes. Indeed, when the Hox gene expression across these two groups was visualized (**Figure 24**), it is evident that SENT display relatively stronger expression of posterior Hox genes while NENT express the anterior ones stronger.
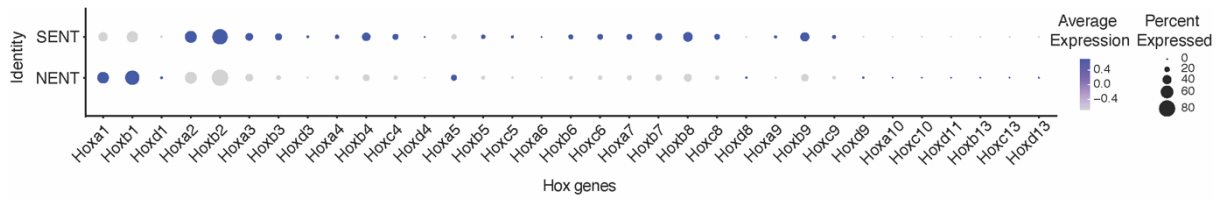
Figure 24. Dot plot visualizing the Hox gene expression in SENT and NENT. NENT only expresses the anterior ones relatively strongly, while SENT expresses the Hox genes spanning throughout the AP axis.

This data suggests that there might be a link between axial elongation and Hox gene expression to explain the elongation of SENT and not of NENT. Deeper insights into the molecular mechanisms involved are required to elucidate the correlation between elongation and the emergence of hindbrain and spinal cord cell identities.

Another finding of this analysis was the existence of premigratory neural crest cells in D6 neural tube organoids, residing between the surface ectoderm and the spinal cord clusters in the UMAP (**Figure 23**). The cells in this cluster express the representative markers of premigratory neural crest cells (**Figure 25**). Accordingly, we detect the expression of not only premigratory markers like *Ets1* and *Phlda2*, but also of pan-neural crest cell markers such *Nes* and *Sox9*[14–20]. These results hint to the prospect of the emergence of neural crest from the neural tube organoid.
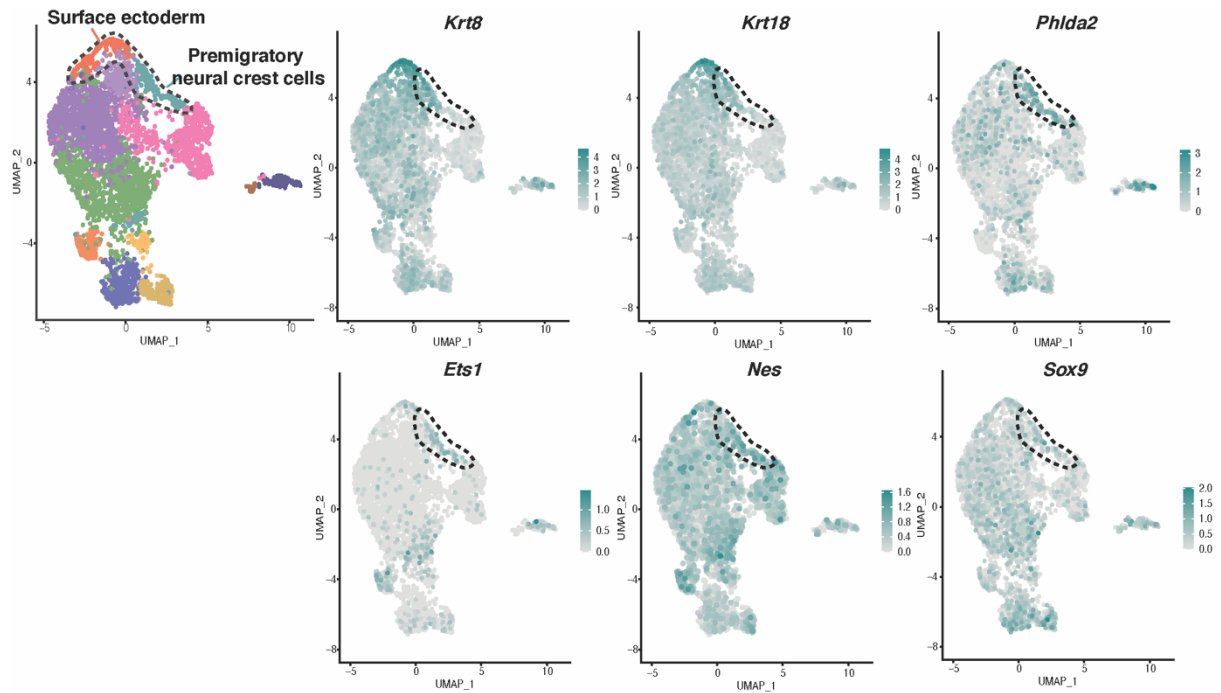
Figure 25. Key markers of premigratory neural crest cells. As the neural crest cells emerge between the dorsal neural tube and surface ectoderm, some cells expressing the surface ectoderm markers (*Krt8* and *Krt18*) are found near the surface ectoderm cluster. Also, there are cells expressing the premigratory neural crest cell markers, *Phlda2* and *Ets1*, and pan-neural crest cell markers, *Nes* and *Sox9* in the cluster. This result hints the potential of the emergence of neural crest cells in the neural tube organoid.

Together, single-cell transcriptomics identified the cell composition of SENT organoid, which thus appear to be made of cells with neuroectoderm identities and of their derivative cell types, from midbrain to spinal cord. Gene ontology (GO) analysis on biological process based on the markers of SENT organoids further supports these results (**Figure 26**).
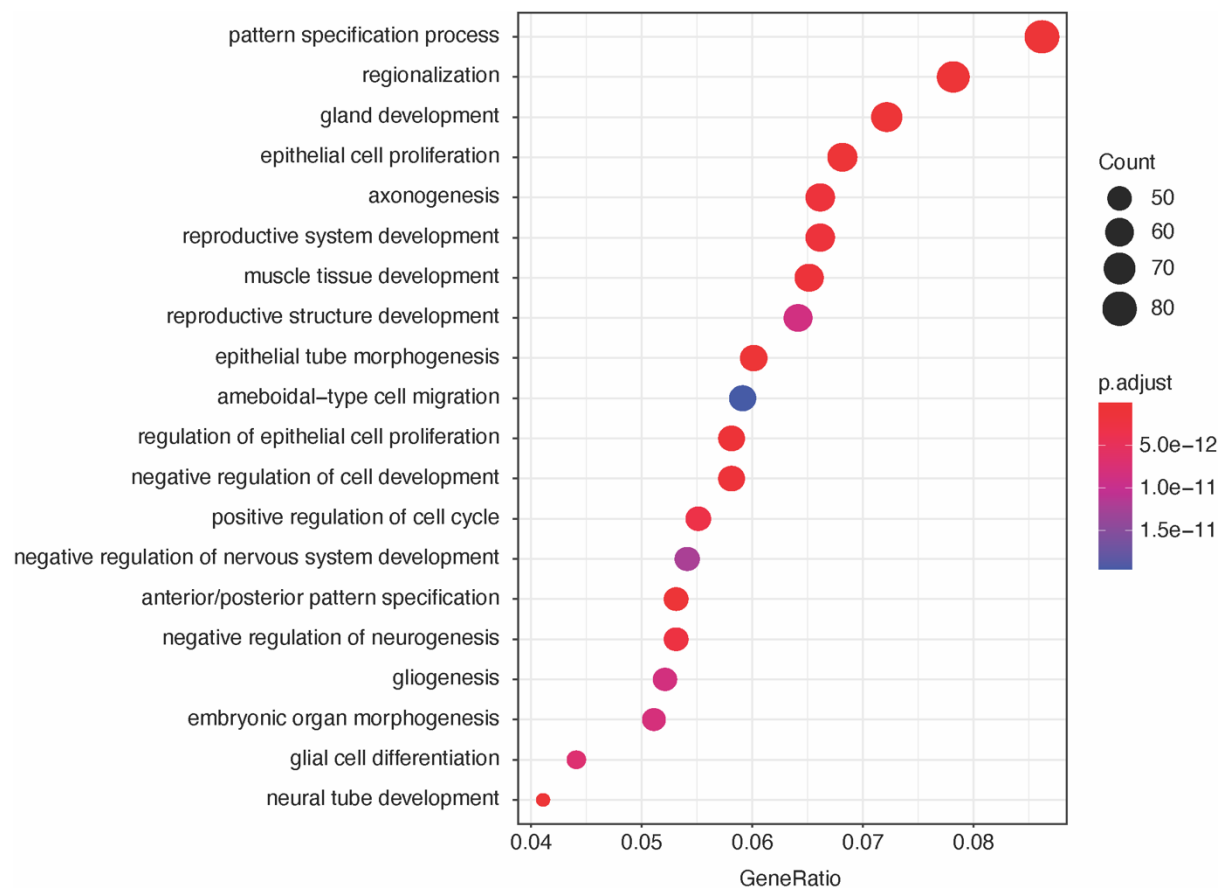
Figure 26. Gene ontology (GO) analysis showing the most significant function enrichment terms in biological process.

First, GO terms like pattern specification, regionalization, and anterior-posterior pattern specification are coherent to the cell composition of SENT organoid with different regions of neural tube. Second, epithelial tissue-related GO terms like gland development, epithelial cell proliferation, and epithelial morphogenesis suggest the relation to the distinctive elongating morphogenesis of SENT. Lastly, neural development-related GO terms like axonogenesis, gliogenesis, and neural tube development clearly indicate that SENT organoid resembles the neural tube development *in vivo*. The link between the markers and the GO terms are displayed on **Figure 27**.
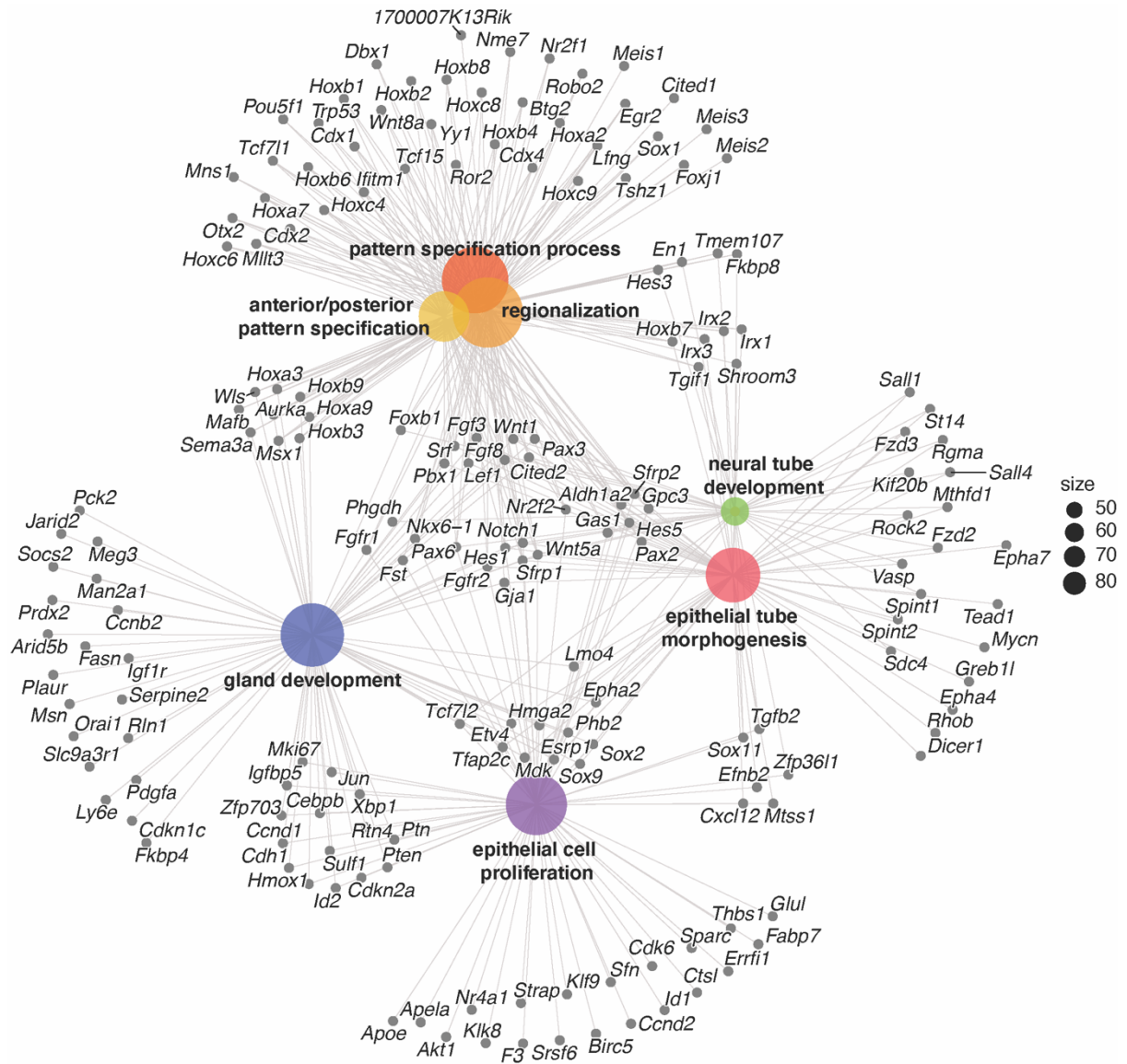
Figure 27. Gene-concept network illustrate the linkage of the genes and the biological significant terms.

Conclusion

To resolve the identity of SENT organoids at a single-cell level, scRNAseq and related bioinformatic analyses were performed. Through this analysis, I could identify the cell types making up D3 and D6 organoids. First, I confirmed that D3 organoids are mainly composed of epiblast cells, reinforcing the time-course qPCR data presented in Chapter 2. Interestingly, scRNAseq-analysis revealed the existence of a small population of caudal epiblast cells. These epiblast cells from D3 develop into neural tube organoid by D6, one half into self-elongating tissue (SENT) and the other half into spherical tissue (NENT). Accordingly, single-cell transcriptomic analysis unveiled neuroectoderm, midbrain, surface ectoderm, and epiblast as common cell types, and hindbrain and spinal cord as exclusive cell types in SENT. Considering that the hindbrain and spinal cord are marked by Hox gene expression, these observations lead to hypothesise that there might be a link between the elongation of SENT and its Hox gene expression which requires to be elucidated in the future. Gene ontology analysis also supports what found in SENT; regionalised cell types, extensive epithelial morphology, and expression of neural developmental markers. Furthermore, a deeper analysis of D6 organoids discovered a small population of cells expressing markers of premigratory neural crest cells in SENT organoids, hinting to the emergence of neural crest from mature SENT organoids. In conclusion, I could better characterize the cellular diversity of the organoids and understand the cellular aspect of organoid differentiation from D3 to D6 by applying scRNAseq strategies. Comparison to *in vivo* mouse embryonic datasets affirms that the SENT organoid recapitulates *in vivo* neural development faithfully.

Materials and methods

Sample preparation for single cell RNA sequencing

The sample preparation was performed according to the instructions from *10x Genomics Single Cell Protocols* (10X Genomics), with some modification. Collected organoids (100 organoids per condition) were washed twice with PBS-/- and trypsinized with TrypLE™ Express (Gibco, Cat# 12605-028) for 7 min in 37 °C. The organoids were dissociated into single cells by pipetting up and down with 1000 μL pipette tip, strained using a 40 μm cell strainer, and collected in 1.5 microcentrifuge tubes. The single cells were centrifuged at 300 rcf for 5 min and resuspended in 1 mL of PBS with 0.04% BSA after removing the supernatant. The cell concentration was determined. After a further round of centrifugation, the cells were resuspended in PBS with 0.04% BSA to achieve a final cell concentration of 1 million cells/mL. After the trysinisation, the cells were always placed on ice.

Single cell RNA sequencing

Single-cell transcriptomics profiling of cells derived from organoids at D3 and D6 of differentiation (NENT, non-elongating neural tube, and SENT, self-elongating neural tube) was done using Chromium Single Cell Gene Expression (10X Genomics), according to manufacturer's recommendations. The cellular suspension was loaded on a Chromium Controller instrument to generate Gel Beads-in-emulsion (GEMs), containing single-cells. Reverse transcription and library preparation were performed using the Single Cell 3' Reagent Kit v3 (10X Genomics), following 10X Genomics protocol.

Single cell RNA sequencing data analysis

Single cell RNA sequencing data analysis was performed using Seurat 3.0.3[5] with raw feature-barcode matrices of D3 (the organoids on D3), SENT (self-elongating neural tube organoids), and NENT (non-elongating neural tube organoids). Genes expressed in less than 3 cells and cells with less than 200 features expressed were removed. Cells with unique feature counts between 3500 and 7500, less than 7.5% mitochondrial counts were used for analysis. Expression level was log normalized, and

the top 2,000 variable genes were calculated using Variance Stabilizing Transformation (VST) algorithm[21]. Three datasets were merged and integrated according to their first 30 dimensions. After integration, the effects of the batch ID, cell cycle, nUMI, and mitochondrial counts were regressed out. The number of cells after filtering was 2185 (D3), 2076 (SENT), and 2225 (NENT). We scaled the data applying a linear transformation and performed principal component analysis (PCA) on the scaled data. Clusters of cells were identified by a shared nearest neighbour (SNN) modularity optimization-based Louvain algorithm with a resolution of 1.0[22]. Clusters were visualized on a two-dimensional Uniform Manifold Approximation and Projection (UMAP)[9]. Cell type of each cluster was identified based on the markers of each cluster expressing more than 0.25 $\log_2$ fold-change different over the others. Also, the markers of each clusters were used for gene ontology (GO) analysis using R package clusterProfiler[23]. To estimate RNA velocity of each cell, velocyto.py[24] was used to generate loom files for each datasets used for Seurat analysis. To do so, the bam file of each dataset produced by Cell Ranger (10X Genomics) and gtf file from 10X Genomics for annotation were used. To integrate the loom file and the Seurat object in R, meta-data like filtered cell IDs, UMAP coordinates, and clusters were extracted. Once the loom files were generated, the loom files and the meta-data were integrated and RNA velocity could be estimated based on the same UMAP coordinates and clusters using scVelo[10]. For the comparison between the neural tube organoid and the mouse embryo *in vivo*, the datasets of E8.0, E8.25, and E8.5 mouse embryo[13] were extracted and integrated with D6 neural tube organoid dataset and aligned.

Immunostaining

The organoids were collected from Matrigel drop by washing with PBS-/- and dissolving the Matrigel using 4 mg/mL Collagenase-IV and 100 µg/mL Dispase I in HBSS+/+ on a shaker in the incubator for 35 minutes. The organoids were fixed in 4% paraformaldehyde (PFA) in PBS-/- for 30 min in room temperature. The organoids were washed with PBS-/- for three times of 20 min, permeabilized in 0.2% Triton-X 100 in PBS-/- for 1 h and blocked in Blocking solution (3% Bovine serum albumin

(BSA) and 0.01% Triton-X 100 in PBS-/-) for 3 h to overnight. Primary antibody (**Table 6**) solution was prepared in Blocking solution, with 2 µg/mL of DAPI (**Table 3**). The organoids were stained overnight on a low-speed orbital shaker in 4 °C. The organoids were thoroughly washed with PBS-/- every 30 min for 4 hours. Secondary antibody (**Table 4**) solution was prepared, treated, and washed the same way as primary antibody solution.

Target	Species	Dilution	Cat. No.	Supplier
KRT8	rabbit	1:200	ab53280	abcam

Table 6. Primary antibodies used in immunostaining surface ectodermal cells

Acknowledgement

Reference

1. Potter, S. S. Single-cell RNA sequencing for the study of development, physiology and disease. *Nat Rev Nephrol* **14**, 479–492 (2018).

2. Buettner, F. *et al.* Computational analysis of cell-to-cell heterogeneity in single-cell RNA-sequencing data reveals hidden subpopulations of cells. *Nat Biotechnol* **33**, 155–160 (2015).

3. Svensson, V. *et al.* Power analysis of single-cell RNA-sequencing experiments. *Nat Methods* **14**, 381–387 (2017).

4. Wu, A. R. *et al.* Quantitative assessment of single-cell RNA-sequencing methods. *Nat Methods* **11**, 41–46 (2014).

5. Stuart, T. *et al.* Comprehensive Integration of Single-Cell Data. *Cell* **177**, 1888-1902.e21 (2019).

6. Andrews, T. S., Kiselev, V. Y., McCarthy, D. & Hemberg, M. Tutorial: guidelines for the computational analysis of single-cell RNA sequencing data. *Nat Protoc* **16**, 1–9 (2021).

7. Hwang, B., Lee, J. H. & Bang, D. Single-cell RNA sequencing technologies and bioinformatics pipelines. *Exp Mol Med* **50**, 1–14 (2018).

8. Luecken, M. D. & Theis, F. J. Current best practices in single-cell RNA-seq analysis: a tutorial. *Mol Syst Biol* **15**, (2019).

9. McInnes, L., Healy, J. & Melville, J. UMAP: Uniform Manifold Approximation and Projection for Dimension Reduction. *arXiv:1802.03426 [cs, stat]* (2018).

10. Bergen, V., Lange, M., Peidli, S., Wolf, F. A. & Theis, F. J. *Generalizing RNA velocity to transient cell states through dynamical modeling.* http://biorxiv.org/lookup/doi/10.1101/820936 (2019) doi:10.1101/820936.

11.   Wheelock, M. J., Shintani, Y., Maeda, M., Fukumoto, Y. & Johnson, K. R. Cadherin switching. *Journal of Cell Science* **121**, 727–735 (2008).

12.   Dady, A., Blavet, C. & Duband, J.-L. Timing and kinetics of E- to N-cadherin switch during neurulation in the avian embryo. *Dev. Dyn.* **241**, 1333–1349 (2012).

13.   Pijuan-Sala, B. *et al.* A single-cell molecular map of mouse gastrulation and early organogenesis. *Nature* **566**, 490–495 (2019).

14.   Simões-Costa, M. & Bronner, M. E. Establishing neural crest identity: a gene regulatory recipe. *Development* **142**, 242–257 (2015).

15.   Théveneau, E., Duband, J.-L. & Altabef, M. Ets-1 Confers Cranial Features on Neural Crest Delamination. *PLoS ONE* **2**, e1142 (2007).

16.   Simoes-Costa, M., Tan-Cabugao, J., Antoshechkin, I., Sauka-Spengler, T. & Bronner, M. E. Transcriptome analysis reveals novel players in the cranial neural crest gene regulatory network. *Genome Research* **24**, 281–290 (2014).

17.   Tani-Matsuhana, S., Vieceli, F. M., Gandhi, S., Inoue, K. & Bronner, M. E. Transcriptome profiling of the cardiac neural crest reveals a critical role for MafB. *Developmental Biology* **444**, S209–S218 (2018).

18.   Gao, Z. *et al.* Ets1 is required for proper migration and differentiation of the cardiac neural crest. *Development* **137**, 1543–1551 (2010).

19.   Nie, S. & Bronner, M. E. Dual developmental role of transcriptional regulator Ets1 in Xenopus cardiac neural crest vs. heart mesoderm. *Cardiovascular Research* **106**, 67–75 (2015).

20.   Angeles Rabadán, M., Usieto, S., Lavarino, C. & Martí, E. Identification of a putative transcriptome signature common to neuroblastoma and neural crest cells:

Genes Common to NB/NC. *Devel Neurobio* n/a-n/a (2013)

doi:10.1002/dneu.22099.

21.   Lin, S. M., Du, P., Huber, W. & Kibbe, W. A. Model-based variance-stabilizing

transformation for Illumina microarray data. *Nucleic Acids Research* **36**, e11–e11

(2008).

22.   Waltman, L. & van Eck, N. J. A smart local moving algorithm for large-scale

modularity-based community detection. *Eur. Phys. J. B* **86**, 471 (2013).

23.   Yu, G., Wang, L.-G., Han, Y. & He, Q.-Y. clusterProfiler: an R Package for

Comparing Biological Themes Among Gene Clusters. *OMICS: A Journal of

Integrative Biology* **16**, 284–287 (2012).

24.   La Manno, G. *et al.* RNA velocity of single cells. *Nature* **560**, 494–498 (2018).

CHAPTER 4

Tissue patterning
in neural tube organoid

Tissue patterning in neural tube organoid

JiSoo Park[1], Dominique Kolly[2], Alexandre Mayran[2], Denis Duboule[2], Matthias P. Lutolf[1,3,*]

[1] Laboratory of Stem Cell Bioengineering, Institute of Bioengineering, School of Life Sciences and School of Engineering, École Polytechnique Fédérale de Lausanne (EPFL), Lausanne, 1015, Vaud, Switzerland

[2] Laboratory of Developmental Genomics, School of Life Sciences, École Polytechnique Fédérale de Lausanne (EPFL), Lausanne, 1015, Vaud, Switzerland

[3] Institute of Chemical Sciences and Engineering, School of Basic Science, École Polytechnique Fédérale de Lausanne (EPFL), Lausanne, 1015, Vaud, Switzerland

[*] Correspondence: matthias.lutolf@epfl.ch

Keyword: neural tube patterning, tissue patterning, tissue specification, anterior-posterior patterning, dorsal-ventral patterning, regionalization, *in situ* hybridization, morphogen-gradient, microfluidics, organ-on-a-chip, spatio-temporal control

Abstract

In vertebrate neural development, the neural tube patterns along two major axes in order to form a fully functional nervous system: AP and DV axis. Here, based on the scRNAseq data from Chapter 3, I characterized the tissue patterning of neural tube organoid in both AP and DV axis. Also, I developed a microfluidic device that could recreate the physiological morphogen gradients of DV axis and thus expose the neural tube organoid to these conditions. Finally, I demonstrate the morphogen gradient-driven DV patterning of the neural tube organoid and show the fidelity of the organoid as an *in vitro* neural tube model.

Introduction

Tissue patterning is essential in embryogenesis to form robust spatial arrangement of specific cell types according to the positional information given from the local microenvironment. The neural tube development specifically evolves by its remarkably sophisticated spatio-temporal patterning process controlled by morphogens and interactions with surrounding tissue types[1,2]. This patterning is a crucial process to establish a functional central nervous system. Along the AP axis, the neural tube is broadly segmented into brain and spinal cord[3,4]. More specifically, the brain is subdivided into forebrain, midbrain, and hindbrain by the local biomolecular signalling. From the hindbrain to the tail, the patterning is governed by a subset of homeobox genes called Hox genes[5–9].

Meanwhile, DV patterning of the spinal cord is largely regulated by the anti-parallel morphogens secreted from two opposite end of DV axis. Especially, the signalling molecule secreted from ventral floor plate together with the notochord, called SHH, is the main player in DV patterning. Numerous studies have reported the neural tube tissue without SHH signalling maintain its default dorsal fate. The gradient of morphogens from the two ends of the DV axis; i.e., BMP4 and Wnt from dorsal pole and SHH from ventral pole, provides positional information and induces a precise spatial cell specification pattern across the DV axis. This morphogen-governed

patterning process drives the distinct spatial arrangement of sensory neurons, interneurons, and motor neurons and thus the formation a functional neural circuitry for locomotion[2,10–15].

Such patterning in neural tissue has been demonstrated in several studies *in vitro*. As discussed in Chapter 1, there are elongated neural tube organoid has been suggested. Libby et al. have shown that there is an AP patterning by showing the spatially organized expression of anterior and posterior Hox genes, however, this system is missing the correct tissue morphology of neural tube[16]. On the other hand, Veenvliet et al. have generated the right tissue morphology of neural tube with elongated tubular neuroepithelium, however, it did not demonstrate its AP patterning of the neural tissue, but only the AP patterning of somites[17]. Collectively, there is no neural tube organoid that resembles both the structure and AP patterning of *in vivo* embryo yet to date. The neural tube organoid mimicking DV patterning are achieved by self-organisation upon RA treatment[18–20], but these organoids are only spherical structures missing the right elongated tubular morphology of the neural tube *in vivo*.

Also, there are a few studies to mimic the morphogen-mediated tissue patterning of neural tube on microfluidic device as discussed in Chapter 1. However, both systems have their limitations in mimicking the 3D neuroepithelial tissue structure of neural tube and in demonstrating distinct spatial patterning of two cell types with clear boundary. Meanwhile, Zagorski et al. have demonstrated DV patterned tissue in microfluidic device by anti-parallel morphogen gradient[21], however, it was only limited to chick embryo neural plate explant, not a 3D *in vitro* tissue model.

Here, I characterize the tissue patterning of the neural tube organoid. To do so, I show the expression of a set of markers showing AP patterning that were detected in the above-described scRNAseq analysis using qPCR and their spatial organisation using *in situ* hybridization (ISH). To study the ability of the neural tube organoid to be patterned by morphogen, I investigated a variety of approaches. First, I verified whether the organoids can be ventralized using ventral morphogens and demonstrated the emergence of ventral cell types. Then, I assayed the cell fate

decisions within the organoids when exposed to various ratios of concentration of DV morphogens in bulk according to the chick embryo neural plate explant culture approach[14,21]. Finally, I developed a novel microfluidic device to prove, for the first time, the possibility of morphogen gradient-mediated tissue patterning on the organoids as of the *in vivo* neural tube.

Results and discussion

AP Patterning

Single-cell transcriptomics revealed the presence a variety of cell types in the neural tube organoids. The main contributors included neuroectoderm, midbrain, hindbrain, and spinal cord specialised cell types. Precisely, the two major cell types that preferentially exist in SENT comparing to NENT were specialized towards hindbrain and spinal cord (**Figure 28**). Most importantly, I could identify a wide range of Hox genes ranking as top markers of these cell clusters (**Figure 29**).
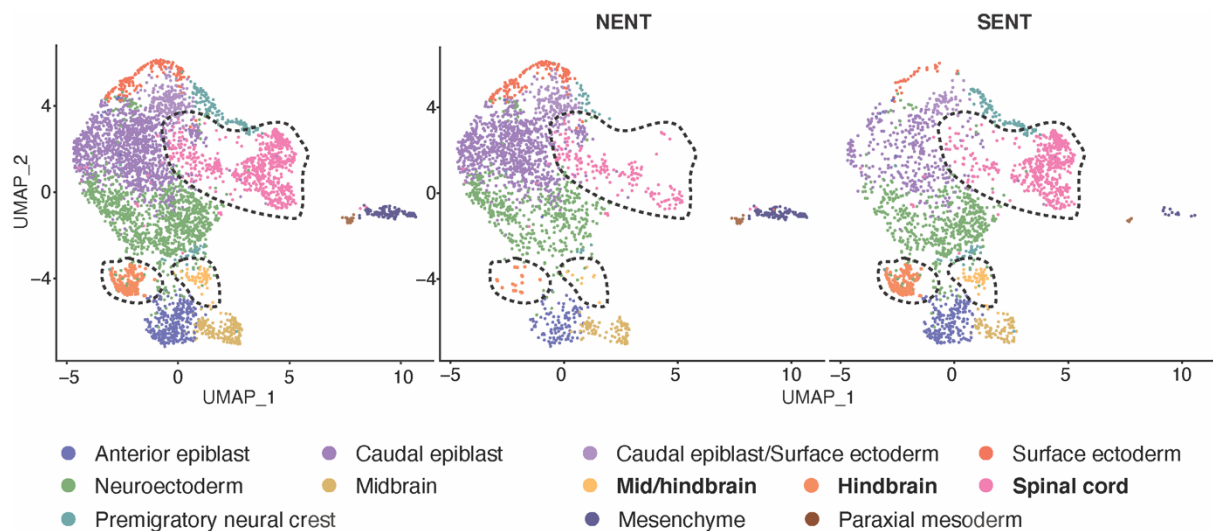

Figure 28. Single-cell transcriptomics revealed the difference in cell type composition between NENT and SENT. The cell clusters identified as mid/hindbrain, hindbrain, and spinal cord were preferentially found in SENT in comparison to NENT.
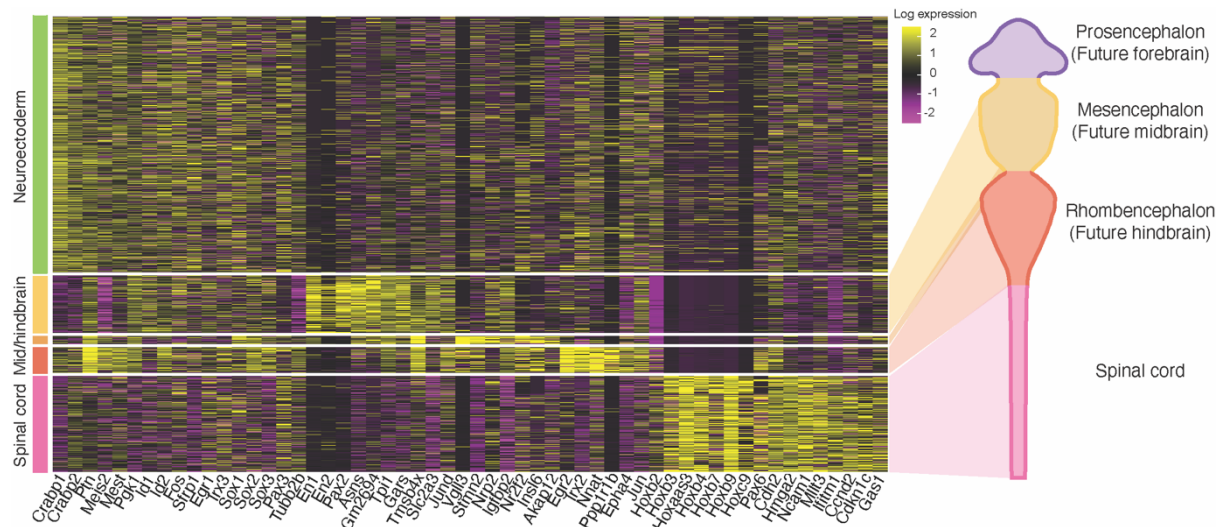
Figure 29. Regionalized cell types along anterior-posterior axis of neural tube organoid. Heatmap with scaled gene expression of the main cell types found in the neural tube organoid showing the regional identity from midbrain to spinal cord of the neural tube *in vivo*. The neuroectoderm cluster shows *Crabp1*, *Crabp2*, *Sox1*, *Sox2*, and *Sox3*, the midbrain cluster shows *En1* and *En2*, the hindbrain cluster shows *Vgll3*, *Egr2, Nnat,* and *Ppp1r1b,* and the spinal cord cluster shows various Hox genes and *Pax6* as its top markers.

Here, I was able to demonstrate a link between the two differential cell types in the elongating neural tube organoids only as well as their appropriate Hox genes expression. Accordingly, I used scRNAseq and qPCR to better characterize such expression patterns and to verify whether this expression has spatial pattern using ISH. As shown in **Figure 30A**, anterior Hox genes were indeed expressed in the majority of the cells composing the organoids, and the posterior Hox genes were expressed in more restricted cell populations. Notably, the range of Hox gene expression found in the organoids spanned from Hox1 to Hox9, corresponding to regions of the embryonic neural tube ranging from the cervical to beginning of lumbar levels[9]. The same range of Hox genes expression could be confirmed by qPCR analysis (**Figure 30B**).
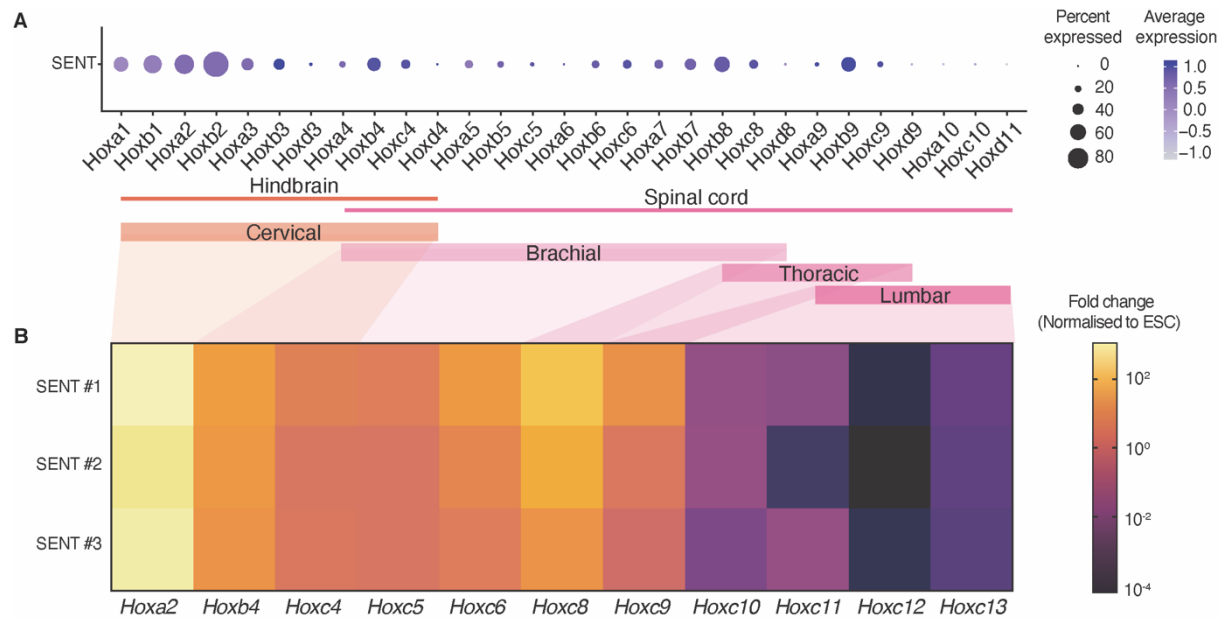
Figure 30. Hox gene expression in SENT. (A) Dot plot showing Hox genes and their expression level in neural tube organoids on D6. The percentage of cells expressing anterior Hox genes is larger but shows lower expression levels, whereas posterior Hox genes are expressed in fewer cells but these show higher expression level. The range of Hox gene expression spans between the cervical level (hindbrain) to the beginning of lumbar level (spinal cord). (B) Reproducible Hox gene expression in three biological replicates of D6 neural tube organoids analyzed by qPCR also range from cervical to the lumbar neural tube level.

To spatially examine Hox gene expression, I performed ISH of the organoids using specific probes against transcripts of the HoxB cluster (**Figure 31**). As expected from scRNAseq results (**Figure 30A, Figure 31A**), *Hoxb1* transcripts could be detected throughout the organoids. Essentially, the more posterior the Hox genes (e.g., *Hoxb4*, *Hoxb9*), the more restricted the signal was toward one end of the organoids (**Figure 31B**).
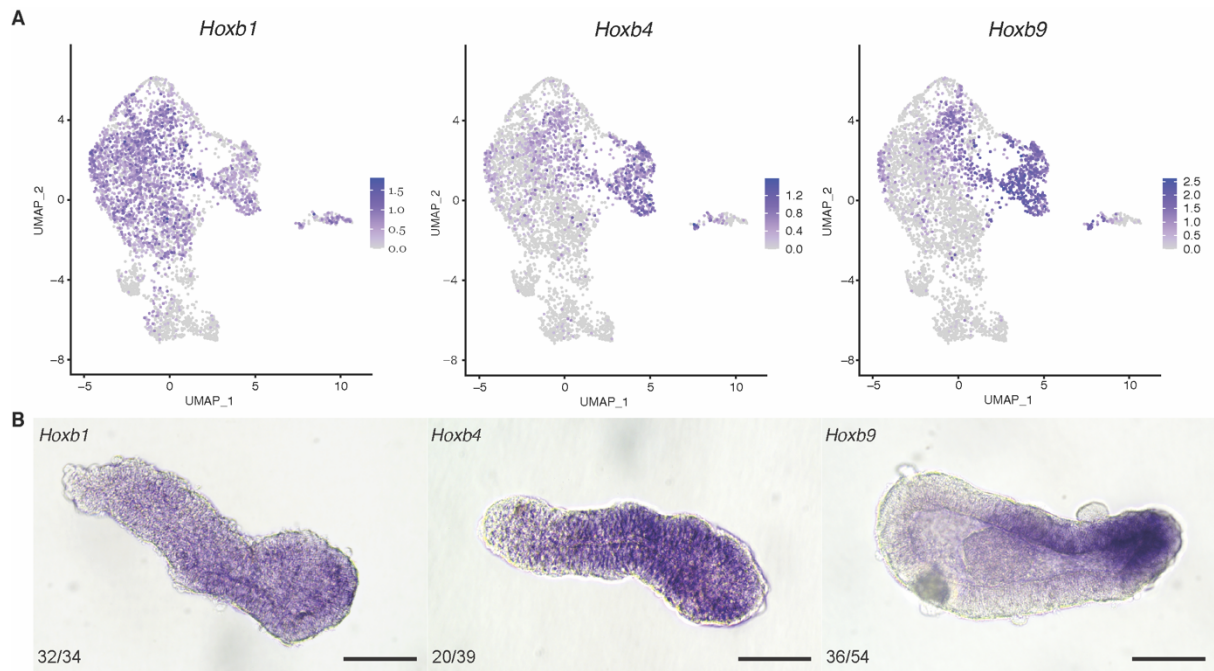
Figure 31. Spatial patterning of Hox genes. (A) UMAP showing HoxB cluster gene expression in D6 organoids. (B) *In situ* hybridization (ISH) of HoxB cluster genes in D6 organoids confirm the spatial distribution of the Hox genes. Anterior genes, *Hoxb1*, spread over the entire organoids tissue, while more posterior genes, *Hoxb4* and *Hoxb9*, are spatially restricted to one end of the tissue. Fractions on the bottom left corner indicate the number of positive samples over the total sample number. Scale bar is 100 μm.

The ISH analysis correlates with the scRNAseq as well as the qPCR findings and thus confirms that these patterns of expression correspond to the spatial AP patterning along the elongation axis of our organoids. Importantly, the self-organizing neural tube organoid with AP patterning could be obtained without the need for artificial posterization, such as through the use of CHIR99021 or RA, as in previous studies[18,22–24]. Collectively, the data suggests that the elongation of SENT is linked to Hox genes which governs the AP patterning.

DV Patterning

In order to understand the variety of cell types involved in DV patterning in the neural tube organoid, I investigated in the DV patterning markers present in the scRNAseq data. Considering the absence of specific DV morphogens in the classical neural tube organoid culture system, I hypothesized the cells would have default dorsal fate as previously reported from other neural tube organoid studies[18,20]. Indeed, I could confirm that no ventral marker genes were detected in the SENT organoid (**Figure 32**) in the scRNAseq data.
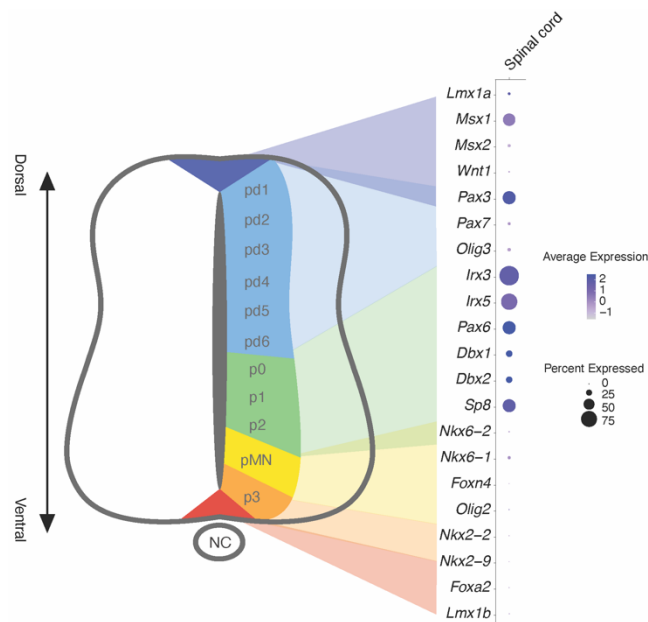

Figure 32. DV patterning markers in spinal cord cluster of SENT organoid. It expresses the genes biased towards the dorsal fate, such as *Msx1*, *Pax3*, *Pax6* and *Irx3* are expressed in the neural tube organoids where no ventral side markers were found.

In consequence, I hypothesized that their cell fates could be directed towards a more ventral fate. To promote ventralization, I chose smoothened agonist (SAG, SHH signalling pathway activator), a small molecule that activates SHH signalling pathway. Upon exposure of SAG at 500 nM SAG from D3 to D5, the naturally dorsal neural tube organoids could be ventralized (**Figure 33A**). qPCR analysis of the organoids for DV patterning marker genes show that the control organoids exhibit standard dorsal identity with low expression of ventral marker genes, while the ventralized organoids

show upregulated ventral marker genes, such as *Olig2*, *Nkx2-2*, *Foxa2*, and *Shh* (**Figure 33B**). Immunostaining images against PAX3/7 (dorsal marker) and OLIG2 (ventral marker) on the neural tube organoids also show that the organoids can acquire a ventral identity at the protein level when exposed to ventral morphogens at an earlier time point (**Figure 33A, Figure 34**).
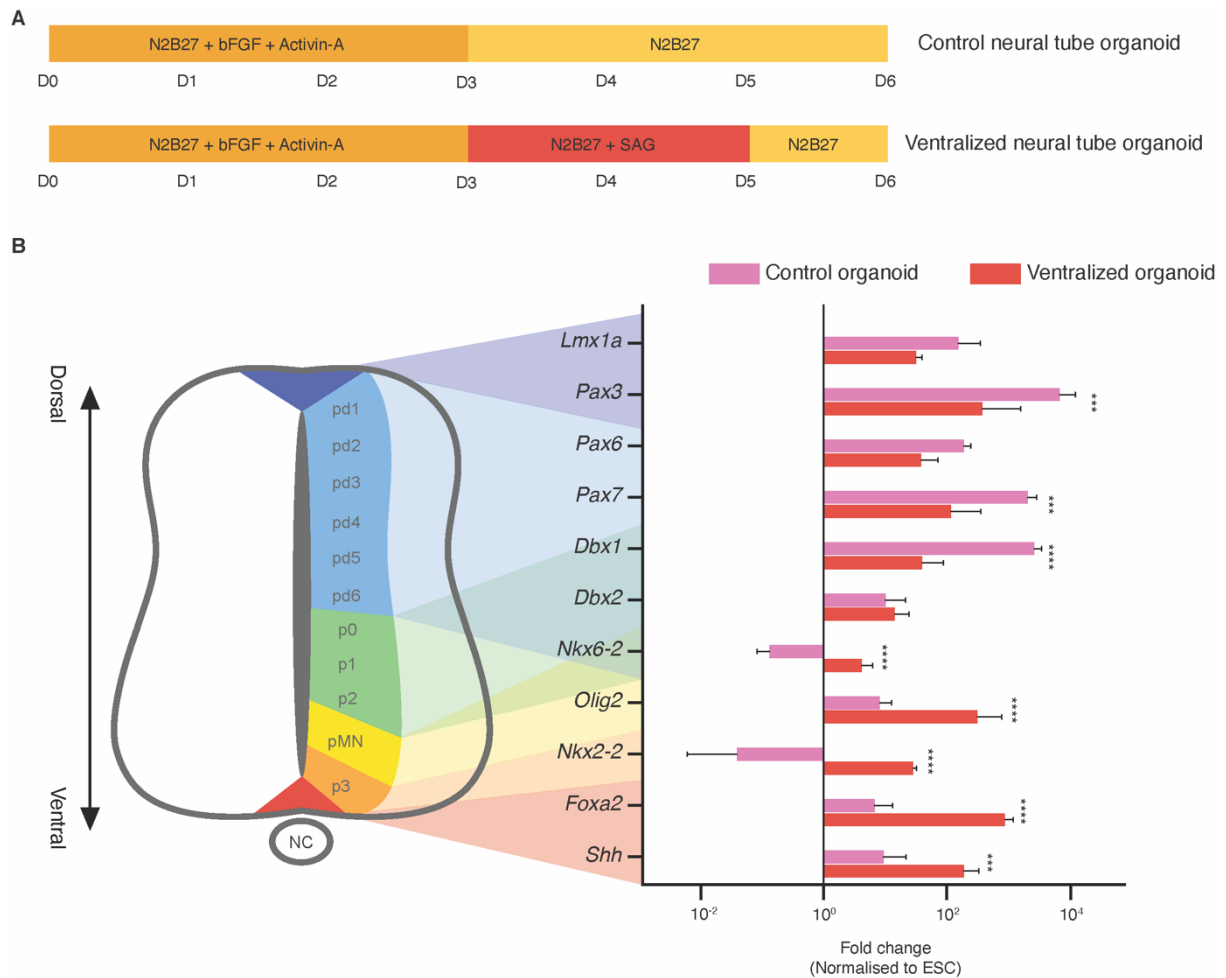

Figure 33. Ventralization of neural tube organoids. (A) Schematic representation of the optimized protocol to ventralize the organoids. After a pre-differentiation in epiblast medium, control neuroepithelial cysts are cultured in N2B27 or in N2B27 with supplemented with 500 nM smoothened agonist (SAG, SHH signalling pathway activator) between D3 and D5 to promote organoid ventralization. (B) qPCR analysis of dorsal-ventral patterning markers of the embryonic neural tube, in control organoid and ventralized organoids. Control organoids show high expression of dorsal markers and low expression of ventral markers, while ventralized organoids show strong upregulation of ventral markers and also retain a substantial expression of dorsal markers. These results shows that the organoids have default dorsal fates unless treated with ventral morphogens. Values are mean ±SEM. Statistical analysis by 2-way ANOVA with Sidak's multiple comparisons test, ***$p<0.001$, ****$p<0.0001$.
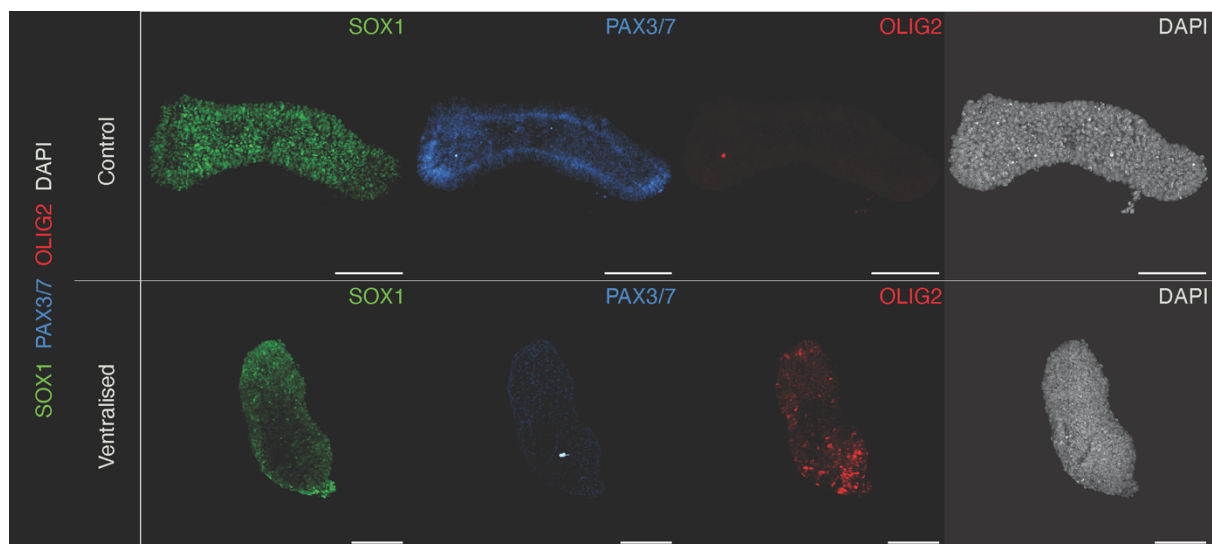
Figure 34. Ventralized neural tube organoids adopt ventral cell fate. Confocal imaging revealed the predominant presence of ventral marker OLIG2 at the protein level in ventralized organoids comparing to the control organoids. This result suggests that selective dorsal or ventral fate of neural tube organoids can be obtained by following according culture condition. All the scale bars are 100 µm.

Based on this result, I could confirm that the cells in neural tube organoid are primed to respond to the ventral morphogens. Thus, I hypothesized that DV patterning of the neural tube organoids via antiparallel morphogen gradient is feasible *in vitro* recapitulating that of *in vivo*. For the initial development of the patterning device, I first assayed the responsiveness of the cells in neural tube organoids to different bulk concentration combinations of the antiparallel morphogens involved in DV patterning. For that, I adopted the classical neural plate explant culture approach used in previous DV patterning studies[14,21]. On D6, I harvested the neural tube organoids and re-embedded them to Matrigel drops at a lower density and cultured them with different concentration combinations of BMP4 (dorsal morphogen) as well as SAG (ventral morphogen) for 18 hours (**Figure 35A**). As PAX3/7 is the flagship dorsal marker and OLIG2 the flagship ventral marker of the neural tube (**Figure 35B**), I quantified the proportion of PAX3/7$^+$ and OLIG2$^+$ expression of confocal images from accordingly immunostained organoids (**Figure 35C, D**). Control neural tube organoids without any morphogen exposure show a clear default dorsal identity, consistent with previous reports[18,20]. Without BMP4 exposure, we observed that the ratio of OLIG2$^+$ over PAX3/7$^+$ pixels increased along with increasing SAG concentration. When organoids were exposed to 500 nM SAG and no BMP4, the organoid showed a ventral identity.

However, with increasing BMP4 concentration, the ratio of PAX3/7[+] over OLIG2^{+} pixels increased accordingly. This shows that the organoids responded to the morphogens in a dose-dependent manner yet without any spatially controlled exposure and the results show the similar trends as the chick embryo explants analysis[14,21]. These results suggest that the organoids can be confidently used as a neural tube tissue model that resemble the cell behavior and responsiveness *in vivo* as an alternative for avian embryo explants.
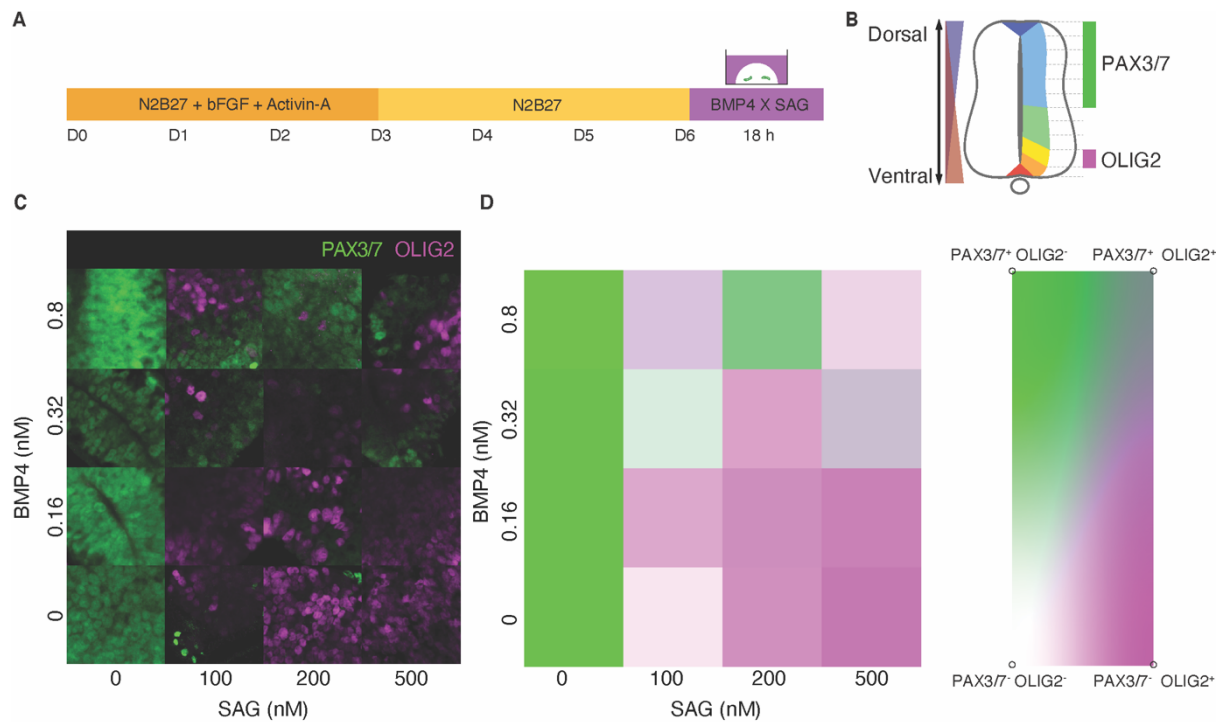

Figure 35. Neural tube organoids respond similarly to the native tissue. (A) Schematic of DV patterning protocol using the traditional approach wherein the organoids were kept in different concentration combinations of BMP4 and SAG. (B) Schematic to show the of dorsal/ventral localization of markers, PAX3/7 and OLIG2, that were used as the readout in this experiment. (C) Confocal microscopy images of organoids cultured in different combination of BMP4 (0, 0.16, 0.32, or 0.8 nM) and SAG (0, 100, 200, or 500 nM) immunostained for dorsal marker PAX3/7 and ventral marker OLIG2. (D) Heatmap of the quantified ratio of PAX3/7[+] pixels and OLIG2^{+} pixels from the images from C.

Next, I explored the possibility to mature the neural organoids in a microfluidic device designed to mimic the tissue patterning driven by anti-parallel morphogen gradients. I developed a microfluidics design able to provide a steep antiparallel gradient of BMP4 and SAG along the perpendicular axis of elongation of the organoid. I expected this novel design to be able to mimic the physiological effect of the morphogen gradient in

the DV patterning. The proposed microfluidic chip includes a novel feature to easily and precisely place any organoid by simply using hydraulic resistance created when loading a gel (**Figure 36**). The key of this device to form steep gradient for the organoid is its small gradient window (**Figure 36A**). Since the gradient is formed by diffusion of the morphogens, it should have a limited space to keep the steep gradient for a long time. For that, the technique enabling to place the organoid at the exact desired spot, at the gradient window, is essential. Hydraulic resistance together with lengthy channels were applied as the mechanism of choice to precisely place the organoids at the desired position (**Figure 36B, Figure 37A**).
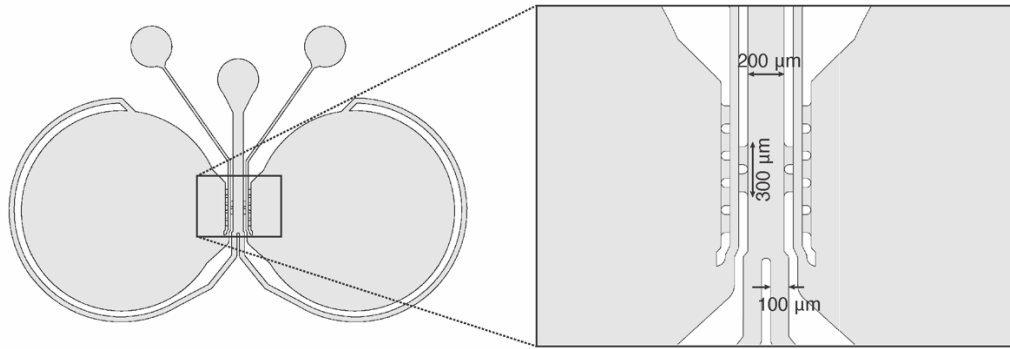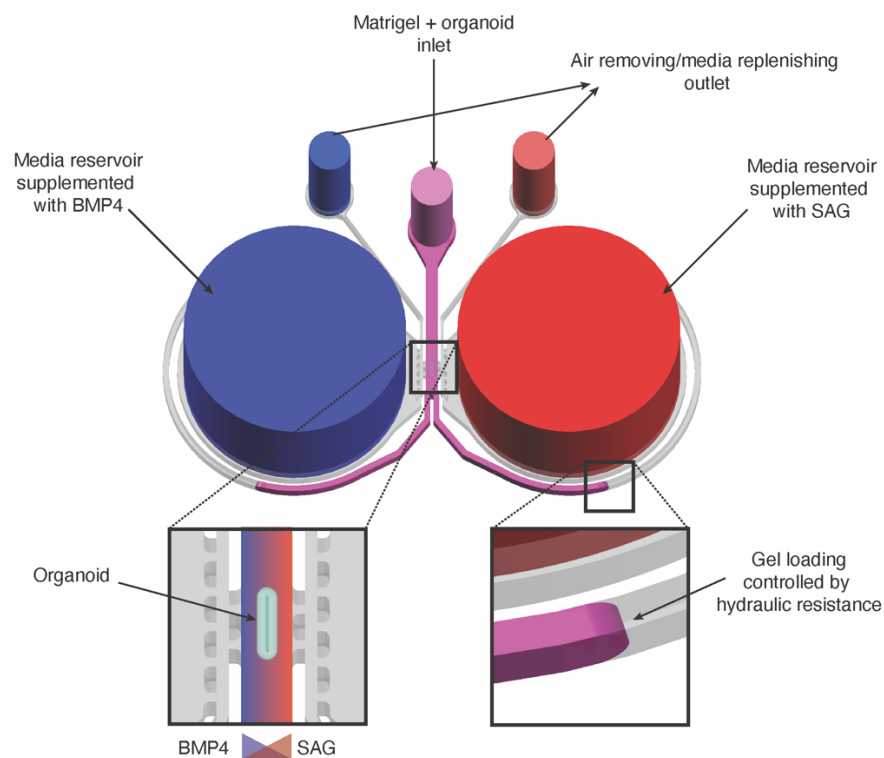
Figure 36. Microfluidic device for DV patterning of neural tube organoids. (A) Overall layout of our novel microfluidic device for DV patterning of neural tube and its dimensions. The width of the organoid loading channel is 200 µm and the gradient window is about 300 µm long where the organoid has to be placed and exposed to the morphogen gradient. After the gradient window, the organoid loading channel divides into two symmetrical channels with 100 µm of width that go around the reservoir and end up connecting to the reservoir of each side. (B) Schematic representation of the key novel features of the microfluidic chip. The organoid loading channel divides into two which increases the total hydraulic resistance of the liquid that brings a mechanical equilibrium in force of loading liquid that the organoid can be precisely placed at a desired spot in a very simple and accurate manner. Also, through the air removing/media replenishing outlet, the residual air in the chip can be easily removed and the media in the reservoir can be replenished to be in contact with the organoid. On each side of the chamber, reservoirs can be filled with two different morphogens in order to guarantee a stable gradient at the gradient window for further patterning the organoid.

Once the microfluidic device was designed, the diffusion of the morphogen on this device was simulated computationally (**Figure 37B**). The simulation result shows the steep of the gradient would be stable over 18 hours along the width of the gradient axis. In addition, I could confirm the simulation results with time-lapse imaging of morphogen-sized fluorophores in the chip (**Figure 37C**). Images captured hourly revealed the diffusion of the fluorophores and confirmed that a linear gradient stabilizes within approximately three hours and is kept over 19 hours (**Figure 37C**). D6 organoids were loaded into the microfluidic devices with Matrigel and placed precisely in the middle of the gradient window to then were exposed to the morphogen gradient for 18 hours (**Figure 37A**).
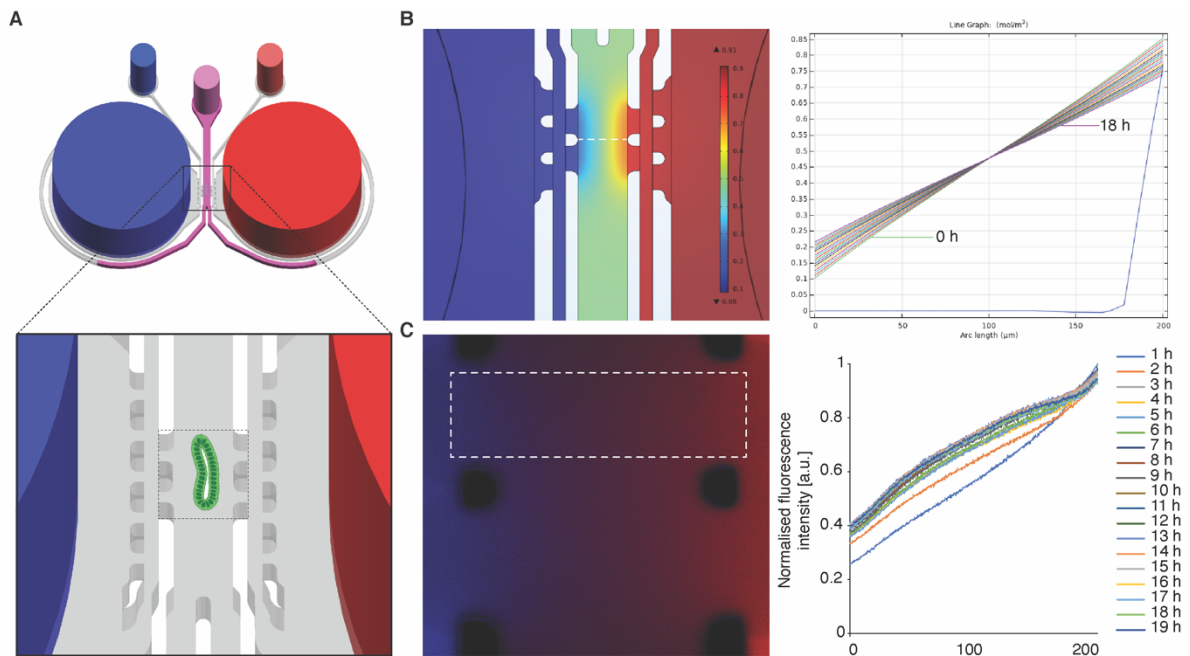
Figure 37. Characterization of gradient formation in the microfluidic device designed for tissue patterning. (A) Scheme of the novel microfluidic chip wherein the organoid can be placed precisely at the gradient window. (B) The diffusion of the morphogens was computationally simulated. (C) A stable gradient formation was experimentally validated by time-lapse imaging of morphogen-sized fluorophore diffusion over 19 hours on a confocal microscope. The fluorescence intensity was quantified every hour.

Upon exposure to the opposing gradient of BMP4 (1.6 nM) and SAG (500 nM), the neural tube organoids showed symmetry-breaking tissue patterning along morphogen gradient axis (**Figure 38A**). The asymmetric expression of PAX3/7 and OLIG2 was quantified and I could show the predominant localization of PAX3/7+ cells towards

BMP4 and OLIG2⁺ cells towards SAG source (**Figure 38B**), using the custom-made image analysis quantification (**Figure 39**).
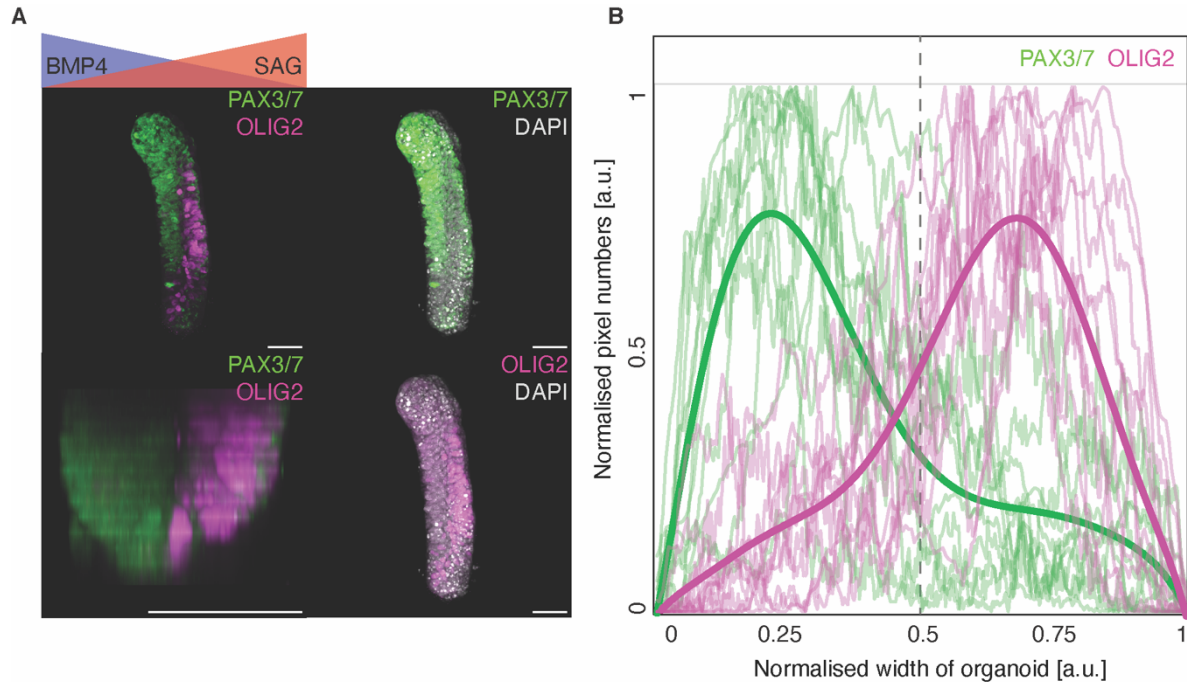
Figure 38. Dorsal-ventral patterning of neural tube organoids. (A) Representative confocal images of the immunostained organoid against PAX3/7 as dorsal marker and OLIG2 as ventral marker shows the symmetry breaking patterning in the organoid along the short axis and directional to the source of the morphogen gradient. (B) The confocal images of immunostained organoids (n=11) were quantified by their profile, and each replicate was plotted along the normalized width of the organoid. The trendline obtained via polynomial regression (degree=6) clearly shows an asymmetric DV patterning in each organoid. Scale bars are 50 µm.
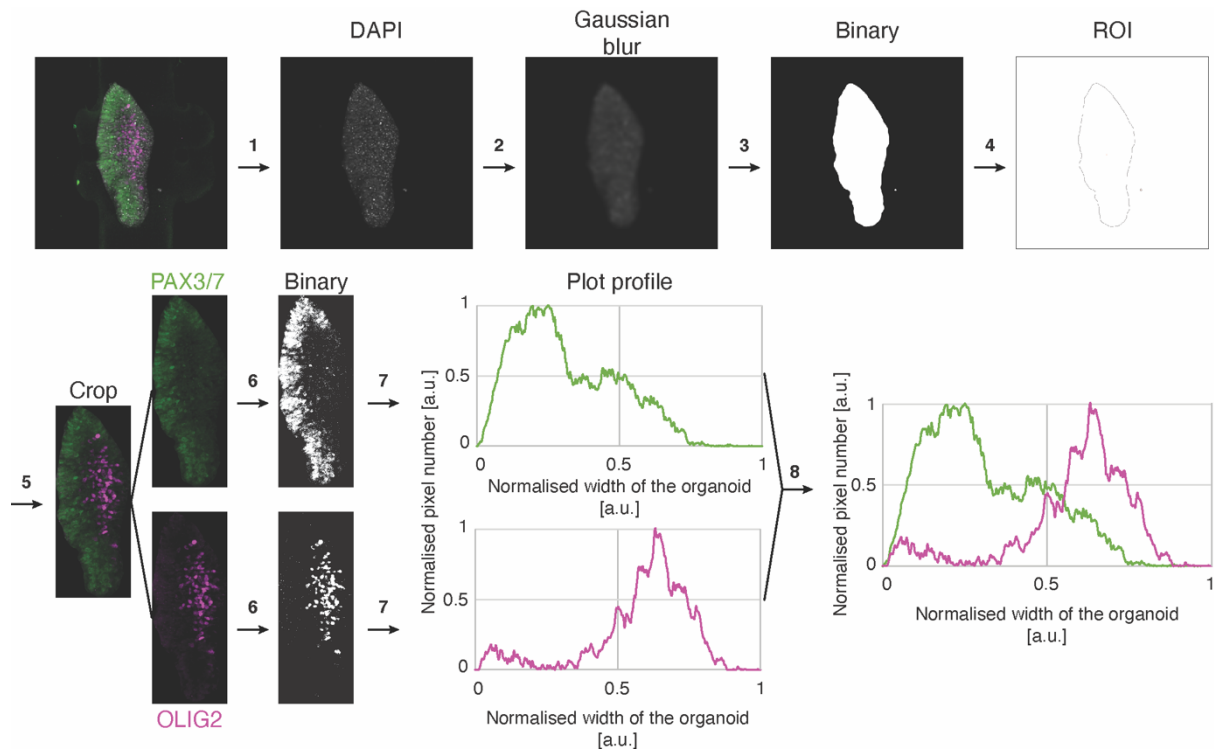
Figure 39. Quantitative analysis pipeline of organoid DV patterning. The immunostained organoids against PAX3/7 in green, OLIG2 in magenta, nuclei (DAPI) in grey were imaged by confocal microscopy in z-stack. The images were projected in maximum intensity and split into each channel (1). The DAPI channel image was filtered by Gaussian blur function (2) and converted to binary images by thresholding the fluorescence intensity (3). Based on this binary image, the outline of the organoid could be obtained and saved as ROI (Region-Of-Interest) region (4). Green and Magenta channel images were cropped based on this ROI region (5) and converted to binary images by thresholding (6). Then, the number of pixels along the width axis of the organoid were normalised to the maximum value of each channel and plotted on the axis of normalised width of the organoid (7). Combining the plots of the two channels evidently shows the clear symmetry-breaking and further DV patterning of the organoids (8).

To verify that the DV patterning requires the anti-parallel gradient, the organoids were exposed to different morphogen combinations in the same microfluidic setup (**Figure 40**). The control neural tube organoid without any morphogen exposure (N2B27 (left; L) - N2B27 (right; R)) shows a standard dorsal identity. When the neural tube organoids were exposed to either BMP4 (BMP4 (L) - N2B27 (R)) or SAG (N2B27 (L) - SAG (R)), they showed fully biased dorsal PAX3/7[+] identity or ventral OLIG2^{+} identity, respectively. In contrast, when the organoids were exposed to an antiparallel morphogen gradient of BMP4 and SAG (BMP4 (L) - SAG (R)), the organoids showed

expression of PAX3/7 towards the BMP4 source (L) and of OLIG2 towards the SAG source (R).
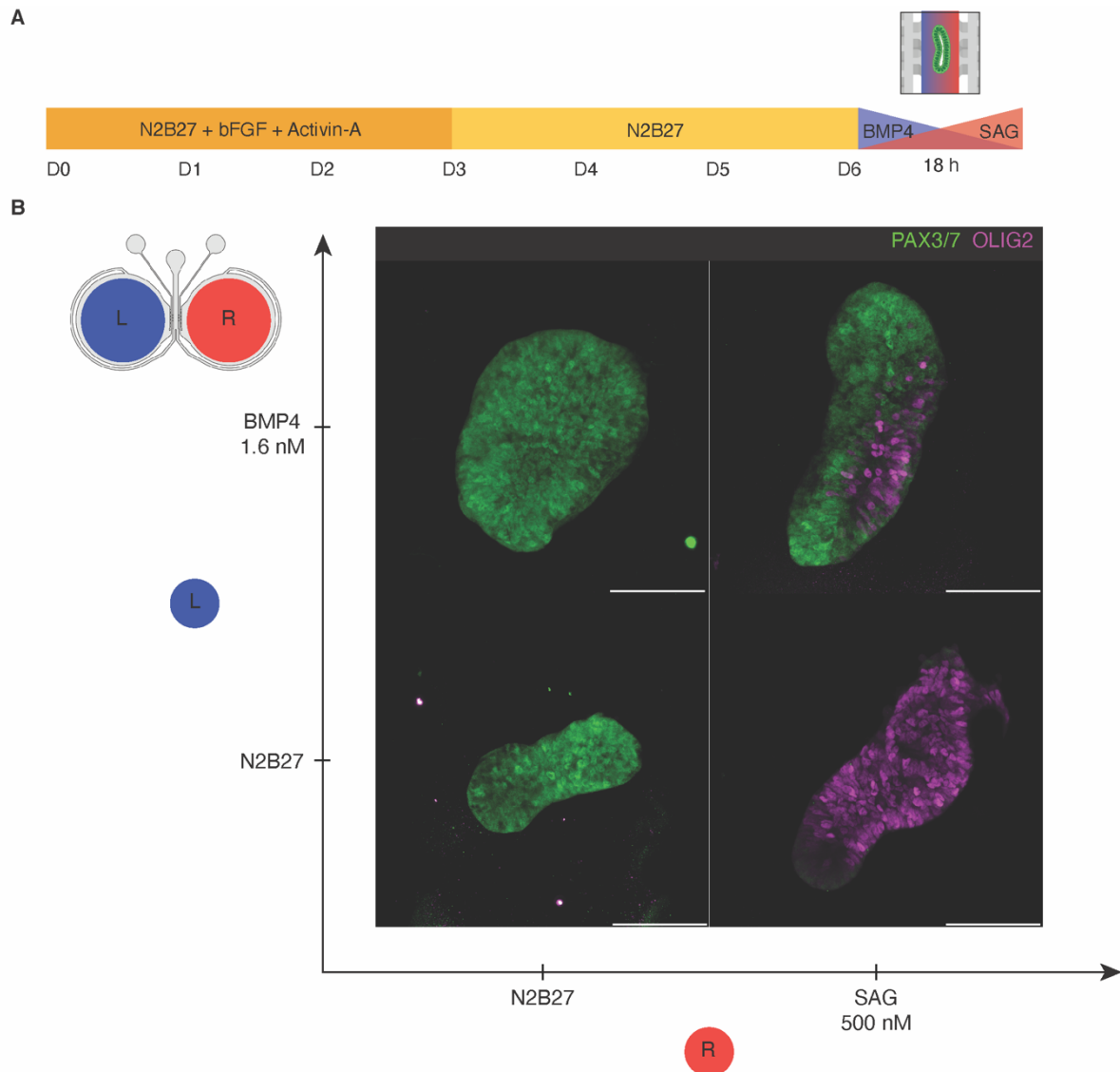
Figure 40. Neural tube organoids respond to morphogen gradient as of _in vivo_. Neural tube organoids from D6 were introduced into the microfluidic devices and exposed to different morphogen gradient for 18 hours. The control organoid with no morphogen exposure (N2B27 (Left; L) – N2B27 (Right; R)) shows a default dorsal identity expressing only PAX3/7+ cells. The organoid exposed only to dorsal morphogen BMP4 (1.6 nM BMP4 (L) – N2B27 (R)) also shows the dorsal identity expressing PAX3/7. Meanwhile, the organoid exposed to ventral morphogen SAG (N2B27 (L) – 500 nM SAG (R)) shows dominant ventral identity expressing OLIG2. Finally, the organoid exposed to the anti-parallel gradient of BMP4 and SAG (1.6 nM BMP4 (L) – 500 nM SAG (R)) shows symmetry-breaking patterning along the gradient axis expressing PAX3/7 biased to the left side and OLIG2 biased to right side. Scale bars are 100 μm.

All together, these results indicate that the cells composing the neural tube organoids are able to form an *in vivo*-like pattern along the axis of the morphogen gradient by differentiating into the appropriate cell type according to spatial morphogen combination. Moreover, I could combine a novel microfluidic design together with the neural tube organoids to demonstrate, for the first time, the morphogen-driven symmetry–breaking-patterning on an organoid *in vitro*.

Conclusion

The self-elongating neural tube organoids do not only mimic the morphology of the neural tube *in vivo*, but can also induce a regionalization of its components along the specific elongation axis. The cell types detected to be exclusively found in elongating organoids (SENT) comparing to non-elongating ones (NENT). were the hindbrain and spinal cord where Hox genes appear as differentially expressed genes within those cell populations. As Hox genes are known for their important role in providing positional information along AP axis for regionalization, I characterized in depth Hox genes expression in the SENT together with their spatial organisation. Using qPCR analysis, I confirmed that there are high expression levels of Hox genes from the occipital level to the beginning of the lumbar level (from Hox1 to Hox9) and is, however, missing the further ahead posterior part. Moreover, the Hox genes visualization (*Hoxb1*, *Hoxb4*, *Hoxb9*) by ISH revealed that there is a clear spatial organisation where the more posterior sets of Hox genes are found more restrictedly in one end of the organoid. From this data, I could confirm that the elongation of the neural tube is related to a series of Hox gene expression and that has a strong impact on the spatial patterning along the long axis of elongation of SENT organoids. Furthermore, I investigated on the ability of SENT to undergo DV patterning. First, by the comparison between the control SENT organoid versus the ventralized SENT organoids using qPCR, I could confirm that the neural tube organoids without any treatment with DV morphogens have default dorsal fate cell types and can be biased towards ventralization upon exposure to ventral morphogens. In addition, the cellular response in SENT organoids to the different concentration combinations of DV morphogens presented in bulk showed that SENT organoids possess the same dose-dependent cell fate decision capacity as the *in vivo* neural tube epithelial tissue. Finally, I demonstrated that SENT organoid can be precisely patterned by anti-parallel morphogen gradient at the single organoid level using a newly design microfluidic system.

For the first time, I show in the present work the induction of symmetry-breaking events in a single organoid via external morphogen patterning in a spatio-temporal controllable way. I offer a radically new way to provide a steep gradient across the

small width of any organoid that has been kept as a challenge for decades. More importantly, the results prove that the SENT organoids are responsive to the local biomolecular signalling faithfully as the neural tube tissue *in vivo*.

Altogether, SENT organoids show a natural self-AP patterning capacity along their long axis giving rise to regionalized cell types of the brain and the spinal cord. Most strikingly, the cells composing these *in vitro* elongated neural tissues are prone to undergo DV patterning as of the native tissue when exposed to the right morphogen micro-environment thanks to a novel microfluidic approach.

Materials and methods

Culture of mouse embryonic stem cells

Sox1[eGFP];*Bra[mCherry]* double reporter[13] (SBr) and *Sox1[eGFP]* reporter[14] (SG) mouse embryonic stem cells (mESCs) were cultured in DMEM supplemented with 10% serum medium (10% ES-grade fetal bovine serum (FBS), 0.1 mM non-essential amino acids (NEAA), 1 mM sodium pyruvate, 3.44 mM GlutaMax, 0.1 mM beta-mercaptoethanol (β-ME), 100 U/mL Penicillin, 100 µg/mL Streptomycin) with 2i (3 µM Chorong, 1 µM PD025901) and 100 µg/mL WIFI in a humidified incubator (5% CO_2, 37 °C). The cells were split every other day, by washing with PBS-/- and dissociating with Accutase for 2 min in room temperature. The cell suspension was collected in a tube and was centrifuged at 200 x g for 5 min. After centrifugation, the cell pellet was resuspended in 1 mL of 10% serum medium and the cells were counted with a haemocytometer. 85,000 cells were plated in 2 mL of 10% serum medium with 2i and LIF per each well of 6 well plate (Corning) and cultured in the humidified incubator. The cells were passaged every 2 days.

Neural tube organoid culture

mESCs were collected by washing with PBS-/- and dissociating with Accutase for 2 min at room temperature. The cell suspension was collected in a centrifuge tube and was centrifuged at 200 x g for 5 min. After centrifugation, the cell pellet was resuspended in 1 mL of 10% serum medium and the cells were counted with a haemocytometer. After cell counting, the cells were washed twice with PBS-/- and were resuspended in N2B27 (47.4% Neurobasal™ Medium, 47.4% DMEM/F-12 with 2.50mM GlutaMAX™, 1 mM GlutaMAX™ Supplement, 100 U/mL Penicillin, 100

μg/mL Streptomycin, 0.1 mM NEAA, 1 mM Sodium Pyruvate, 0.1 mM β-ME, 1% B27 Supplement, 0.5% N-2 Supplement) and embedded in Matrigel to a final concentration of 1125 cells/10μL of Matrigel drop for SBr and 1000 cells/10μL of Matrigel drop for SG. 10 μL of the resulting Matrigel-embedded cell suspension were deposited in each well of a 24 well plate (Corning). The cells in each well were cultured in 500 μL of Epi medium (N2B27 supplemented with 12 ng/mL basic Fibroblast Growth Factor (bFGF, Thermofisher, Cat#PMG0031) and 20 ng/mL activin-A, R&D Systems, Cat#338-AC-010) for the first three days. On D3, the Epi medium of each well was substituted with 1 mL of N2B27. The medium of each well was substituted with 1 mL of N2B27 on D5 and the cells were cultured until D6.

Probe production for *in situ* hybridization

The RNA of the organoids was extracted following the same protocol for quantitative PCR. The extracted RNA was used for retro-transcription using SuperScript Vilo cDNA synthesis kit according to the manufacturer's instructions. CDNA PCR amplification was performed using Phusion DNA polymerase (Cat# M0541S) and primers including T7 promoter sequence according to the manufacturer's instructions. The PCR product was purified using Qiagen MinElute PCR purification kit (Cat# 28004) and the concentration was measured with NanoDrop. 1.5 μg of cDNA was used for *in vitro* transcription using 5X Promega transcription buffer, 100 mM DTT, T7 RNA polymerase (Cat# P2075), RNAsin, and digoxigenin (DIG) labelling mix (Roche, Cat# 11277073910). The probes were purified using Qiagen RNAeasy microplus kit (Cat# 74034).

Whole mount *in situ* hybridization

Whole mount *in situ* hybridization was performed as previously described[23], with some modification. The collected organoids were fixed in 4% PFA at 4 °C for 4 hours or overnight. The fixed organoids were washed with TBS-T (20 mM Tris 137 mM NaCl, 2.7 mM KCl, 0.1% Tween, pH=7.4). The organoids were digested in 1.25 μg/mL

Proteinase K (Roche, Cat# REF03115844001) in TBS-T for 2 min, briefly washed three times with 2 mg/mL Glycine solution in TBS-T, washed with TBS-T for 3 min. The organoids were refixed in 4% PFA for 20 min and washed 5 times of 5 minutes in TBS-T. After post-fixation, the organoids were prehybridized at 68 °C for 4 hours in Hybmix (1.33X SSC; 50% deionized formamide; 10mM EDTA pH 8; 0.1% Tween®-20; 0.1% blocking reagent; 5 mg/mL torula RNA, 125 µg/mL heparin) and hybridized with DIG-labelled probes of 200 ng/mL at 68 °C overnight with agitation (**Table 7**). The next day, the organoids were washed at 68 °C in Hybmix and in 0.1% Tween®-20 2xSSC. The organoids were washed at room temperature in MABT (100 mM maleic acid, 150 mM NaCl, 0.1% Tween, pH 7.5) prior to incubation with blocking buffer (10% Goat serum, 1% blocking reagent in MABT) for 1.5 hours in room temperature. Subsequently, DIG-labelled probes were targeted using anti-DIG antibody coupled to alkaline phosphate (Roche, Cat#093274) at 1:3000 dilution in blocking solution for 4 hours at room temperature. Non-specific antibody background was removed by washing overnight in MABT. The next day, the organoids were washed 3 times of 5 min with TBS-T in alkaline phosphatase buffer (0.1M Tris pH 9.5, 100 mM NaCl, 0.1% Tween) and stained with BM purple solution (Roche, #REF 11442074001) without being exposed to light. After staining, the organoids were washed 3 times of 5 min with TBS-T, fixed in 4% PFA for 20 min in room temperature, and stored in TBST.

	Forward	**Reverse**	**Digest with**	**Transcribe with**
Hoxb1	CTTAGCCCAACTCTTCTTTC	GGAAACTCTGTCACCATTC	- (PCR direct probe synthesis)	T7
Hoxb4	GCCCATCTGTCTTGTTTAC	CTGCAACATTGTCCTTCC	- (PCR direct probe synthesis)	T7
Hoxb9	-	-	Ncol	Sp6

The probes for *Hoxb9* were provided by Denis Duboule lab, EPFL, Switzerland.

Table 7. Primer sequences used for whole mount *in situ* hybridisation

Single-cell RNA sequencing data analysis

Single cell RNA sequencing data analysis was performed using Seurat 3.0.3[25] with raw feature-barcode matrices of D3 (the organoids on D3), SENT (self-elongating neural tube organoids), and NENT (non-elongating neural tube organoids). Genes expressed in less than 3 cells and cells with less than 200 features expressed were removed. Cells with unique feature counts between 3500 and 7500, less than 7.5% mitochondrial counts were used for analysis. Expression level was log normalized, and the top 2,000 variable genes were calculated using Variance Stabilizing Transformation (VST) algorithm[26]. Three datasets were merged and integrated with the dimension of 1:30. After the integration, the effects of the batch ID, cell cycle, nUMI, and mitochondrial counts were regressed out. The number of cells after filtering was 2185 (D3), 2076 (SENT), and 2225 (NENT). We scaled the data applying a linear transformation and performed principal component analysis (PCA) on the scaled data. Clusters of cells were identified by a shared nearest neighbour (SNN) modularity optimization-based Louvain algorithm with a resolution of 1.0[27]. Clusters were visualized on a two-dimensional Uniform Manifold Approximation and Projection (UMAP)[28]. Cell type of each cluster was identified based on the markers of each cluster expressing more than 0.25 $\log_2$ fold-change different over the others. Also, the markers of each clusters were used for gene ontology (GO) analysis using R package clusterProfiler[29]. To estimate RNA velocity of each cell, velocyto.py[30] was used to generate loom files for each datasets used for Seurat analysis. To do so, the bam file of each dataset produced by Cell Ranger (10X Genomics) and gtf file from 10X Genomics for annotation were used. To integrate the loom file and the Seurat object in R, meta-data like filtered cell IDs, UMAP coordinates, and clusters were extracted. Once the loom files were generated, the loom files and the meta-data were integrated and RNA velocity could be estimated based on the same UMAP coordinates and clusters using scVelo[31].

Ventralization of the neural tube organoid

mESCs were collected by washing with PBS-/- and dissociating with Accutase for 2 min at room temperature. The cell suspension was collected in a centrifuge tube and was centrifuged at 200 x g for 5 min. After centrifugation, the cell pellet was resuspended in 1 mL of 10% serum medium and the cells were counted with a haemocytometer. After cell counting, the cells were washed twice with PBS-/- and were resuspended in N2B27 (47.4% Neurobasal™ Medium, 47.4% DMEM/F-12 with 2.50mM GlutaMAX™, 1 mM GlutaMAX™ Supplement, 100 U/mL Penicillin, 100 µg/mL Streptomycin, 0.1 mM NEAA, 1 mM Sodium Pyruvate, 0.1 mM β-ME, 1% B27 Supplement, 0.5% N-2 Supplement) and embedded in Matrigel to a final concentration of 1125 cells/10µL of Matrigel drop for SBr and 1000 cells/10µL of Matrigel drop for SG. 10 µL of the resulting Matrigel-embedded cell suspension were deposited in each well of a 24 well plate (Corning). The cells in each well were cultured in 500 µL of Epi medium (N2B27 supplemented with 12 ng/mL basic Fibroblast Growth Factor (bFGF, Thermofisher, Cat#PMG0031) and 20 ng/mL activin-A, R&D Systems, Cat#338-AC-010) for the first three days[32,33]. On D3, the Epi medium of each well was substituted with 1 mL of N2B27 supplemented with 500 nM smoothened agonist (SAG, Sigma Aldrich, Cat# 566660). The medium of each well was substituted with 1 mL of N2B27 on D5 and the cells were cultured until D6.

Gene expression analysis by quantitative PCR

The collected organoids were washed with PBS-/- and resuspended in lysis buffer. RNA was extracted immediately using the RNAeasy micro kit (Qiagen, Cat#74004) according to the manufacturer instructions with on-column DNase I (Qiagen) digestion. The extracted RNA concentration was measured using NanoDrop. cDNA was synthesised using iScript™ cDNA Synthesis Kit (BIORAD, Cat# 170-8891) according

to the manufacturer's instructions using 1 µg of RNA of each sample replicate in Biorad thermocycler. Quantitative PCR analysis of mRNA levels for the genes on Primer list was performed using *Power* SYBR™ Green PCR Master Mix (ThermoFisher Scientific, Cat# 4367659) on Applied Biosystems Quantstudio 6 Flex Real-Time PCR system. PCR primers were designed using NCBI Primer-Blast software (**Table 8**). Expression values of each gene was normalized to Gapdh expression value of each sample replicate using delta-delta CT method. The graph was plotted using Prism 8 (GraphPad) and error bars represent the standard deviation across three biological replicate samples.

Probe	Primer Forward	Primer Reverse
Hoxa2	CTC GGC CAC AAA GAA TCC CT	GGG GTC TGC AAA GGT ACT TG
Hoxb4	CAC GGT AAA CCC CAA TTA CGC	CGC GTC AGG TAG CGA TTG
Hoxc4	AGC ACG GTG AAC CCC AAT TA	GGC GAT CTC GAT CCT TCT CC
Hoxc5	ATG AGC CAC GAG ACG GAT G	GCG AGT GAG GTA GCG GTT AAA
Hoxc6	ACA CAC AGA CCT CAA TCG CT	ACC CCA CTG TGC GAA TTC AT
Hoxc8	GAT GAG ACC CCA CGC TCC T	CTT CAA TCC GGC GCT TTC TG
Hoxc9	GGA CCC TAG CAA CCC CGT	CGA CGG TCC CTG GTT AAA TAC A
Hoxc10	GTT TTG GGG TGT TGT GTG TG	TTG CAT GGA GAA CAG AAT GC
Hoxc11	CCG TCT CTT CCT TCC TAC CC	CGA GTA GCT GTT CCG ATG GT
Hoxc12	GCG AGT TTC TGG TCA ACG A	TTT TCA TTC TCC GGT TCT GG
Hoxc13	TCC CTG TTG AAG GCT ACC AG	CTC ACT TCG GGC TGT AGA GG
Lmx1a	CCC TTG TCT GGA CTC TAC CC	CGG TTG AGT CTA GCT TCC CG
Pax3	TGC CCA CAT CTC AGC CCT AT	AAT GAA AGG CAC TTT GTC CAT ACT
Pax7	CGA CTC CGG ATG TGG AGA AAA	TCT GAG CAC TCG GCT AAT CG
Dbx1	AAG CCC TGG AGA AGA CGT TC	CGC CAT TTC ATG CGT CGA TT
Dbx2	CCG AAG GAT GAA ATG GCG GA	TGG CTG GGA GAC TTC CCA TA
Nkx6-2	AGT ATT TGG CAG GCC CAG AG	GCT TCT TTT TAG CCG ACG CC
Olig2	TTA CAG ACC GAG CCA ACA CC	TGG CCC CAG GGA TGA TCT AA
Nkx2-2	GGT TCC AGA ACC ATC GCT ACA	TCC ACC TTG CGG ACA CTA TG
Foxa2	TTT AAA CCG CCA TGC ACT CG	CTC ACG AAA GAG TAG CCC TC
Shh	ATG TGT TCC GTT ACC AGC GA	ATA TAA CCT TGC CTG CCG CT
Gapdh	GCA CAG TCA AGG CCG AGA AT	GTG GTT CAC ACC CAT CAC AA

Table 8. Primer sequences used for quantitative PCR

Response assay of neural tube organoid cells to DV patterning morphogens

To harvest the organoids, on D6, the Matrigel drops with organoids were washed once with PBS and then treated with 3 mg/mL Collagenase IV and 1 mg/mL Dispase in HBSS+/+ for 30 minutes on a shaker to dissolve the Matrigel. After Matrigel was dissolved, the organoids were collected with cut 1000 µL pipette tips coated with 10% serum and centrifuged at 900 rpm for 5 minutes. The supernatant was removed and the organoids were suspended in N2B27 medium. The organoids were collected and re-embedded in 10 µL of Matrigel and plated on glass-bottom 24 well plate and further cultured in N2B27 medium in 5% CO_2 and 37 °C incubator. To investigate the effect of the DV patterning morphogens on cell differentiation of the organoid, the medium was supplemented with various concentration combination of BMP4 (BioLegend, Cat#595302, 0, 0.16, 0.32, 0.8 nM) as a dorsal morphogen and SAG (0, 100, 200, 500 nM) as a ventral morphogen and cultured in the for 18 hours in 5% CO_2 and 37 °C incubator.

Microfluidic device fabrication

The chip design was generated using CleWin (v3, Phoenix Software). The microfluidic device was fabricated using standard photolithography and soft lithography methods from Center of MicroNanoTechnology (CMi, EPFL). The first layer for gel loading channel was 150 µm and second layer for phase guidance was 50 µm thickness of SU-8. Once the master mold is fabricated, the wafer was treated with vaporized trichloro(1H, 1H, 2H, 2H-perfluorooctyl) silane (Sigma) for overnight. Using standard soft lithography methods, PDMS (Sylgard 184, Dow Corning) mold was made from the master mold and was punched with biopsy punchers. Then, PDMS chips were plasma-bonded onto 0.5mm-thck glass cover slips (TEDPELLA) using plasma treatment machine (Femto, diener electronic). Finally, PDMS Chips were sterilized with UV and kept at 37°C under humidified air prior to use.

Time-lapse imaging of gradient formation in microfluidic device

To characterize the gradient formation in microfluidic device, time-lapse imaging was performed to capture the diffusion of fluorophore every hour. First, Matrigel was loaded into the gel-loading channel and filled the gradient window chamber. A small drop of N2B27 medium was placed in each medium reservoir for humidification and the chip was incubated in 5% CO_2 and 37 °C incubator for 5 minutes to let the Matrigel polymerise. After, the reservoirs were filled with N2B27 media supplemented with 10 mg/mL of 20 kDa FITC or 40 kDa TexasRed and residual air in the chip was removed from the air outlets. The device with the organoid were incubated in 5% CO_2 and 37 °C incubator for 19 hours. The image was taken every hour with multiple z-stack by LSM700 (Zeiss) on Inverted Zeiss AxioObserver Z1 (Bioimaging and Optics Core Facility, EPFL), equipped with 20×/0.80 air 488-nm and 555-nm and controlled by ZEN 2010 imaging software (Zeiss). Images were analyzed using FIJI (NIH). Before the imaging, the incubation chamber on the microscope was thermally stabilized for 2 hours with the microfluidic chip and the fluorophore solution inside.

DV patterning of neural tube organoid in microfluidic device

The harvested organoids by dissolving the Matrigel drop on D6 were suspended in Matrigel and loaded into the culture chamber and were placed at the gradient window in the middle of the chip. A small drop of N2B27 medium was placed in each medium reservoir for humidification and the chip was incubated in 5% CO_2 and 37 °C incubator for 5 minutes to let the Matrigel polymerise. After, the reservoirs were filled with N2B27 media supplemented with 1.6 nM of BMP4 or 500 nM of SAG and residual air in the chip was removed from the air outlets. The device with the organoid were incubated in 5% CO_2 and 37 °C incubator for 18 hours. For imaging, we used SG mESCs-based neural tube organoids to secure two channels available to detect the fluorescent signals from either dorsal or ventral marker from immunostained samples.

Immunostaining and confocal microscopy

The organoids embedded in Matrigel drop or in microfluidic device were washed with PBS-/- twice and fixed in 4% paraformaldehyde (PFA) in PBS-/- for 30 min in room temperature. After, the organoids were washed with PBS-/- for three times of 20 min and treated with 0.3 M Glycine in PBS-/- for 2 hours in room temperature. Then, the organoids were permeabilized and blocked with PBS-FT (0.2% Triton-X 100 and 10% FBS in PBS-/-) for 3 hours to overnight 4 °C. Primary antibody solution (**Table 9**) was prepared in PBS-FT (following the dilution ratio on **Table 9**) with 2 µg/mL of DAPI. The organoids were stained overnight on a low-speed orbital shaker in 4 °C. The organoids were thoroughly washed with PBS-/- every 30 min for 4 hours to remove the residual primary antibody. Secondary antibody solution (**Table 10**) was prepared, treated, and washed the same way as primary antibody solution (following the dilution ratio on **Table 10**). Confocal images of organoids were generated using LSM700 (Zeiss) on Inverted Zeiss AxioObserver Z1 (Bioimaging and Optics Core Facility, EPFL), equipped with 10×/0.30 air, 20×/0.80 air, and 63×/1.40 oil objectives, 405-nm, 488-nm, 555-nm and 639-nm lasers and controlled by ZEN 2010 imaging software (Zeiss). Images were analyzed using FIJI (NIH).

Target	Species	Dilution	Cat. No.	Supplier
PAX3/7	mouse	1:200	sc-365843	Santa Cruz Biotechnology
OLIG2	rabbit	1:500	AB9610	Millipore

Table 9. Primary antibodies used in immunostaining

	Dilution	Cat. No	Supplier
Donkey anti-mouse Alexa Fluor 568	1:500	A-10037	ThermoFisher Scientific
Donkey anti-rabbit Alexa Fluor 647	1:500	A-31573	ThermoFisher Scientific

Table 10. Secondary antibodies and dyes used in immunostaining

Image analysis-based quantification of DV patterned organoid

Image analysis was done on FIJI (NIH). The immunostained organoids against PAX3/7 in green, OLIG2 in magenta, nuclei (DAPI) in grey were imaged by confocal microscopy in z-stack. The images were projected in maximum intensity and split into each channel. The DAPI channel image was filtered by Gaussian blur function and converted to binary images by thresholding the fluorescence intensity. Based on this binary image, the outline of the organoid could be obtained and saved as ROI (Region-Of-Interest) region. Green and Magenta channel images were cropped based on this ROI region and converted to binary images by thresholding. Then, the number of pixels along the width axis of the organoid were normalised to the maximum value of each channel and plotted on the axis of normalised width of the organoid. Combining the plots of the two channels evidently shows the clear DV patterning of the organoid in symmetry-breaking manner. Finally, the trendline of combined plots were generated by polynomial regression (degree=6) to visualize the general tendency.

Acknowledgement

Reference

1. Kiecker, C. & Lumsden, A. The Role of Organizers in Patterning the Nervous System. *Annu. Rev. Neurosci.* **35**, 347–367 (2012).

2. Briscoe, J. & Small, S. Morphogen rules: design principles of gradient-mediated embryo patterning. *Development* **142**, 3996–4009 (2015).

3. Schilling, T. F. Anterior-posterior patterning and segmentation of the vertebrate head. *Integrative and Comparative Biology* **48**, 658–667 (2008).

4. Yamaguchi, T. P. Heads or tails: Wnts and anterior–posterior patterning. *Current Biology* **11**, R713–R724 (2001).

5. Aulehla, A. & Pourquie, O. More Than Patterning—Hox Genes and the Control of Posterior Axial Elongation. *Developmental Cell* **17**, 439–440 (2009).

6. Deschamps, J. & Duboule, D. Embryonic timing, axial stem cells, chromatin dynamics, and the Hox clock. *Genes Dev.* **31**, 1406–1416 (2017).

7. Deschamps, J. & van Nes, J. Developmental regulation of the Hox genes during axial morphogenesis in the mouse. *Development* **132**, 2931–2942 (2005).

8. Forlani, S., Lawson, K. A. & Deschamps, J. Acquisition of Hox codes during gastrulation and axial elongation in the mouse embryo. *Development* **130**, 3807–3819 (2003).

9. Philippidou, P. & Dasen, J. S. Hox Genes: Choreographers in Neural Development, Architects of Circuit Organization. *Neuron* **80**, 12–34 (2013).

10. Dessaud, E., McMahon, A. P. & Briscoe, J. Pattern formation in the vertebrate neural tube: a sonic hedgehog morphogen-regulated transcriptional network. *Development* **135**, 2489–2503 (2008).

11. Le Dréau, G. & Martí, E. Dorsal-ventral patterning of the neural tube: A tale of three signals. *Devel Neurobio* **72**, 1471–1481 (2012).

12. Jessell, T. M. Neuronal specification in the spinal cord: inductive signals and transcriptional codes. *Nat Rev Genet* **1**, 20–29 (2000).

13. Wilson, L. & Maden, M. The mechanisms of dorsoventral patterning in the vertebrate neural tube. *Developmental Biology* **282**, 1–13 (2005).

14. Dessaud, E. *et al.* Interpretation of the sonic hedgehog morphogen gradient by a temporal adaptation mechanism. *Nature* **450**, 717–720 (2007).

15. Sagner, A. & Briscoe, J. Establishing neuronal diversity in the spinal cord: a time and a place. *Development* **146**, dev182154 (2019).

16. Libby, A. R. G. *et al.* Axial elongation of caudalized human organoids mimics aspects of neural tube development. *Development* **148**, dev198275 (2021).

17. Veenvliet, J. V. *et al.* Mouse embryonic stem cells self-organize into trunk-like structures with neural tube and somites. *Science* **370**, eaba4937 (2020).

18. Meinhardt, A. *et al.* 3D Reconstitution of the Patterned Neural Tube from Embryonic Stem Cells. *Stem Cell Reports* **3**, 987–999 (2014).

19. Ranga, A. *et al.* Neural tube morphogenesis in synthetic 3D microenvironments. *Proc Natl Acad Sci USA* **113**, E6831–E6839 (2016).

20. Zheng, Y. *et al.* Dorsal-ventral patterned neural cyst from human pluripotent stem cells in a neurogenic niche. *Sci. Adv.* **5**, eaax5933 (2019).

21. Zagorski, M. *et al.* Decoding of position in the developing neural tube from antiparallel morphogen gradients. *Science* **356**, 1379–1383 (2017).

22. Ranga, A. *et al.* Neural tube morphogenesis in synthetic 3D microenvironments. *Proc Natl Acad Sci USA* **113**, E6831–E6839 (2016).

23. Beccari, L. *et al.* Multi-axial self-organization properties of mouse embryonic stem cells into gastruloids. *Nature* **562**, 272–276 (2018).

24. Turner, D. A. *et al.* Anteroposterior polarity and elongation in the absence of extra-embryonic tissues and of spatially localised signalling in gastruloids: mammalian embryonic organoids. *Development* **144**, 3894–3906 (2017).

25. Stuart, T. *et al.* Comprehensive Integration of Single-Cell Data. *Cell* **177**, 1888-1902.e21 (2019).

26. Lin, S. M., Du, P., Huber, W. & Kibbe, W. A. Model-based variance-stabilizing transformation for Illumina microarray data. *Nucleic Acids Research* **36**, e11–e11 (2008).

27. Waltman, L. & van Eck, N. J. A smart local moving algorithm for large-scale modularity-based community detection. *Eur. Phys. J. B* **86**, 471 (2013).

28. McInnes, L., Healy, J. & Melville, J. UMAP: Uniform Manifold Approximation and Projection for Dimension Reduction. *arXiv:1802.03426 [cs, stat]* (2018).

29. Yu, G., Wang, L.-G., Han, Y. & He, Q.-Y. clusterProfiler: an R Package for Comparing Biological Themes Among Gene Clusters. *OMICS: A Journal of Integrative Biology* **16**, 284–287 (2012).

30. La Manno, G. *et al.* RNA velocity of single cells. *Nature* **560**, 494–498 (2018).

31. Bergen, V., Lange, M., Peidli, S., Wolf, F. A. & Theis, F. J. *Generalizing RNA velocity to transient cell states through dynamical modeling*. http://biorxiv.org/lookup/doi/10.1101/820936 (2019) doi:10.1101/820936.

32. Vallier, L. *et al.* Early Cell Fate Decisions of Human Embryonic Stem Cells and Mouse Epiblast Stem Cells Are Controlled by the Same Signalling Pathways. *PLoS ONE* **4**, e6082 (2009).

33.   Hayashi, K., Ohta, H., Kurimoto, K., Aramaki, S. & Saitou, M. Reconstitution of the Mouse Germ Cell Specification Pathway in Culture by Pluripotent Stem Cells. *Cell* **146**, 519–532 (2011).

CHAPTER 5

Maturation of neural tube organoid

Maturation of neural tube organoid

JiSoo Park[1], Matthias P. Lutolf[1,2,*]

[1] Laboratory of Stem Cell Bioengineering, Institute of Bioengineering, School of Life

Sciences and School of Engineering, École Polytechnique Fédérale de Lausanne

(EPFL), Lausanne, 1015, Vaud, Switzerland

[2] Institute of Chemical Sciences and Engineering, School of Basic Science, École

Polytechnique Fédérale de Lausanne (EPFL), Lausanne, 1015, Vaud, Switzerland

[*] Correspondence: matthias.lutolf@epfl.ch

Abstract

During early vertebrate development, neural crest cells emerge from the dorsal side of the neural tube and give rise to a myriad of different cell types thus contributing to various tissues as multipotent cells. Surprisingly, the maturation of neural tube organoids gave rise to the emergence of neural crest cells and mature neurons. In this chapter, I characterized the neural crest cells and neurons from the mature neural tube organoids and their further derivative cell types. Time-lapse imaging revealed the detailed progress of delamination and migration of neural crest cells, and even phagocytosis events that have never been shown in a mammalian model to date because of its limited accessibility. The observations presented here suggest further potential of neural tube organoids as mammalian neural crest models to understand their emergence, development, and derivative cells, with better accessibility and tractability.

Introduction

Neural crest cells emerge from the dorsal part of the neural tube and possess stem cell-like properties such as self-renewal and multipotency[1–6]. They delaminate from their neighbouring neuroepithelial cells through epithelium-to-mesenchymal transition (EMT) and migrate to various part of the body and contribute to diverse range of tissues such as those of the peripheral nervous system, to craniofacial skeletal structures, and to cardiac structures[7,8]. For these significant properties, they are often referred to as "the fourth germ layer". Given that neural crest cells contribute to divergent tissues, abnormalities in their development can cause neurocristopathies such as Treacher Collins syndrome and DiGeorge syndrome, which are congenital malfunctions[9–11]. Most of these neurocristopathies result from abnormal cell specification or migration of neural crest cells. Hence, better understanding of the migration of the neural crest cells would be essential. During their migration, it is indeed important for the neural crest cells to interpret local environmental signals that guide them to their target regions[7,12]. Studies shows that this migratory behaviour is

guided by chemotaxis. However, to date, there are no accessible and tractable mammalian *in vitro* systems available to study its mechanism. Here, an *in vitro* neural tube model would permit a deeper understanding of neural crest cell development and its related diseases.

Insofar as the neural tube organoid resembles the morphology, the patterning, and the cell behaviour of the *in vivo* neural tube, I wanted to explore the later maturation of neural tube organoids. Surprisingly, I observed the emergence of mature neurons and neural crest cells. Thanks to the accessibility of the neural tube organoid system, I could characterize the maturation of the neural tube organoid into neurons and neural crest cells by live imaging. I could also capture the detailed process of neural crest cell emergence and migration. Furthermore, by long-term culturing the neural tube organoid, I could examine diverse derivatives of neural crest cells, demonstrating the multipotency of the latter. I believe mature SENT organoids can be a great model to study the development of neural crest cells and neurons.

Results and discussion

As the neural tube develops and expands, neural crest cells emerge from the dorsal side of the neural tube, and then migrate out to contribute to the development of various tissues ranging from the peripheral nervous system to the facial skeleton. Despite such an important role of this so-called "fourth germ layer", to date, there is no available *in vitro* 3D model to help dissect the mechanisms behind neural crest emergence, delamination, and migration[1–3,6,8]. Because the neural tube organoids exhibit the major hallmarks of the native neural tube, I hypothesized that they would also retain the capacity to generate neural crest cells and mature neurons *in vitro*. To test this, I harvested and re-embedded the organoids at a low density in a Matrigel drop to investigate whether they could further mature past D6 (**Figure 41A**).
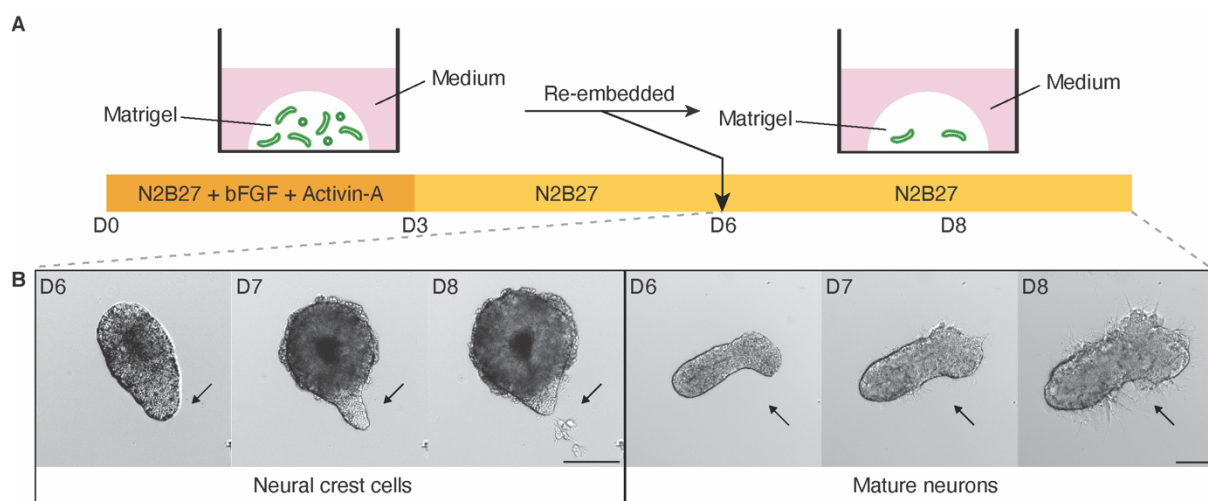

Figure 41. Neural tube organoids mature into neural crest cells and mature neurons. (A) Schematic representation of long-term organoid culture from D6 onward. (B) The brightfield time-course imaging between D6 and D8 revealed two types of organoid maturation: neural crest cells (left box) and mature neurons (right box). The arrows in the left box indicate the emergence, delamination, and migration of neural crest cells from the neural tube organoid. The arrows in the right box indicate the neurite outgrowths from mature neurons of the neural tube organoid. All the scale bars are 100 µm.

Already two days after organoid re-embedding, migrating neural crest cells and neurite extension were observed. Time-course imaging of these re-embedded organoids, from D6 to D8, revealed two main maturing organoid types (**Figure 41B**). One type

exhibited neural crest cells emerging and migrating in 3D outward from the organoids. A time-lapse of this process captured its progress in more detail (**Figure 42A**).

A Neural crest cells
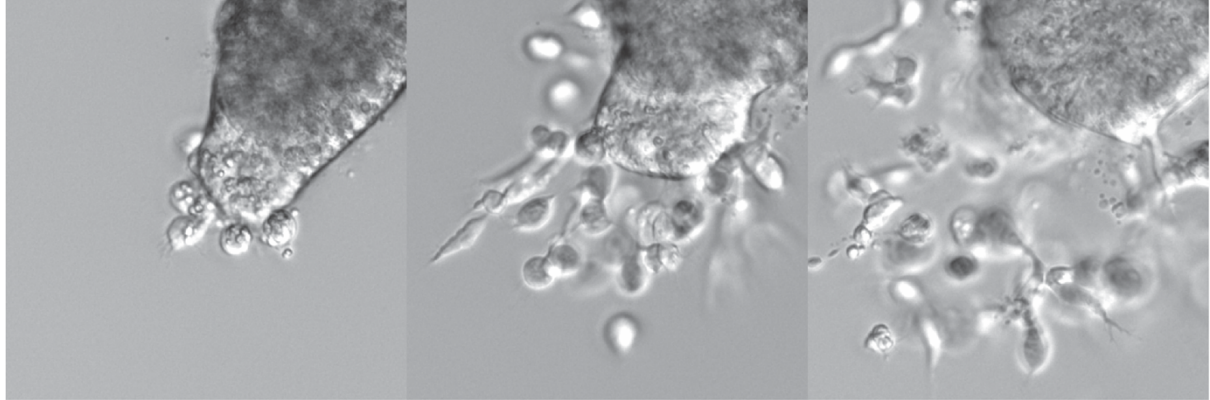
B Neurites
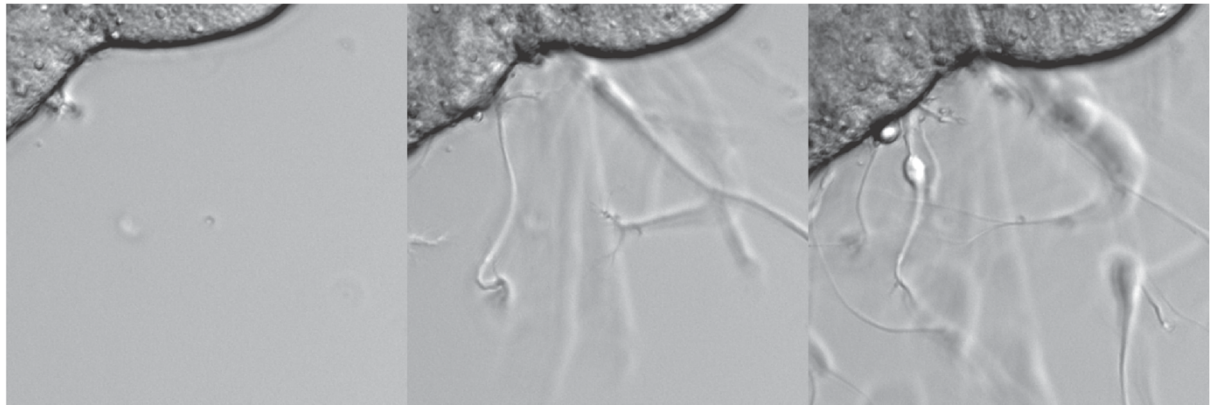
Figure 42. Time-lapse imaging captured the moment of neural crest cell migration and neurite extension. A time-lapse between D6 and D8 revealed the emergence, delamination, and migration of neural crest cells (A) and the neurite extension meaning the existence of mature neurons (B).

Observed migratory cells were later confirmed to be neural crest cells expressing neural crest cell markers[6] such as AP2α, SOX9, PAX3/7, NESTIN, and SOX10 by immunofluorescence and confocal imaging (**Figure 43**).
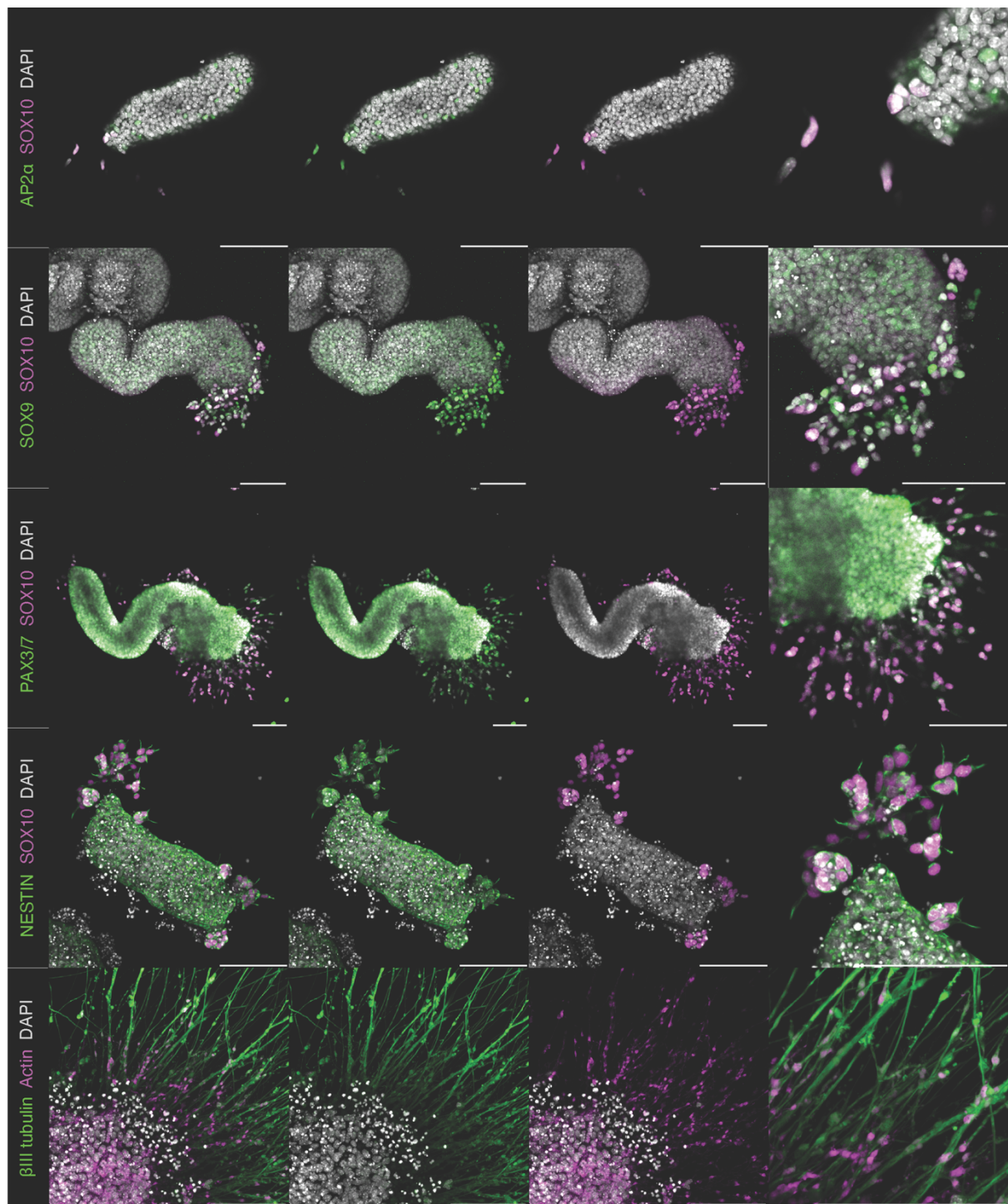
Figure 43. The emergence of neural crest cells and mature neurons from the mature neural tube organoid are confirmed by immunofluorescence by their key markers. Confocal images of 8-day-old organoids confirmed the neural crest cells that migrated out from the organoid express neural crest cell markers, AP2α, SOX9, PAX3/7, NESTIN, and SOX10. The neurite extended out from the 12-day-old organoid express βIII tubulin confirming the existence of mature neurons. All scale bars are 100 μm.

Notably, and given that AP2α is a premigratory neural crest marker, AP2α+ cells were also detected on the surface of the organoid. In addition, PAX3/7 positivity was detected all over the organoid and also among neural crest cells, as these markers are expressed in both dorsal neural tube tissue and neural crest cells *in vivo*. Meanwhile, immunofluorescent staining against NESTIN (an intermediate filament protein) highlights the cytoskeleton of neural crest cells and co-immunostaining with actin clearly shows the general cytoskeletal structure of migrating neural crest cells (**Figure 43** and **Figure 44**). As actin marks the filopodia of migrating neural crest cells, a live cell imaging-based deeper exploration of protrusion dynamics underlying neural crest migration would be feasible. This is a good example to demonstrate the accessibility of neural tube organoids. In turn, this accessibility would facilitate studies in the field addressing unresolved questions about mammalian neural crest cell development.
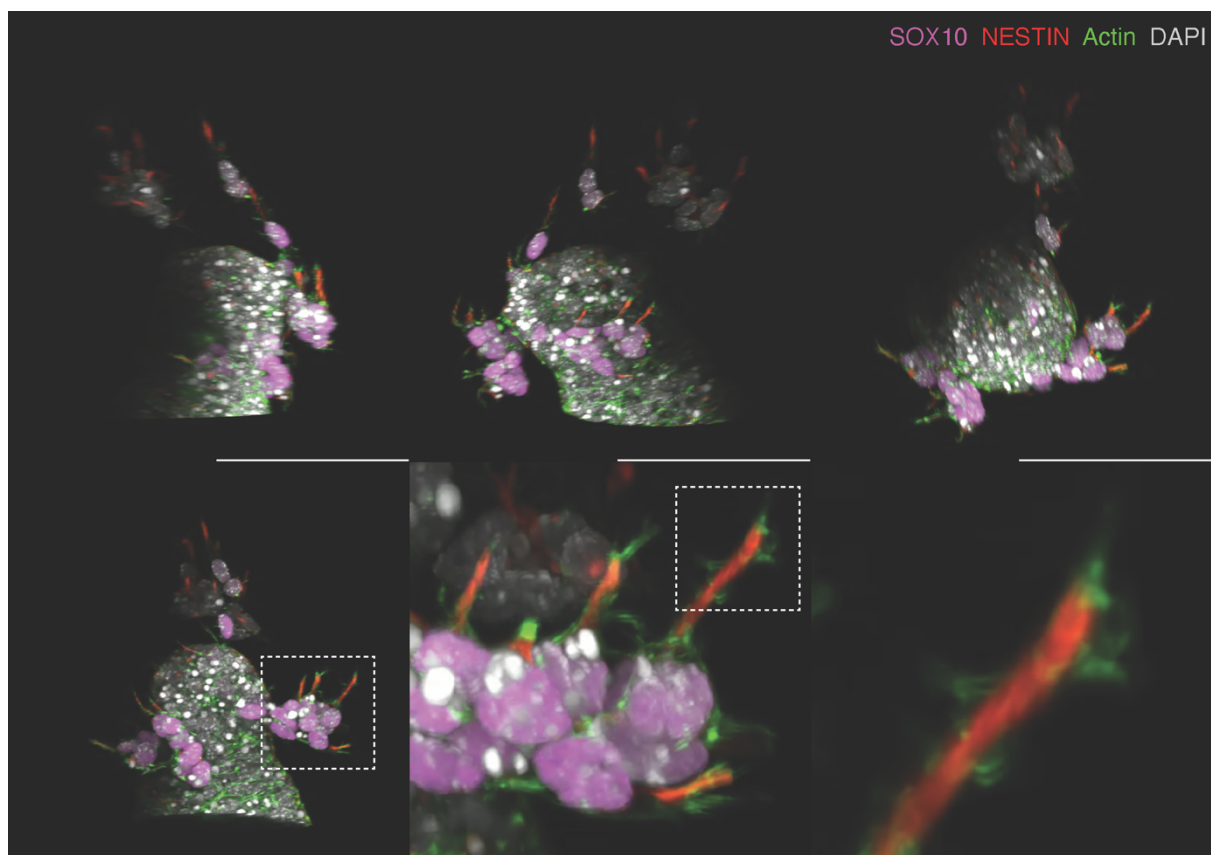

Figure 44. 3D projection of migrating neural crest cells. Co-immunostaining of NESTIN and actin clearly shows the protrusion of migrating neural crest cells. This result shows the accessibility of this system that could be potentially used for deciphering the mechanism of migration. All the scale bars are 100 μm.

The other maturing organoid type contained outgrowing neurites, indicating neuron maturation, and these could also be monitored in detail by live imaging (**Figure 42B**), Neurite identity was confirmed by βIII tubulin expression (**Figure 43**). Altogether, this data demonstrates that neural tube organoids can be a new tool for studying the emergence, delamination, and migration of neural crest cells and mature neuronal differentiation of the neural tube in an easily accessible and tractable fashion.

To assess the multipotency of emerging neural crest cells, I cultured neural tube organoids for 28 days. Since they were only cultured in N2B27 without any other morphogens, neural crest cells were not directed to differentiate into any specific cell type. On Day 28, I fixed the samples and performed immunofluorescence against the markers of several neural crest cell derivatives[4,13] (**Figure 45A**). As ectodermal derivatives, mature neurons expressing βIII tubulin (**Figure 45B**) and glial cells expressing GFAP and S100β (**Figure 45C**) were detected. As mesenchymal derivatives, adipocytes identified by the presence of the lipid droplets in their cytoplasm (detected by Bodipy staining) and smooth muscle cells expressing SM22α (**Figure 45D**) were detected. These results certainly show neural crest cells migrating out of neural tube organoids have the potential to differentiate into various cell types, not only ectodermal cells but also mesenchymal cells as well, just as is the case *in vivo*.
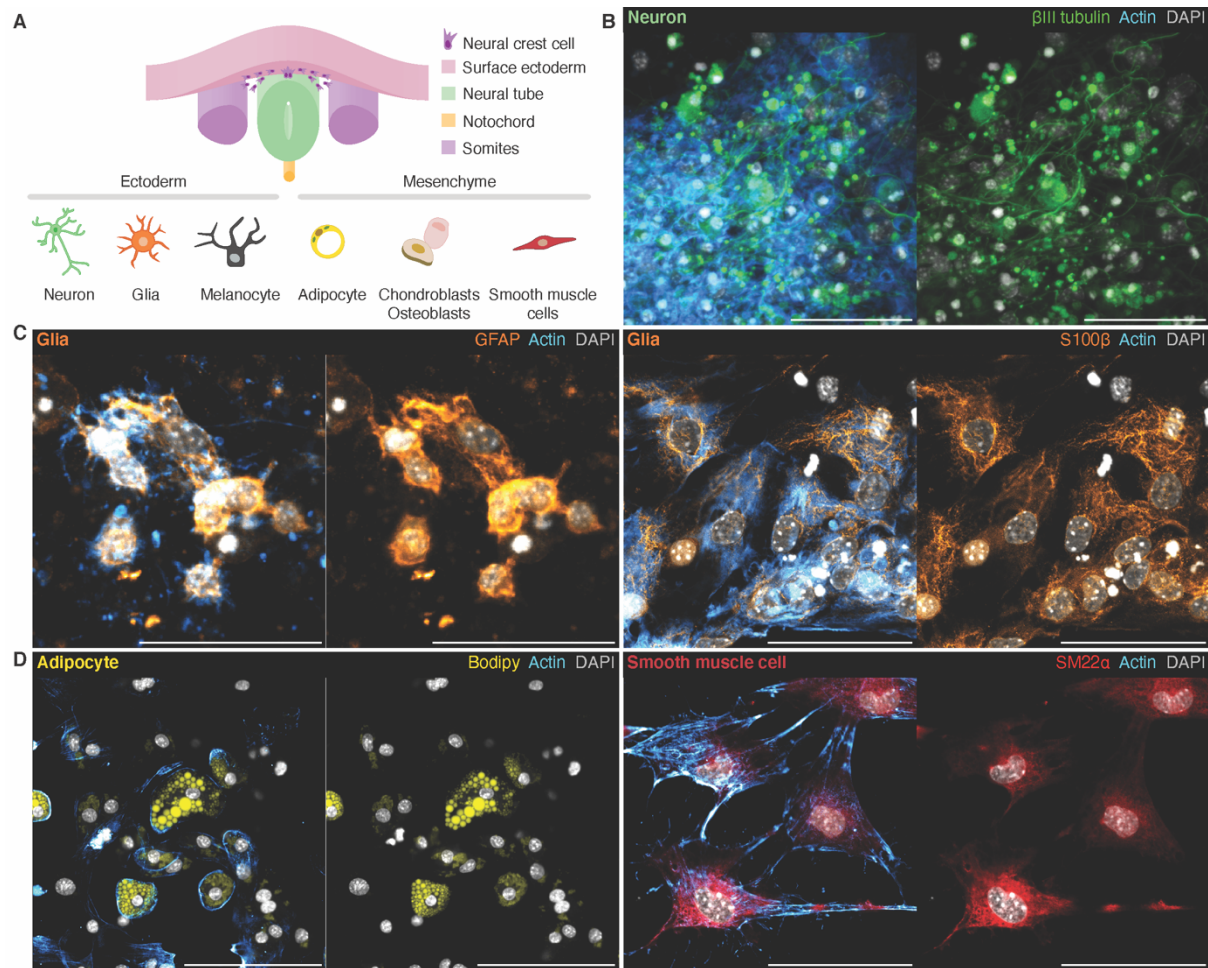
Figure 45. The emerged neural crest cells from the neural tube organoid are multipotent. (A) Illustration of multipotency of neural crest cells. Neural crest cells can be derived into ectodermal cells, such as neuron and glia, and mesenchymal derivatives, such as adipocyte and smooth muscle cells. (B-D) Culturing the neural tube organoid for 28 days revealed the multipotency of the neural crest cells. Confocal imaging confirmed that the neural crest cells have differentiated into various cell types: (B) neurons expressing βIII tubulin, (C) glial cells expressing GFAP and S100β, (D) mesenchymal derivatives like adipocyte with the lipid droplets visualized by Bodipy and smooth muscle cells expressing SM22α. All the scale bars are 50 μm.

As discussed in the introduction to this chapter, the migration of neural crest cells is critical for proper development of a wide range of embryonic tissues. However, due to the limited accessibility of mammalian models, most of the studies on this topic have been performed on avian embryos or zebrafish. A lack of information about mammalian neural crest development thus remains, especially regarding details about their delamination and migration. Since the neural crest cells emerge from neural tube organoids, and neural tube organoids are an accessible model, I wanted to explore how delamination and migration of their neural crest cells happens. For this, I

combined time-lapse imaging with live actin staining and observes the process in real time. As a result, I could observe three main processes: delamination, self-renewal, and phagocytosis.

Where a cell was seen delaminating, and prior to the delamination event itself, it could be seen constantly extending its filopodia out of the neuroepithelium, and then changed its shape to move onto the surface of the neuroepithelium (**Figure 46**). Then, the cell completely detached from the epithelium and migrated way from the organoid, extending its protrusions towards the direction of migration.
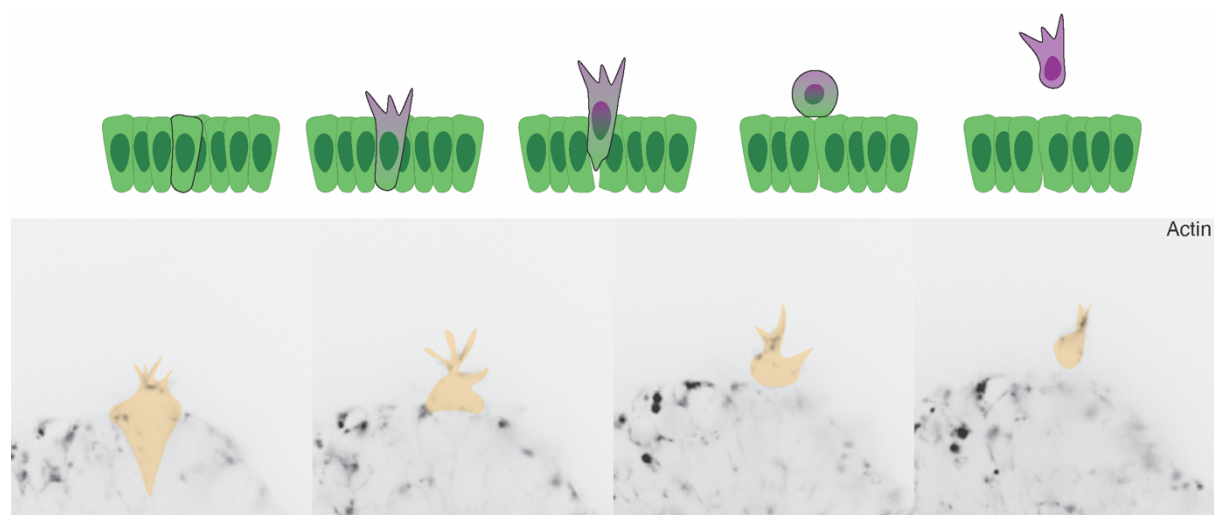
Figure 46. Delamination and migration of neural crest cells. The schematic and the time-lapse images depict the process of delamination and migration of the neural crest cells emerged from neural tube organoid. First, the cell protrudes out its filopodia out of the neuroepithelium and changes its morphology to go on the surface of the neuroepithelium. Then, the cell is entirely separated from the neural tube organoid and migrate away from the organoid having the filopodia towards the direction of migration.

After delamination, cells were proliferating actively throughout migration. Neural crest cells are known to have stem cell-like properties such as self-renewal and multipotency. From the time-lapse imaging, I indeed could capture self-renewing neural crest cells (**Figure 47**). A cell was migrating away from the organoid (as indicated by the orientation of its filopodia protrusions) and just before the division, its shape changed to big round shape with shrunken filopodia (**Figure 47A**). Then, it divided and kept on migrating away from the organoid. This active proliferation of

neural crest cells could be visualized by immunostaining against the mitosis marker, pH3 (**Figure 47B**).
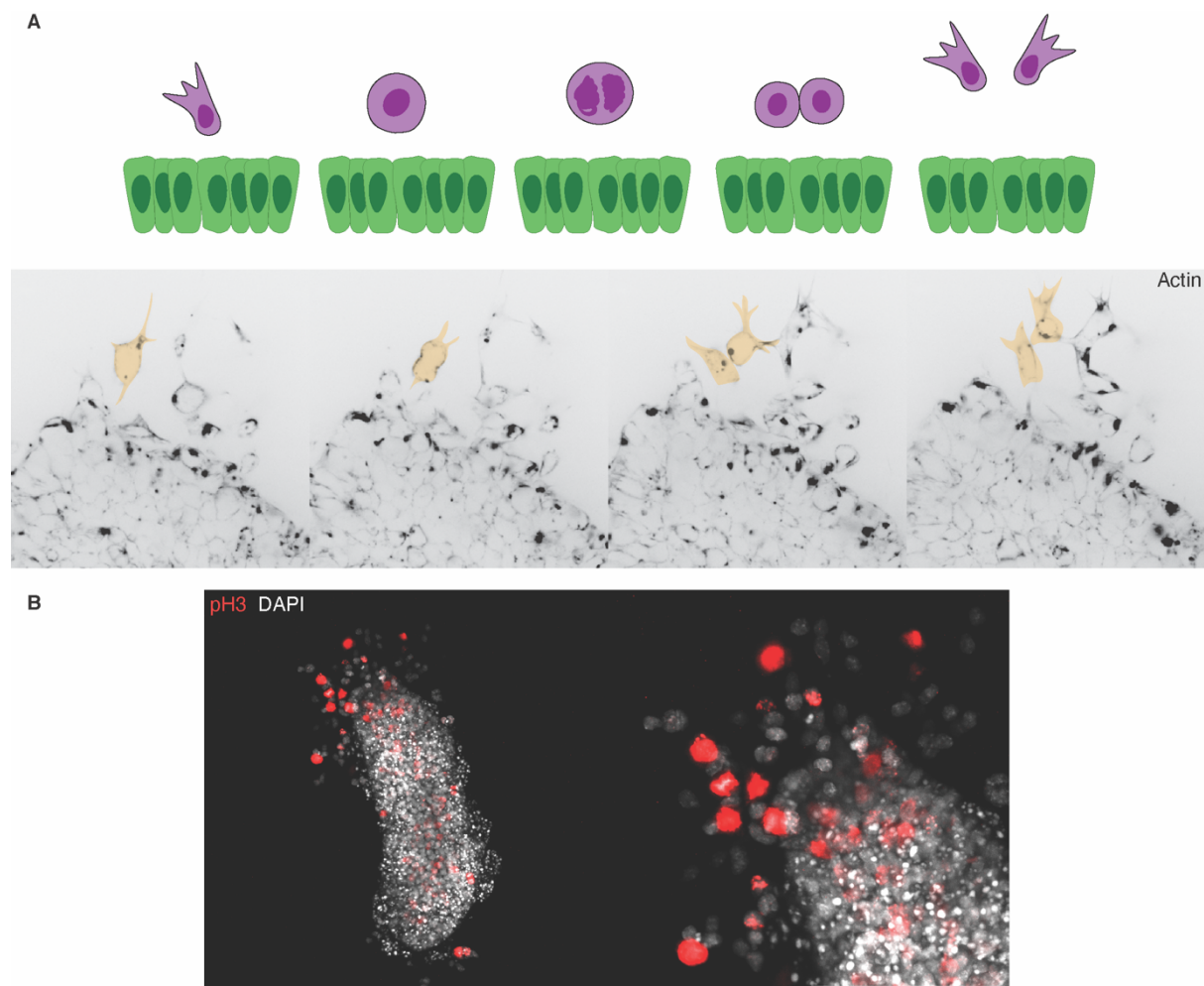
Figure 47. Self-renewal of migratory neural crest cells. (A) The schematic and the time-lapse images show the self-renewal of migratory neural crest cell. (B) pH3, mitosis marker, signal shows the neural crest cells proliferate actively during migration. The scale bars are 100 µm.

Another process that I unexpectedly observed from this time-lapse imaging was phagocytosis among neural crest cells. When one of the neural crest cells died while migrating, a neighbouring neural crest cell migrated towards the dead cell and engulfed the apoptotic debris (**Figure 48**). After phagocytosis, the neural crest continued migration. Such an intriguing process was only recently reported in zebrafish[14] in a study suggesting that the phagocytic activity of neural crest cells is important during early development before professional phagocytes populate the developing nervous system. The discovery of phagocytic capabilities among neural

crest cells finally answered the unresolved question of how apoptotic cells are removed in the developing nervous system, and would not have been revealed in the absence of accessible models such as zebrafish. Thus, this observation of phagocytic activity among mammalian neural crest cells is thus a good example of the possible applications of *in vitro* neural tube models to reveal undiscovered aspects of neural development. This result is the first observation of phagocytic activity of neural crest in a mammalian tissue.
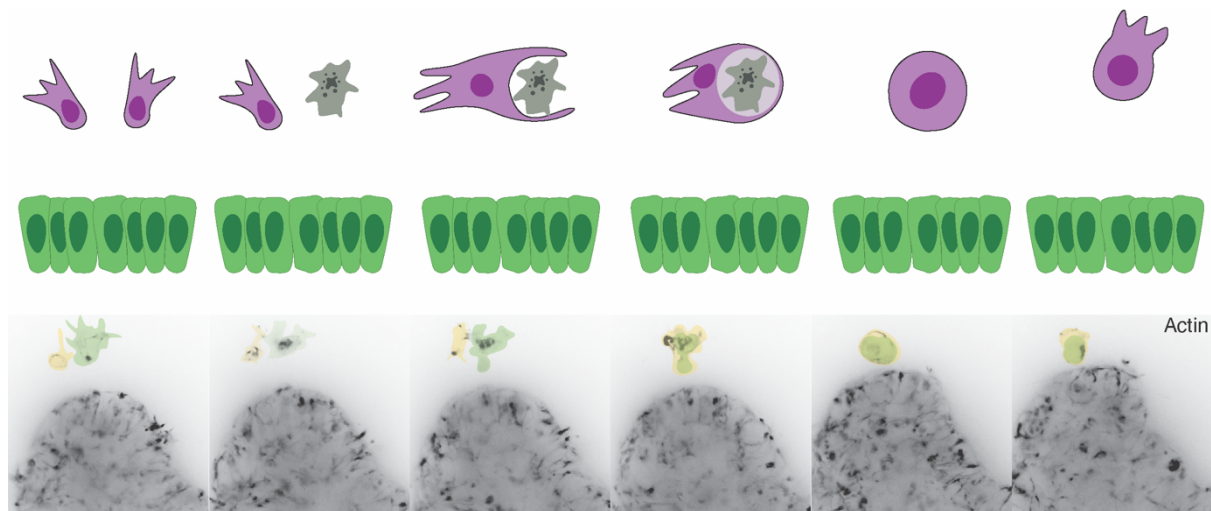
Figure 48. Phagocytosis of migrating neural crest cells. The schematic and the time-lapse images demonstrate the phagocytosis of migration neural crest cells. When there was an apoptotic cell, the neighbouring migratory neural crest cell migrated towards the apoptotic debris, engulfed, and continued migrating.

Together, the maturation of neural tube organoids revealed the emergence of neural crest cells and mature neurons. Long-term culture of the organoids revealed the multipotency of neural crest cells, differentiating into ectodermal and mesenchymal derivatives. Finally, thanks to the accessibility of the system, the process of emergence, migration, and phagocytosis of neural crest cell could be inspected by time-lapse imaging. These results suggest that neural tube organoids can be a good *in vitro* model to answer unresolved questions in neural crest cell development.

Conclusion

Maturation of neural tube organoids revealed the emergence of neural crest cells and mature neurons. Long-term culture revealed various cell types, from ectodermal to mesenchymal derivatives, derived from migrating neural crest cells. Through time-lapse imaging, detailed aspects of neural crest cell development could be captured. Particularly, it discovered phagocytic activity of neural crest cells, a behaviour that has only recently been reported but in zebrafish[14]. Observing such phenomenon in mammalian system is still impossible given the absence of mammalian models with adequate accessibility. This suggests that neural tube organoids could be used as a suitable tool to study neural crest cell development. Specifically, as defective migration is an important common factor for most neurocristopathies, these organoids can provide a good tractability to understand the pathological aspects of these disorders. Altogether, this data demonstrates that neural tube organoid can be a new tool for studying neural crest cell development and mature neuronal differentiation of the neural tube in an easily accessible and tractable fashion. It would help in elucidating the unknown mechanism of neural crest cell development and related congenital disorders.

Materials and methods

Maturation of neural tube organoids

To harvest the organoids, on D6, the Matrigel drops with organoids were washed once with PBS and then treated with 3 mg/mL Collagenase IV and 1 mg/mL Dispase in HBSS+/+ for 30 minutes on a shaker to dissolve the Matrigel. After Matrigel was dissolved, the organoids were collected with cut 1000 μL pipette tips coated with 10% serum and centrifuged at 900 rpm for 5 minutes. The supernatant was removed and the organoids were suspended in N2B27 medium. The organoids were collected and re-embedded in 10 μL of Matrigel and plated on glass-bottom 24 well plate and further cultured in N2B27 medium in 5% CO_2 and 37 °C incubator.

Immunostaining and confocal microscopy

The organoids embedded in Matrigel drop or in microfluidic device were washed with PBS-/- twice and fixed in 4% paraformaldehyde (PFA) in PBS-/- for 30 min in room temperature. After, the organoids were washed with PBS-/- for three times of 20 min and treated with 0.3 M Glycine in PBS-/- for 2 hours in room temperature. Then, the organoids were permeabilized and blocked with PBS-FT (0.2% Triton-X 100 and 10% FBS in PBS-/-) for 3 hours to overnight 4 °C. Primary antibody solution was prepared in PBS-FT (following the dilution ratio on **Table 11**) with 2 μg/mL of DAPI. The organoids were stained overnight on a low-speed orbital shaker in 4 °C. The organoids were thoroughly washed with PBS-/- every 30 min for 4 hours to remove the residual primary antibody. Secondary antibody solution was prepared, treated, and washed the same way as primary antibody solution (following the dilution ratio on **Table 12** and **Table 13**). Confocal images of organoids were generated using LSM700 (Zeiss) on Inverted Zeiss AxioObserver Z1 (Bioimaging and Optics Core Facility, EPFL), equipped with 10×/0.30 air, 20×/0.80 air, and 63×/1.40 oil objectives, 405-nm, 488-nm, 555-nm and 639-nm lasers and controlled by ZEN 2010 imaging software (Zeiss). Images were analyzed using FIJI (NIH) and IMARIS (Oxford Instruments).

Target	Species	Dilution	Cat. No.	Supplier
Phospho-Histone H3 (Ser10)	rabbit	1:500	06-570	Merck
PAX3/7	mouse	1:200	sc-365843	Santa Cruz Biotechnology
SOX9	rabbit	1:100	ab185966	abcam
AP2α	mouse	1:50	sc-12726	Santa Cruz Biotechnology
Nestin	mouse	1:100	ab11306	abcam
SOX10 [SP267]	rabbit	1:25	ab227680	abcam
Tuj1 (βIII-tubulin)	mouse	1:500	MMS-435P	Covance
GFAP	rabbit	1:500	Z0334	DAKO
S100β (EP1576Y)	Rabbit	1:100	ab52642	abcam
SM22a	rabbit	1:200	ab14106	Abcam

Table 11. Primary antibodies used in immunostaining

	Dilution	Cat. No	Supplier
Donkey anti-mouse Alexa Fluor 568	1:500	A-10037	ThermoFisher Scientific
Donkey anti-rabbit Alexa Fluor 647	1:500	A-31573	ThermoFisher Scientific
Donkey anti-rabbit Alexa Fluor 568	1:500	A-10042	ThermoFisher Scientific
Donkey anti-mouse Alexa Fluor 647	1:500	A-31571	ThermoFisher Scientific

Table 12. Secondary antibodies and dyes used in immunostaining

	Cat. No	Supplier	Purpose
sir-actin	SC001	Spirochrome	Live cell actin dye
BODIPY™ 493/503	D3922	ThermoFisher Scientific	Lipid droplet

Table 13. Dyes used in staining

Time-lapse imaging

To observe how the organoid and its lumen elongate between D6 and D8, the organoids of each well were treated with 1 mL of N2B27 with 500 nM Sir-actin (**Table 13**) for 4 hours before imaging. Time-lapse imaging was acquired by either Nikon Eclipse Ti inverted microscope system (equipped with a 10×/0.30 air objective, 632-nm filters, DS-Qi2 and Andor iXon Ultra DU888U (Oxford Instruments) cameras and controlled by NIS-Elements AR 5.11.02 (Nikon Corporation) software) for bright-field imaging or Visitron CSU-W1 (equipped with U PLAN S APO 60×/1.42 oil objective, sdc Cy5 filter, 50 µm Spinning Disk, ImagEMX2 camera, and controlled by VisiView software) and 647 nm laser for Sir-actin signal, and bright-field. The image was captured every hour between D6 and D8 (Nikon Eclipse Ti) or every 5 min between D6 and D8 (Visitron). Temperature was maintained at 37 °C with 5% CO_2.

Reference

1. Achilleos, A. & Trainor, P. A. Neural crest stem cells: discovery, properties and potential for therapy. *Cell Res* **22**, 288–304 (2012).

2. Baggiolini, A. *et al.* Premigratory and Migratory Neural Crest Cells Are Multipotent *In Vivo*. *Cell Stem Cell* **16**, 314–322 (2015).

3. Cheung, M. Neural Crest Stem Cells/Progenitors and Their Potential Applications in Disease Therapies. *JSRT* **1**, (2016).

4. Dupin, E. & Coelho-Aguiar, J. M. Isolation and differentiation properties of neural crest stem cells. *Cytometry* **83A**, 38–47 (2013).

5. Le Douarin, N. M., Creuzet, S., Couly, G. & Dupin, E. Neural crest cell plasticity and its limits. *Development* **131**, 4637–4650 (2004).

6. Simões-Costa, M. & Bronner, M. E. Establishing neural crest identity: a gene regulatory recipe. *Development* **142**, 242–257 (2015).

7. Theveneau, E. & Mayor, R. Neural Crest Cell Migration. in *Neural Crest Cells* 73–88 (Elsevier, 2014). doi:10.1016/B978-0-12-401730-6.00004-1.

8. Theveneau, E. & Mayor, R. Neural crest delamination and migration: From epithelium-to-mesenchyme transition to collective cell migration. *Developmental Biology* **366**, 34–54 (2012).

9. Sato, T. S. *et al.* Neurocristopathies: Enigmatic Appearances of Neural Crest Cell–derived Abnormalities. *RadioGraphics* **39**, 2085–2102 (2019).

10. Vega-Lopez, G. A., Cerrizuela, S., Tribulo, C. & Aybar, M. J. Neurocristopathies: New insights 150 years after the neural crest discovery. *Developmental Biology* **444**, S110–S143 (2018).

11.   Pilon, N. Treatment and Prevention of Neurocristopathies. *Trends in Molecular Medicine* **27**, 451–468 (2021).

12.   Shellard, A. & Mayor, R. Chemotaxis during neural crest migration. *Seminars in Cell & Developmental Biology* **55**, 111–118 (2016).

13.   Moghadasi Boroujeni, S. *et al.* Neural crest stem cells from human epidermis of aged donors maintain their multipotency *in vitro* and *in vivo*. *Sci Rep* **9**, 9750 (2019).

14.   Zhu, Y. *et al.* Migratory Neural Crest Cells Phagocytose Dead Cells in the Developing Nervous System. *Cell* **179**, 74-89.e10 (2019).

CHAPTER 6

Conclusion and outlook

In this thesis, I present a novel *in vitro* neural tube model that recapitulates key features of the developing neural tube *in vivo*. Starting from single mESCs cultured in Matrigel, the cells self-organize to form an elongated neuroepithelial tissue in 6 days harbouring a single neural canal-like tubular structure with primary cilia, expressing the key markers found in the developing neural tube tissue *in vivo*. The efficiency of this elongation by D6 is about fifty percent. Self-elongating neural tube organoids and the cysts remaining spherical were hereafter named SENT organoids and NENT organoids, respectively for comparative investigation. To identify the cell types composing the organoids, I used single-cell transcriptomics on both three (D3) and six (D6) days old organoids. In addition, both SENT and NENT organoids were analysed as separate conditions of D6 organoids. This scRNAseq results revealed that the D3 organoids are composed of mainly epiblast cells and D6 organoids are comprised of mainly neuroectoderm and midbrain cell types. This confirms the mESCs differentiated from pluripotent cell to epiblast and to neuroprogenitors sequentially by D6. Moreover, the respective cellular compositions of SENT and NENT organoids were compared. Strikingly, two main cell types were exclusively found in SENT organoid: hindbrain and spinal cord. In order to uncover the set of genes responsible for the drastically different morphology between the two groups of organoids developing in the exact same condition, I investigated the differentially expressed markers in these two specific cell type clusters As a result, I could demonstrate that the Hox genes were the markers exclusively found in SENT organoid. Considering the role of Hox genes in embryogenesis[1–5], I hypothesized that there might be a link between the morphological axial elongation and the AP patterning and this over expression of the Hox genes. I could validate the key contribution of this gene panel by performing qPCR and ISH to confirm the presence of Hox gene expression as well as their *in vivo*-like spatial localisation. Indeed, these results showed that SENT organoids express Hox genes from Hox1 to Hox9, which are typically found from the hindbrain to the spinal cord lumbar level. In addition, the spatial expression of the HoxB cluster genes were restricted towards a single end of the organoids as they are typically found in more posterior tissues. Accordingly, the scRNAseq analysis revealed the presence of cell types in SENT organoid mainly corresponding to neuroectoderm and its derivatives spanning from midbrain, hindbrain, and spinal cord. This indicates that the axial

elongation of SENT organoids was formed by self-organization and the AP patterning along the elongation axis spontaneously occurred alongside the elongation.

Another important aspect in neural tube development is its DV patterning. As shown by scRNAseq and immunofluorescence analyses, D6 neural tube organoid when developing without any specific morphogens involved in DV patterning was composed of dorsal fate cells. This result aligns with previously reported studies that demonstrated neuroepithelial cells adopting a default dorsal fate without exposure to any morphogens. Since *in vivo* DV patterning is governed by anti-parallel morphogen gradients from each end of dorsal and ventral part of the neural tube, I investigated the possibility to control DV patterning on single SENT organoids via external morphogen exposure and thus inspecting whether the organoids could respond similarly to the native neural tube tissue *in vivo*[6,7]. First, I investigated whether the neural tube organoids can be biased to have ventral cell types. Indeed, exposing the cells during the organoid development with ventral morphogen (SAG) resulted in a ventralized organoid. Then, I tested different concentration combinations of dorsal morphogen (BMP4) and ventral morphogen (SAG) added in bulk culture medium on the organoids. This approach is a standard experiment setup in the developmental biology field to study the effect of morphogens on tissue explants dissected from avian embryos. From this experiment, I could confidently confirm that the cells in the organoids are indeed responsive to the morphogens in dose-dependent manner. Based on these results, I designed another approach to examine the capacity to recapitulate the DV patterning of a developing neural tube on single organoid by providing exogenous morphogen gradients. To achieve the desired exposure conditions, I developed a novel microfluidic device where the organoids can be loaded in a 3D Matrigel matrix and then can be exposed to a stable anti-parallel gradient of dorsal morphogen (BMP4) and ventral morphogen (SAG). As a result, the organoids were patterned along the axis of morphogen gradient expressing dorsal cell marker (PAX3/7[+]) towards BMP4 source, where higher ratio of BMP4 over SAG presents, and ventral cell marker (OLIG2^{+}) towards SAG source, where higher ratio of SAG over BMP4 presents. The key features in the system enabling symmetry-breaking patterning on such a small tissue were (i) the use of a small gradient window where

the gradient can be kept stable for extended times and (ii) the possibility to have a precise control over organoid positioning at the desired location (i.e., at the gradient window). Taken together, I developed a novel neural tube organoid that resembles the morphology and key hallmarks of the developing neural tube *in vivo* and can be patterned with exogenous sources of effectors.

Tissues emerging from the developing neural tube do not only contribute to the nervous system, but also to other, more remote, tissue types such as craniofacial skeleton and connective tissue, through a specialized cell type called neural crest cell. Often the neurocristopathies are caused by the abnormal migration of neural crest cells. As neural crest cells emerge from the dorsal part of neural tube and our neural tube organoid comprises of dorsal cell types, I hypothesized that neural crest cells would emerge from the organoid, if it is a true mirror of the neural tube *in vivo*. The neural tube organoids developing further than 6 days revealed the emergence of neural crest cells and mature neurons, confirmed at the protein level by immunofluorescence of neural crest cells major markers. Long-term culture of the organoids demonstrated the multipotency of neural crest cells to differentiate into ectodermal derivatives like neuron and glia, mesenchymal derivatives like adipocytes as well as smooth muscle cells[8]. Furthermore, thanks to the accessibility of the organoid, I could easily observe at high resolution the process of delamination and migration of the neural crest and neurite extension of mature neurons using time-lapse imaging. Most importantly using this strategy, I could discover a phagocytotic activity of migratory neural crest cells. I, for the first time, showcase this phenomenon in a mammalian tissue, a fascinating discovery only seen in zebrafish models up to today[9]. Collectively, I demonstrated another potential application of the neural tube organoid where the development of neural crest cells, from delamination, migration, and differentiation, can be monitored in real time. The presented neural tube extraordinary accessibility and resemblance to its *in vivo* counterpart overcomes the current hurdle in the neural crest cell field and open new avenues to study deeper, investigate mechanisms and potentially answer yet unresolved questions in the field.

As described above, I have developed an *in vitro* neural tube model that closely mimics the developing neural tube in the embryo. I expect these organoids to open new paths to study tissue mechanics, patterning, and neural crest development in mammalian neural tube at the cellular and molecular level. Yet, various unanswered questions about the self-organisation and *in vivo*-like responsiveness of our neural tube organoid model remain.

First, the mechanism of elongation should be elucidated. Gastruloid as an example of axial elongating embryo-like structure is known to elongate from the tail-bud like structure comprised of NMP cells types resembling of the axial extension of tail-bud *in vivo*. Based on these gastruloid studies[10], I inspected the existence of NMP cells in the organoid, however, I could not find it in the neural tube organoid. Also, exposure to retinoic acid (RA) inhibited the elongation of the neural tube organoid (data not shown)[5]. A number of studies described how RA inhibits axial elongation, however, this inhibition was due to Wnt signaling inhibition in NMPs, a cell type missing in the neural tube organoid[5,11,12]. Thus, the elongation mechanism in the neural tube organoids is yet to be uncovered. Additionally, further investigation is needed to understand the novel neural tube tissue mechanical link to its herein described morphogenesis. For example, the PCP pathway is known to be involved in axial elongation, especially in convergent extension[13,14]. The scRNAseq analysis have exhibited higher expression level of PCP pathway genes in SENT than NENT (**Figure 49**) suggesting that the axial elongation might occur via convergent extension. Overall, a clearer and deeper study on the mechanism of the elongation would be beneficial to better understand and thus control in its entirety this novel system.
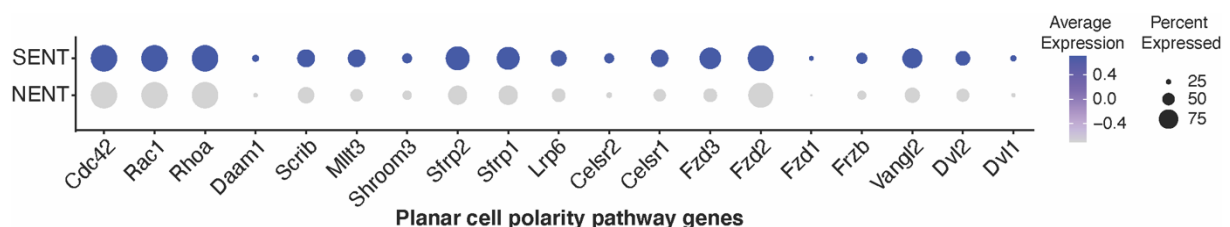

Figure 49. Higher expression level of PCP pathway genes found in SENT comparing to NENT.

Second, dissecting a series of shorter timepoints in single-cell transcriptomics would help understanding the emergence, the trajectory and the differentiation of each cell populations and. Furthermore, single-cell transcriptomics could be used to decipher the trajectory from D6 organoids to the emergence of neural crest cells around D8. Also, to study the multipotency of neural crest cells in a more controlled manner, sorting the neural crest cell specifically out of the neural tube organoid cells and culturing in a specific culture condition to differentiate into a distinct cell type would be more appropriate method[15]. With this, the neural tube organoids could act as a source of desired specialized cell type for regenerative medicine applications.

Lastly, more characterization of AP patterning and DV patterning is needed to investigate further maturation. The Hox genes involved in AP patterning are known to be expressed from the anterior to the posterior region of the embryo over time. Hox gene expression was revealed solely at D6 as the end of the experiment and the most posterior Hox genes expressed was Hox9 level, lumbar level of spinal cord. I expect that investigating Hox gene expression in a more mature neural tube organoid might have more posterior Hox gene expression. Also, DV patterning in the neural tube organoid could be examined to a greater extent. For this study, only one marker each of dorsal and ventral part of the neural tube were employed as a readout of DV patterning in neural tube organoid by morphogen gradient. The presence of more specified and various cell types along DV axis showing a variety of sensory neurons, interneurons, and motor neurons remains to be characterized. Ultimately, exploring the connections between the three cell types would reveal yet pending questions on the establishment of the neural circuitry for locomotion.

Overall, I herein present a novel *in vitro* organoid model that faithfully recapitulates the hallmarks of the developing embryonic neural tube, from its architecture with neural canal to its patterning by self-organization. This system allows real time observations of cellular rearrangements during morphogenesis, elongation as well as symmetry-breaking patterning along the appropriate axes with the emergence of region-specific cell identities. The accessibility of this system allows migration and development of neural crest cells to be studied *in vitro*. Especially, many

neurocrepathies are caused by abnormalities in migration of neural crest cells, thus dissecting the migration of neural crest cells having control over chemotaxis using notably microfluidics approach would allow us to better understand the nature and mechanisms involved in these pathologies[16,17]. Notably, the presented model is a unique knowledge base enabling the development of a physiologically relevant human neural tube model (**Figure 50**).
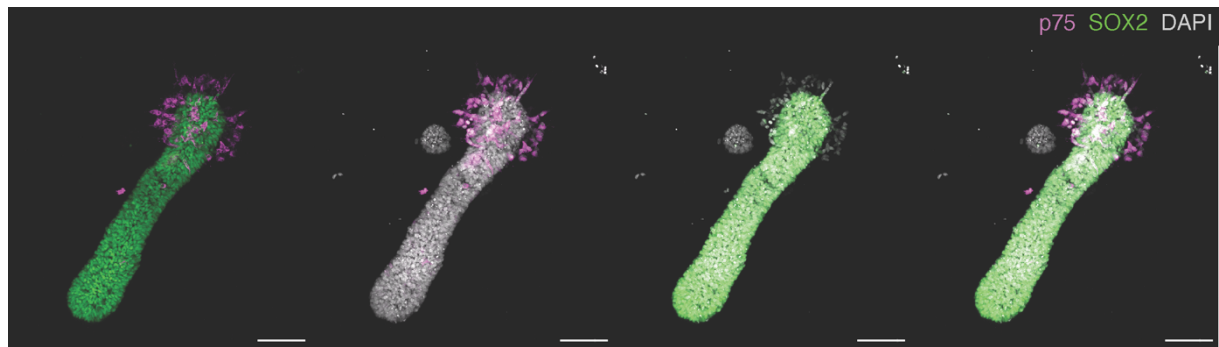
Figure 50. hPSC-based elongated neural tube-like structure with emergence of neural crest cells. SOX2 demonstrates the neuroprogenitor cells and p75 indicates the neural crest cells. This preliminary data shows the promising potential in developing an *in vitro* human neural tube organoid. Scale bars are 100 µm.

Collectively, this model should contribute to understanding and facilitating the exploration of mammalian neural tube developmental processes as well as neurodevelopmental diseases in scalable and tractable manner.
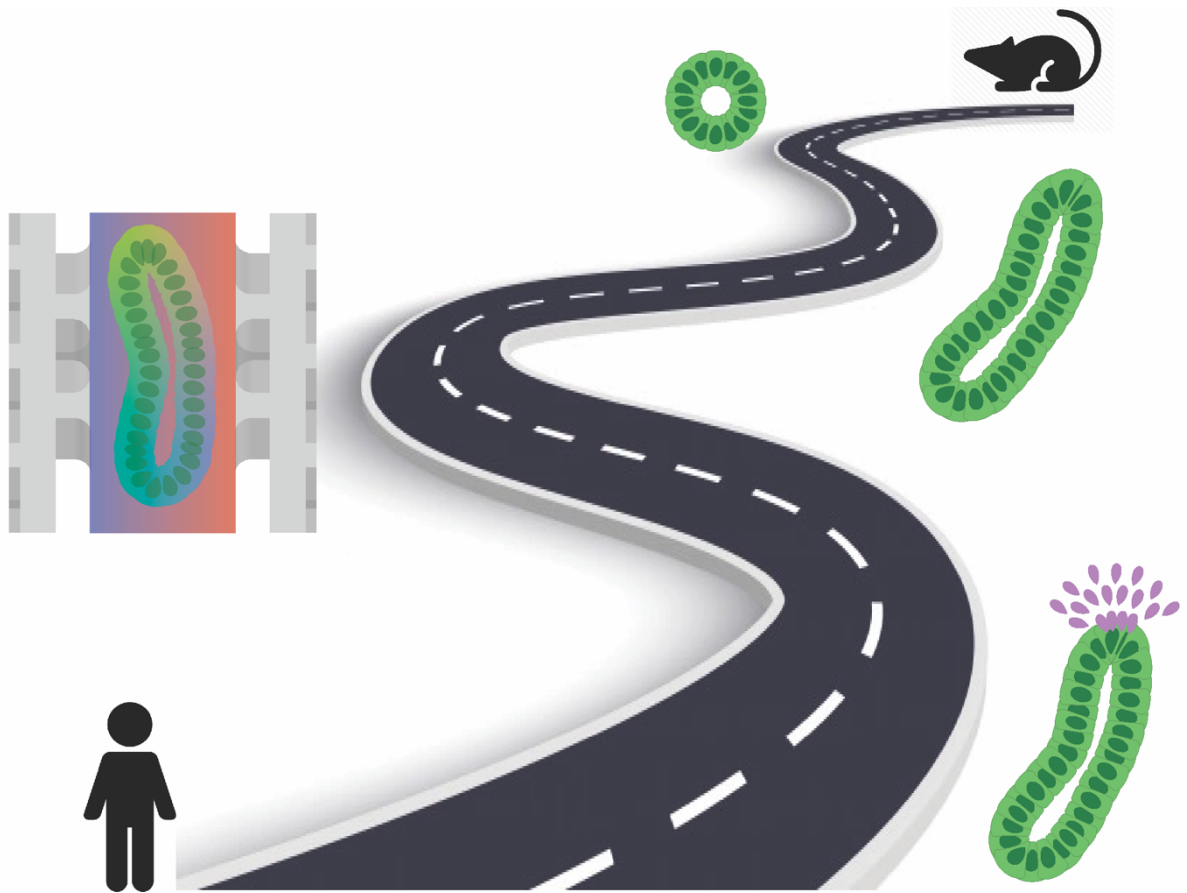
Figure 51. Summary of the thesis journey. I developed mESC-based neural tube organoid that resembles the morphology and hallmarks of developing neural tube *in vivo*. This organoid could be spatially patterned by morphogen gradient provided by microfluidic device recapitulating DV patterning of neural tube *in vivo*. Further maturation of this organoid demonstrated emergence and migration of multipotent neural crest cells. I believe this experience and knowledge could facilitate the development of physiologically relevant human neural tube model in the future.

Reference

1. Philippidou, P. & Dasen, J. S. Hox Genes: Choreographers in Neural Development, Architects of Circuit Organization. *Neuron* **80**, 12–34 (2013).

2. Forlani, S., Lawson, K. A. & Deschamps, J. Acquisition of Hox codes during gastrulation and axial elongation in the mouse embryo. *Development* **130**, 3807–3819 (2003).

3. Deschamps, J. & Duboule, D. Embryonic timing, axial stem cells, chromatin dynamics, and the Hox clock. *Genes Dev.* **31**, 1406–1416 (2017).

4. Aulehla, A. & Pourquie, O. More Than Patterning—Hox Genes and the Control of Posterior Axial Elongation. *Developmental Cell* **17**, 439–440 (2009).

5. Deschamps, J. & van Nes, J. Developmental regulation of the Hox genes during axial morphogenesis in the mouse. *Development* **132**, 2931–2942 (2005).

6. Zagorski, M. *et al.* Decoding of position in the developing neural tube from antiparallel morphogen gradients. *Science* **356**, 1379–1383 (2017).

7. Dessaud, E. *et al.* Interpretation of the sonic hedgehog morphogen gradient by a temporal adaptation mechanism. *Nature* **450**, 717–720 (2007).

8. Moghadasi Boroujeni, S. *et al.* Neural crest stem cells from human epidermis of aged donors maintain their multipotency *in vitro* and *in vivo*. *Sci Rep* **9**, 9750 (2019).

9. Zhu, Y. *et al.* Migratory Neural Crest Cells Phagocytose Dead Cells in the Developing Nervous System. *Cell* **179**, 74-89.e10 (2019).

10. Beccari, L. *et al.* Multi-axial self-organization properties of mouse embryonic stem cells into gastruloids. *Nature* **562**, 272–276 (2018).

11.   Sambasivan, R. & Steventon, B. Neuromesodermal Progenitors: A Basis for Robust Axial Patterning in Development and Evolution. *Front. Cell Dev. Biol.* **8**, 607516 (2021).

12.   Edri, S., Hayward, P., Baillie-Johnson, P., Steventon, B. & Arias, A. M. An Epiblast Stem Cell derived multipotent progenitor population for axial extension. *Development* dev.168187 (2019) doi:10.1242/dev.168187.

13.   Ybot-Gonzalez, P. *et al.* Convergent extension, planar-cell-polarity signalling and initiation of mouse neural tube closure. *Development* **134**, 789–799 (2007).

14.   Shindo, A. Models of convergent extension during morphogenesis: Models of convergent extension during morphogenesis. *WIREs Dev Biol* **7**, e293 (2018).

15.   Kawaguchi, J., Nichols, J., Gierl, M. S., Faial, T. & Smith, A. Isolation and propagation of enteric neural crest progenitor cells from mouse embryonic stem cells and embryos. *Development* **137**, 693–704 (2010).

16.   Pilon, N. Treatment and Prevention of Neurocristopathies. *Trends in Molecular Medicine* **27**, 451–468 (2021).

17.   Vega-Lopez, G. A., Cerrizuela, S., Tribulo, C. & Aybar, M. J. Neurocristopathies: New insights 150 years after the neural crest discovery. *Developmental Biology* **444**, S110–S143 (2018).

JiSoo Park

Professional contact: EPFL SV IBI-SV UPLUT
                        AI 1116 (Bâtiment AI)
                        Station 15
                        1015 Lausanne
                        jisoo.park@epfl.ch
                        +41 (0)21 693 17 89

Personal contact: Avenue Floréal 2
                        1006 Lausanne
                        jisooo.park@gmail.com
                        +41 (0)78 689 88 17

Date of birth: October 11, 1988
Place of birth: Seoul, South Korea
Nationality: South Korean

EDUCATION

June 2016 – Present

Ph.D. candidate
Laboratory of Stem Cell Bioengineering,
École Polytechnique Fédérale de Lausanne, Lausanne, Switzerland
Advisor: Matthias P. Lütolf

Mar 2013 – Feb 2015

Master in Engineering,
NBIT, KU-KIST Graduate School of Converging Science and Technology,
Korea University, Seoul, South Korea
Advisor: Sang-Hoon Lee
Co-advisor: C. Justin Lee

Mar 2008 – Feb 2013

Bachelor in Engineering,
Department of Biomedical Engineering, College of Health Science,
Korea University, Seoul, South Korea
Advisor: Sang-Hoon Lee

PROFESSIONAL EXPERIENCES

Mar 2015 – May 2016

Researcher
Intelligent BioMEMS Laboratory,
Korea University, Seoul, South Korea
Advisor: Sang-Hoon Lee

Feb 2011 – July 2011

Research assistant
Neuroeconomics and Social Neurosciences,
Department of Economics, University of Zurich, Zurich, Switzerland
Advisor: Philippe Tobler

June 2010 – Aug 2010

Research assistant
Neuroengineering & Biomedical Instrumentation Lab,
Department of Biomedical Engineering,
Johns Hopkins University, Baltimore, USA
Advisor: Nitish Thakor

Honors and Awards

Sep 2015	TERMIS-SYIS Travel Awards
Mar 2013 – Feb 2015	KU-KIST Full Scholarship, Korea University
May 2012	Best Presenter Award, The Korean Society of Medical&Biological Engineering
May 2010	Best Presenter Award, The Korean Society of Medical&Biological Engineering
Mar 2009 – Feb 2010	Student President Scholarship, Department of Biomedical Engineering, Korea University
July 2008 – Feb 2010	Student Leader Scholarship, Department of Biomedical Engineering, Korea University

PUBLICATIONS GeonHui Lee, Jaeho Lim, **JiSoo Park**, Wonseok Lee, Dae Sung Yoon, Soo Hyun Kim, Myung-Ki Kim, Sang-Hoon Lee, Dong-Hwee Kim. Construction of neurospherioids via surface modified concave microwells. *Journal of industrial and engineering chemistry*, 62, 341-351 (2018)

DoYeun Park*, **JiSoo Park***, Heeyeong Jang, Jie Cheng, Soo Hyun Kim, Sang-Hoon Lee. Simultaneous microfluidic spinning of multiple strands of submicron fiber for the production of free-standing porous membranes for biological application. *Biofabrication*, 9(2). (2017)

Yoon Young Yi, **JiSoo Park**, Jaeho Lim, C. Justin Lee, Sang-Hoon Lee. Central nervous system and its disease models on a chip. *Trends in Biotechnology*, 33, no. 12: 762-776. (2015)

Gi Seok Jeong, Joon Young Chang, **JiSoo Park**, Seung-A Lee, DoYeun Park, Junsung Woo, Heeyoung An, C. Justin Lee, Sang-Hoon Lee. Networked neural spheroid by neuro-bundle mimicking nervous system created by topology effect. *Molecular Brain*, 8(1), 1-12. (2015)

JiSoo Park*, Bo Kyeong Lee*, Gi Seok Jeong, Jung Keun Hyun, C. Justin Lee, Sang-Hoon Lee. Three dimensional brain-on-a-chip with an interstitial level of flow and its application as an *in vitro* model of Alzheimer's disease. *Lab on a Chip*, 15(1), 141-150. (2015)

AhRan Kang*, **JiSoo Park***, Jongil Ju*, Gi Seok Jeong, Sang-Hoon Lee. Cell encapsulation via microtechnologies. *Biomaterials*, 35(9), 2651-2663. (2014)

Yoon Jung Choi*, **JiSoo Park***, Sang-Hoon Lee. Size-controllable networked neurospheres as a 3D neuronal tissue model for Alzheimer's disease studies. *Biomaterials*, 34(12), 2938-2946. (2013)

Dong-Hyun Baek, **JiSoo Park**, Eun-Joong Lee, SuJung Shin, Jin-Hee Moon, James Jungho Park, Sang-Hoon Lee. Interconnection of multichannel polyimide electrodes using anisotropic conductive films (ACFs) for biomedical applications. *IEEE Transactions on Biomedical Engineering*, 58(5), 1466-1473. (2011)

*Indicates shared first-authorship.

SELECTED PRESENTATIONS **JiSoo Park**, Sang-Hoon Lee. "Noodle fiber" overcoming limitations of electrospinning and microfluidics-based microfiber. *The 19th International Conference on Miniaturized Systems for Chemistry and Life Sciences (MicroTAS)*. Gyeongju, Korea, October 25-29, 2015.

JiSoo Park, Bo Kyeong Lee, Gi Seok Jeong, C. Justin Lee, Sang-Hoon Lee. 3D Brain-on-a-chip with an interstitial level of flow and its application as an in vitro Alzheimer's disease model. *The 4th TERMIS World Congress*. Boston, MA, USA, September 8-11, 2015.

JiSoo Park, Bo Kyeong Lee, Gi Seok Jeong, C. Justin Lee, Sang-Hoon Lee. 3D Brain-on-a-chip with an interstitial level of flow and its application as an in vitro Alzheimer's disease model. *The 7th International Symposium on Microchemistry and Microsystems (ISMM)*. Kyoto, Japan, June 8-10, 2015.

JiSoo Park, Bo Kyeong Lee, Gi Seok Jeong, C. Justin Lee, Sang-Hoon Lee. Development of a three-dimensional brain-on-a-chip with an interstitial level of flow and its application as an in vitro model of Alzheimer's disease. *The 18th International Conference on Miniaturized Systems for Chemistry and Life Sciences (MicroTAS)*. San Antonio, TX, USA, October 26-30, 2014.

JiSoo Park, Yoon Jung Choi, Sang-Hoon Lee. Uniform-sized 3D neuronal tissue model for Alzheimer's disease studies. *The 9th World Congress of Chemical Engineering*. Seoul, Korea, August 18-23, 2013.

Selected Presentations

Sep 8-11, 2015   **JiSoo Park**, Bo Kyeong Lee, Gi Seok Jeong, C. Justin Lee, Sang-Hoon Lee. 3D Brain-on-a-chip with an interstitial level of flow and its application as an in vitro Alzheimer's disease model. *The 4th TERMIS World Congress*. Boston, MA, USA

Jun 8-10, 2015   **JiSoo Park**, Bo Kyeong Lee, Gi Seok Jeong, C. Justin Lee, Sang-Hoon Lee. 3D Brain-on-a-chip with an interstitial level of flow and its application as an in vitro Alzheimer's disease model. *The 7th International Symposium on Microchemistry and Microsystems (ISMM)*. Kyoto, Japan

Oct 26-30, 2014   **JiSoo Park**, Bo Kyeong Lee, Gi Seok Jeong, C. Justin Lee, Sang-Hoon Lee. Development of a three-dimensional brain-on-a-chip with an interstitial level of flow and its application as an in vitro model of Alzheimer's disease. *The 18th International Conference on Miniaturized Systems for Chemistry and Life Sciences (MicroTAS)*. San Antonio, TX, USA

Aug 18-23, 2013   **JiSoo Park**, Yoon Jung Choi, Sang-Hoon Lee. Uniform-sized 3D neuronal tissue model for Alzheimer's disease studies. *The 9th World Congress of Chemical Engineering*. Seoul, Korea

Activities

Dec 2020 – Feb 2020   Marketing manager, SciFilmIt Lausanne 2020, Lausanne, Switzerland

Jan 2020 – Present   Soprano, Philophonia, Lausanne, Switzerland

Sep 2019 – Dec 2019   Innosuisse Business Concept Course (First prize), Lausanne, Switzerland

Nov 2018 – Dec 2018   Scientist (First prize), Exposure Science Film Hackathon, Lausanne, Switzerland

July 2018 – Present   Active member, Bio Science Network Lausanne (BSNL), Lausanne, Switzerland

Dec 2014 – June 2015   Bartender, Fundoori, Seoul, South Korea

Dec 2012 – May 2016   Designer, Intelligent BioMEMS Laboratory, Seoul, South Korea

Jan 2010 – Feb 2011   Moderator of Seoul Group, Couch Surfing, Seoul, South Korea

Feb 2009 – Feb 2010   Student President, Department of Biomedical Engineering, Korea University

Feb 2009 – Feb 2010   Leader of Class, Department of Biomedical Engineering, Korea University

June 2008 – Feb 2009   Leader of Class, Department of Biomedical Engineering, Korea University

Mar 2008 – Feb 2009   Acoustic Guitar Club, Seoul, South Korea

Languages

Korean : Native
English : Fluent
French : B1 (learning)

Hobbies

Acoustic guitar, singing, skiing, photography, climbing, cooking